

# Nitrogen oxides in the free troposphere: Implications for tropospheric oxidants and the interpretation of satellite NO<sub>2</sub> measurements

5 Viral Shah<sup>1,a</sup>, Daniel J. Jacob<sup>1,2</sup>, Ruijun Dang<sup>1</sup>, Lok N. Lamsal<sup>3,4</sup>, Sarah A. Strode<sup>3,5</sup>, Stephen D. Steenrod<sup>3,4</sup>, K. Folkert Boersma<sup>6,7</sup>, Sebastian D. Eastham<sup>8,9</sup>, Thibaud M. Fritz<sup>8</sup>, Chelsea Thompson<sup>10,11</sup>, Jeff Peischl<sup>10,11</sup>, Ilann Bourgeois<sup>10,11,b</sup>, Ilana B. Pollack<sup>12</sup>, Benjamin A. Nault<sup>13</sup>, Ronald C. Cohen<sup>14,15</sup>, Pedro Campuzano-Jost<sup>16,17</sup>, Jose L. Jimenez<sup>16,17</sup>, Simone T. Andersen<sup>18</sup>, Lucy J. Carpenter<sup>18</sup>, Tomás Sherwen<sup>18,19</sup>, Mat J. Evans<sup>18,19</sup>

- 10 <sup>1</sup> Harvard John A. Paulson School of Engineering and Applied Sciences, Harvard University, Cambridge, MA 01238, USA  
<sup>2</sup> Department of Earth and Planetary Sciences, Harvard University, Cambridge, MA 02138, USA  
<sup>3</sup> Atmospheric Chemistry and Dynamics Laboratory, NASA Goddard Space Flight Center, Greenbelt, MD 20771, USA  
<sup>4</sup> University of Maryland Baltimore County, Baltimore, MD 21250, USA  
<sup>5</sup> GESTAR II, Morgan State University, Baltimore, MD 21251, USA  
15 <sup>6</sup> Royal Netherlands Meteorological Institute (KNMI), De Bilt, the Netherlands  
<sup>7</sup> Wageningen University, Wageningen, the Netherlands  
<sup>8</sup> Laboratory for Aviation and the Environment, Department of Aeronautics and Astronautics, Massachusetts Institute of Technology, Cambridge, MA 02139, USA  
<sup>9</sup> Joint Program on the Science and Policy of Global Change, Massachusetts Institute of Technology, Cambridge, MA 02139, USA  
20 <sup>10</sup> NOAA Chemical Sciences Laboratory, Boulder, CO 80305, USA  
<sup>11</sup> Cooperative Institute for Research in Environmental Sciences, University of Colorado Boulder, Boulder, CO 80309, USA  
<sup>12</sup> Department of Atmospheric Sciences, Colorado State University, Fort Collins, CO 80523, USA  
<sup>13</sup> Center for Aerosols and Cloud Chemistry, Aerodyne Research, Inc., Billerica, MA 01821, USA  
25 <sup>14</sup> Department of Earth and Planetary Science, University of California Berkeley, Berkeley, CA 94720, USA  
<sup>15</sup> Department of Chemistry, University of California Berkeley, Berkeley, CA 94720, USA  
<sup>16</sup> Cooperative Institute for Research in Environmental Sciences, University of Colorado, Boulder, CO 80309, USA  
<sup>17</sup> Department of Chemistry, University of Colorado, Boulder, CO 80309, USA  
<sup>18</sup> Wolfson Atmospheric Chemistry Laboratories, Department of Chemistry, University of York, York, YO10 5DD, UK  
30 <sup>19</sup> National Centre for Atmospheric Science, University of York, York YO10 5DD, UK.  
<sup>a</sup> Now at Global Modeling and Assimilation Office, NASA Goddard Space Flight Center, Greenbelt, MD 20771, USA, and Science Systems and Applications, Inc., Lanham, MD 20706, USA  
<sup>b</sup> Now at Extreme Environments Research Laboratory, École Polytechnique Fédérale de Lausanne Valais Wallis, Sion, Switzerland, and Plant Ecology Research Laboratory, École Polytechnique Fédérale de Lausanne, Lausanne, Switzerland.
- 35 *Correspondence to:* Viral Shah (vshah@seas.harvard.edu)

**Abstract.** Satellite-based retrievals of tropospheric NO<sub>2</sub> columns are widely used to infer NO<sub>x</sub> (≡NO+NO<sub>2</sub>) emissions. These retrievals rely on model information for the vertical distribution of NO<sub>2</sub>. The free tropospheric background above 2 km is particularly important because the sensitivity of the retrievals increases with altitude. Free tropospheric NO<sub>x</sub> also has a strong effect on tropospheric OH and ozone concentrations. Here we use observations from three aircraft campaigns (SEAC<sup>4</sup>RS, DC3, and ATom) and four atmospheric chemistry models (GEOS-Chem, GMI, TM5, and CAMS) to evaluate the model capabilities for simulating NO<sub>x</sub> in the free troposphere and attribute it to sources. NO<sub>2</sub> measurements during the SEAC<sup>4</sup>RS and

40

DC3 campaigns over the southeastern US in summer show increasing concentrations in the upper troposphere above 10 km, which are not replicated by GEOS-Chem although the model is consistent with the NO measurements. Using concurrent NO, NO<sub>2</sub>, and ozone observations from a DC3 flight in a thunderstorm outflow, we show that the NO<sub>2</sub> measurements in the upper troposphere are biased high, plausibly due to interference from thermally labile NO<sub>2</sub> reservoirs such as peroxyacetic acid (HNO<sub>4</sub>) and methyl peroxy nitrate (MPN). We find that NO<sub>2</sub> concentrations calculated from the NO measurements and NO-NO<sub>2</sub> photochemical steady state (PSS) are more reliable to evaluate the vertical profiles of NO<sub>2</sub> in models. GEOS-Chem reproduces the shape of the PSS-inferred NO<sub>2</sub> profiles throughout the troposphere for SEAC<sup>4</sup>RS and DC3 but overestimates NO<sub>2</sub> concentrations by about a factor of 2. The model underestimates MPN and alkyl nitrate concentrations, suggesting missing organic NO<sub>x</sub> chemistry. On the other hand, the standard GEOS-Chem model underestimates NO observations from the ATom campaigns over the Pacific and Atlantic Oceans, indicating a missing NO<sub>x</sub> source over the oceans. We find that we can account for this missing source by including in the model the photolysis of particulate nitrate on sea salt aerosols at rates inferred from laboratory studies and field observations of nitrous acid (HONO) over the Atlantic. The median PSS-inferred tropospheric NO<sub>2</sub> column density for the ATom campaign is  $1.7 \pm 0.44 \times 10^{14}$  molec cm<sup>-2</sup> and the NO<sub>2</sub> column density simulated by the four models is in the range of  $1.4\text{--}2.4 \times 10^{14}$  molec cm<sup>-2</sup>, implying that the uncertainty from using modeled NO<sub>2</sub> tropospheric columns over clean areas in the retrievals for stratosphere-troposphere separation is about  $1 \times 10^{14}$  molec cm<sup>-2</sup>. We find from GEOS-Chem that lightning is the main primary NO<sub>x</sub> source in the free troposphere over the tropics and southern midlatitudes, but aircraft emissions dominate at northern midlatitudes in winter and in summer over the oceans. Particulate nitrate photolysis increases ozone concentrations by up to 5 ppbv in the free troposphere in the northern extratropics in the model, which would largely correct the low model bias relative to ozonesonde observations. Global tropospheric OH concentrations increase by 19%. The contribution of the free tropospheric background to the tropospheric NO<sub>2</sub> columns observed by satellites over the contiguous US increases from  $25 \pm 11$  % in winter to  $65 \pm 9$  % in summer according to the GEOS-Chem vertical profiles. This needs to be accounted for when deriving NO<sub>x</sub> emissions from satellite NO<sub>2</sub> column measurements.

## 1 Introduction

Retrievals of NO<sub>2</sub> tropospheric columns from satellite measurements of solar backscatter are used extensively to infer anthropogenic NO<sub>x</sub> ( $\equiv$ NO+NO<sub>2</sub>) emissions near the surface and their trends (e.g., Martin et al., 2003; Richter et al., 2005; Beirle et al., 2011; Krotkov et al., 2016). This is complicated by the presence of background NO<sub>2</sub> in the free troposphere, the part of the atmosphere between the top of the boundary layer (~2 km altitude) and the tropopause. NO<sub>x</sub> sources in the free troposphere include lightning, aircraft, transport from the boundary layer and the stratosphere, and chemical recycling from HNO<sub>3</sub> and organic nitrates (Singh et al., 1996; Jaeglé et al., 1998a; Levy et al., 1999; Hudman et al., 2007). As fossil fuel NO<sub>x</sub> emissions have decreased in the US and other post-industrial countries, the relative contribution of the free tropospheric background to the tropospheric NO<sub>2</sub> columns has increased (Silvern et al., 2019). Satellite instruments are more sensitive to NO<sub>2</sub> in the free troposphere than in the boundary layer because of atmospheric scattering, so the NO<sub>2</sub> column retrievals must

assume a vertical distribution of NO<sub>2</sub> (shape factor) specified by an atmospheric chemistry model for the local conditions (Martin et al., 2002; Eskes and Boersma, 2003). However, these models may be subject to large errors in the free troposphere (Travis et al., 2016; Silvern et al., 2018). Here we use the vertical distribution of tropospheric NO<sub>x</sub> from aircraft measurements over land and ocean, simulated with GEOS-Chem and other atmospheric chemistry models, to diagnose the confidence to be had in these models and in the aircraft observations. We discuss the implications for global tropospheric oxidants and the retrieval and interpretation of satellite NO<sub>2</sub> measurements in terms of surface NO<sub>x</sub> emissions.

80

Accurate *in situ* measurements of NO<sub>2</sub> in the free troposphere are challenging because of low NO<sub>2</sub> concentrations and interferences from labile non-radical NO<sub>x</sub> reservoirs (HNO<sub>4</sub>, N<sub>2</sub>O<sub>5</sub>, and organic nitrates) when sampling at cold temperatures (Bradshaw et al., 1999; Browne et al., 2011; Reed et al., 2016; Nussbaumer et al., 2021). Current techniques to measure NO<sub>2</sub> *in situ* involve either (i) the conversion of NO<sub>2</sub> to NO by photolysis followed by measurement of NO through chemiluminescence (photolysis-chemiluminescence; P-CL) (Walega et al., 1991; Ryerson et al., 2000; Bourgeois et al., 2022), or (ii) the direct measurement of NO<sub>2</sub> through laser induced fluorescence (LIF) (e.g. Thornton et al., 2000; Matsumoto et al., 2001; Javed et al., 2019), cavity ring-down spectroscopy (Osthoff et al., 2006), or cavity enhanced differential optical absorption spectroscopy (Platt et al., 2009). Intercomparisons of NO<sub>2</sub> instruments have generally found agreement among the different techniques at high (>1 ppbv) NO<sub>2</sub> concentrations (Thornton et al., 2003; Fuchs et al., 2010; Sparks et al., 2019; Bourgeois et al., 2022), but poor agreement in free tropospheric conditions where NO<sub>2</sub> concentrations are below 50 pptv and close to the instrument detection limits (Gregory et al., 1990a; Sparks et al., 2019). In contrast, NO measurements in the free troposphere are generally found to be reliable down to about 10 pptv (Gregory et al., 1990a; Rollins et al., 2020). The NO<sub>2</sub> photolysis technique has been used for NO<sub>2</sub> measurements from aircraft since the 1980s (Ridley et al., 1988; Sandholm et al., 1990). However, the free tropospheric NO<sub>2</sub> concentrations from these measurements were often found to be higher than expected from NO-NO<sub>2</sub> photochemical steady state (PSS) (Davis et al., 1993; Fan et al., 1994; Crawford et al., 1996). This was later attributed to an artifact in the NO<sub>2</sub> measurements from the decomposition of peroxyacetyl nitrate (PAN), HNO<sub>4</sub> and methyl peroxy nitrate (MPN) in the sample line and the photolysis cell (Bradshaw et al., 1999; Browne et al., 2011; Reed et al., 2016). These species are present at relatively high concentrations at cold temperatures of the upper troposphere (Murphy et al., 2004; Kim et al., 2007; Singh et al., 1986) and can cause significant interference in the NO<sub>2</sub> measurements when the instrument temperature is higher than the ambient temperature (Nault et al., 2015; Reed et al., 2016).

The LIF technique was developed to eliminate interferences associated with the photolytic conversion of NO<sub>2</sub> (Thornton et al., 2000) and has been widely used in aircraft campaigns to measure free tropospheric profiles of NO<sub>2</sub> over North America and remote regions (Murphy et al., 2004; Bertram et al., 2007; Browne et al., 2011; Nault et al., 2015) and to evaluate satellite NO<sub>2</sub> retrievals (Bucsela et al., 2008; Boersma et al., 2008; Laughner et al., 2019). However, Silvern et al. (2018) found that the LIF NO<sub>2</sub> measurements in the upper troposphere over the southeastern US during the Studies of Emissions and Atmospheric Composition, Clouds and Climate Coupling by Regional Surveys (SEAC<sup>4</sup>RS) aircraft campaign were much higher than the

NO<sub>2</sub> concentrations expected from the NO-NO<sub>2</sub> PSS, indicating either an error in the NO-NO<sub>2</sub>-O<sub>3</sub> kinetics at low temperatures or a remaining bias in the measurement.

110

Free tropospheric NO<sub>2</sub> concentrations have also been derived using remote sensing techniques. The Airborne Multi-AXis Differential Optical Absorption Spectroscopy (AMAX-DOAS) instrument has been used to measure vertical profiles of NO<sub>2</sub> in the free troposphere (Baidar et al., 2013; Volkamer et al., 2015). Ground-based MAX-DOAS instruments can measure NO<sub>2</sub> vertical profiles in the boundary layer but have low sensitivity to the free troposphere (Vlemmix et al., 2011). NO<sub>2</sub> concentrations in the upper troposphere (8–12 km) have been retrieved from satellite NO<sub>2</sub> column measurements using cloud-slicing techniques based on measuring differences in partial NO<sub>2</sub> columns above clouds of different heights (Belmonte Rivas et al., 2015; Choi et al., 2014; Marais et al., 2021). These provide extensive spatial coverage but there are inconsistencies among different products and large differences compared to aircraft LIF measurements (Marais et al., 2018, 2021).

115

Atmospheric chemistry models are often used alongside satellite NO<sub>2</sub> measurements to determine surface NO<sub>x</sub> emissions and their trends, as they provide a way to relate changes in NO<sub>2</sub> columns to surface NO<sub>x</sub> emissions (Martin et al., 2003; Lamsal et al., 2011). But the sensitivity of modeled NO<sub>2</sub> columns to surface emissions depends on the relative contribution of the free troposphere to NO<sub>2</sub> columns. Modeled NO<sub>2</sub> vertical profiles over the continents generally agree with aircraft observations below about 6 km (Lamsal et al., 2014; Choi et al., 2020), but underestimate NO<sub>2</sub> measurements in the upper troposphere (Martin et al., 2006; Travis et al., 2016; Williams et al., 2017; Miyazaki et al., 2020). This could reflect model errors in the parametrized lightning NO<sub>x</sub> emissions (Martin et al., 2006; Allen et al., 2010; Hudman et al., 2007; Zhu et al., 2019), convective transport of surface pollutants (Travis et al., 2016), or NO<sub>x</sub> chemistry (Nault et al., 2016; Silvern et al., 2018), but also measurement errors.

125

A number of global modeling studies have evaluated NO simulations over remote regions because of its importance for the production of tropospheric ozone and the hydroxyl radical (OH), and have generally found agreement within a factor of two (e.g., Emmons et al., 1997; Wang et al., 1998; Levy et al., 1999; Bey et al., 2001; Horowitz et al., 2003). However, a recent comparison of six global models with aircraft observations over the Pacific and Atlantic oceans made during the NASA Atmospheric Tomography (ATom) campaign's first deployment (July–August 2016) found significant underestimate of NO in all models below 4 km in the tropics and subtropics (Guo et al., 2021a). Other studies also suggest a missing source of NO<sub>x</sub> in models over the subtropical oceans from fast photolysis of particulate nitrate (Ye et al., 2016b; Reed et al., 2017; Kasibhatla et al., 2018; Andersen et al., 2022) or from oceanic emissions (Fisher et al., 2018).

135

Here we use data from the SEAC<sup>4</sup>RS and the Deep Convective Clouds and Chemistry (DC3) aircraft campaigns to demonstrate the pervasiveness of interference from non-radical NO<sub>x</sub> reservoirs in NO<sub>2</sub> measurements in the upper troposphere. We go on to use the more reliable NO measurements and the NO<sub>2</sub> concentrations derived by applying PSS to the NO measurements to

140

evaluate the NO and NO<sub>2</sub> vertical profiles from different models for the SEAC<sup>4</sup>RS, DC3, and ATom campaigns. We use the model results to examine the sources of NO<sub>x</sub> in the free troposphere, effects on tropospheric ozone and OH, and contribution of the free tropospheric background to satellite NO<sub>2</sub> columns over the US.

145 **2 Methods**

**2.1 Aircraft observations**

We use observations from the SEAC<sup>4</sup>RS (August–September 2013; Toon et al., 2016) and DC3 (April–May 2012; Barth et al., 2015) campaigns over the southeastern US (25°–40°N; 65°–100°W), and the ATom campaign (4 seasonal deployments in 2016–18) over the Pacific and Atlantic oceans (Thompson et al., 2022). For all three campaigns, we use measurements from  
150 the NASA DC-8 aircraft, which has a ~12 km ceiling. Table 1 lists the measurements used in this work. Here, we briefly describe the NO<sub>2</sub> and NO measurements as they are most relevant. NO<sub>2</sub> measurements during the SEAC<sup>4</sup>RS and DC3 campaigns were made using the Berkeley LIF instrument (Thornton et al., 2000; Cleary et al., 2002; Nault et al., 2015). The LIF measurements have little (<5%) interference from HNO<sub>4</sub>, but there is interference from the thermal decomposition of MPN, for which a correction was applied (0–21% for SEAC<sup>4</sup>RS and 0–40% for DC3). The correction was calculated using  
155 concurrent measurements of MPN concentrations (from the same instrument using thermal decomposition in a heated channel) and the fractional thermal decomposition of MPN in the NO<sub>2</sub> channel considering the temperature of the channel (15–25°C) and the instrument residence time (0.23 s for SEAC<sup>4</sup>RS and 0.5 s in DC3), as described by Nault et al. (2015). The LIF measurements have an accuracy of 5% and a detection limit of ~30 pptv for 1 Hz measurements (Thornton et al., 2000; Day et al., 2002; Wooldridge et al., 2010). NO<sub>2</sub> measurements in ATom were made with the NOAA NOyO3 instrument using the  
160 P-CL technique (Ryerson et al., 2000; Bourgeois et al., 2022). The NOAA instrument also provided NO<sub>2</sub> measurements in SEAC<sup>4</sup>RS and DC3. The instrument has an accuracy of ~7% and a detection limit of 20–30 pptv for 1 Hz measurements (Pollack et al., 2010, 2012). Interference from the thermal dissociation of HNO<sub>4</sub> and MPN is reduced, but not eliminated, by maintaining a low sample residence time (0.75 s) and preventing heating of the photolysis cell by using low-power LEDs (Pollack et al., 2010; Bourgeois et al., 2022). The P-CL NO<sub>2</sub> measurements have some photolytic interference from HONO  
165 (5% of the HONO mixing ratio), but this is negligible in much of the troposphere where HONO concentration is generally less than 10 pptv (Ye et al., 2016b; Andersen et al., 2022). NO measurements in all three campaigns were made by the NOAA NOyO3 instrument, with an accuracy of 4% and a detection limit of 6–10 pptv for 1 Hz measurements (Ryerson et al., 2000). For comparison with the model, we exclude measurements influenced by fresh convection (condensation nuclei larger than 10nm > 10<sup>4</sup> cm<sup>-3</sup>), fresh NO<sub>x</sub> emissions (NO<sub>y</sub>/NO < 3 mol mol<sup>-1</sup>), biomass burning plumes (CO > 200 ppbv and CH<sub>3</sub>CN > 200  
170 pptv), and stratospheric intrusions (O<sub>3</sub> > 100 ppbv or CO < 45 ppbv).

**Table 1: Measurements from the SEAC<sup>4</sup>RS, DC3, and ATom aircraft campaigns<sup>a</sup>**

Measurement	Instrument <sup>b</sup>	Campaigns	Uncertainty <sup>c</sup>	References
NO <sub>2</sub> , MPN, alkyl nitrates	Berkeley TD-LIF	SEAC <sup>4</sup> RS, DC3	NO <sub>2</sub> : 5%, MPN: 40%, alkyl nitrates: 15%	Nault et al. (2015)
NO, NO <sub>2</sub> , NO <sub>y</sub> <sup>d</sup> , O <sub>3</sub>	NOAA NO <sub>y</sub> O <sub>3</sub>	SEAC <sup>4</sup> RS, DC3, ATom	NO: 4%, NO <sub>2</sub> : 7%, NO <sub>y</sub> : 12%, O <sub>3</sub> : 2%	Ryerson et al. (1998, 2000); Pollack et al. (2010); Bourgeois et al. (2020, 2022)
OH, HO <sub>2</sub>	Penn State ATHOS	DC3, ATom	35%	Faloona et al. (2004); Brune et al. (2021)
HNO <sub>4</sub>	Georgia Tech CIMS	SEAC <sup>4</sup> RS, DC3	30%	Kim et al. (2007)
Photolysis frequencies	NCAR CAFS	SEAC <sup>4</sup> RS, DC3, ATom	$j_{\text{NO}_2}$ : 12%, $j_{\text{O}_3}$ : 15%	Shetter and Müller (1999); Hall and Ullmann (2021)
Particulate nitrate	CU Boulder HR-AMS <sup>e</sup>	ATom	34%	Hodzic et al. (2020); Nault et al. (2021)
	UNH SAGA <sup>e</sup>	ATom	15%	Dibb (2020); Heim et al. (2020)
HNO <sub>3</sub>	Caltech CIMS	ATom	30%	Allen et al. (2019)
PAN	NOAA PANTHER	ATom	10%	Moore et al. (2022)
Condensation nuclei	NASA Langley CPC (TSI 3772)	SEAC <sup>4</sup> RS, DC3	<sup>f</sup>	<sup>f</sup>
CO	NASA Langley DACOM	SEAC <sup>4</sup> RS, DC3	2%	Sachse et al. (1991)
	NOAA Picarro (G2401)	ATom	9 ppbv	Chen et al. (2013); McKain and Sweeney (2021)
CH <sub>3</sub> CN	Innsbruck PTR-MS	SEAC <sup>4</sup> RS, DC3	30%	Wisthaler et al. (2002)

<sup>a</sup> Measurements used in this work to evaluate the NO<sub>x</sub> simulations and to select data for analysis

175 <sup>b</sup> Instrument acronyms: TD-LIF: Thermal Dissociation, Laser Induced Fluorescence; ATHOS: Airborne Tropospheric Hydrogen Oxides Sensor; CIMS: Chemical Ionization Mass Spectrometer; CAFS: CCD Actinic Flux Spectroradiometer; HR-AMS: High Resolution Aerosol Mass Spectrometer; SAGA: Soluble Acidic Gases and Aerosols; PANTHER: PAN and Trace Hydrohalocarbon Experiment; CPC: Condensation Particle Counter; DACOM: Differential Absorption Carbon monoxide Monitor; PTR-MS: Proton Transfer Reaction - Mass Spectrometry

180 <sup>c</sup> Estimated accuracy at analyte concentrations well above the detection limit

<sup>d</sup> Total reactive nitrogen oxides including NO<sub>x</sub> and its oxidation products

<sup>e</sup> The AMS measures the composition of non-refractory submicron aerosols. SAGA measures the ionic composition of water-soluble bulk aerosols of diameter less than about 4 μm.

<sup>f</sup> Commercial instrument operated by the NASA Langley Aerosol Research Group Experiment

## 185 2.2 GEOS-Chem model

We use the GEOS-Chem atmospheric chemistry model (12.9.3; doi: 10.5281/zenodo.3959279), with modification to include inorganic particulate nitrate (pNO<sub>3</sub><sup>-</sup>) photolysis as described below. Our simulations are driven by assimilated meteorology from NASA GMAO's Modern-Era Retrospective analysis for Research and Applications, Version 2 (MERRA-2; Gelaro et al., 2017). We conduct global simulations at 4°×5° horizontal resolution (47 levels in the vertical) for the time periods

190 corresponding to the aircraft campaigns: SEAC<sup>4</sup>RS (July–August 2013), DC3 (May–June 2012), ATom (July–August 2016,

January–February 2017, September–October 2017, and April–May 2018), as well as an annual simulation for 2015. Previous work on the SEAC<sup>4</sup>RS campaign used finer resolution simulations (Travis et al., 2016), but these are not needed here as the free tropospheric NO<sub>2</sub> concentrations do not vary much at regional scales and finer resolution tests showed similarity in results (Yu et al., 2016). The horizontal grid resolution can lead to localized differences in the upper troposphere from stratospheric intrusions, convective transport, and lightning NO<sub>x</sub> emissions (Schwantes et al., 2022), and we minimize these effects by filtering out data influenced by the stratosphere, fresh convection, and fresh NO<sub>x</sub> emissions, as described above. The spin-up period for our simulations is six months. Comparison to aircraft measurements is done by sampling the model along the flight path as an online diagnostic during the model simulation.

**Table 2: Global NO<sub>x</sub> emissions in 2015<sup>a</sup>**

Source <sup>b</sup>	Emission rate (TgN a <sup>-1</sup> )
Fuel combustion	35.2
Fires	6.6
Soils & fertilizer use	8.1
Aircraft	1.2
Lightning	5.8
Total <sup>c</sup>	56.9

<sup>a</sup> as used in our GEOS-Chem simulation  
<sup>b</sup> references for the different sources are given in the text  
<sup>c</sup> not including the NO<sub>x</sub> source of ~0.5 TgN a<sup>-1</sup> from downwelling of stratospheric NO<sub>y</sub> produced from N<sub>2</sub>O

Table 2 lists the global NO<sub>x</sub> emissions in our 2015 simulation. Anthropogenic NO<sub>x</sub> emissions are from the Community Emissions Data System (CEDS) global inventory (Hoesly et al., 2018), superseded with regional emission inventories for the US (US EPA 2011 NEI, 2016), Canada (Air Pollutant Emissions Inventory, 2017), Africa (Marais and Wiedinmyer, 2016), and China (Zheng et al., 2018). The US EPA 2011 NEI is scaled annually using EPA-estimated emissions trends (US EPA Air Pollutant Emissions Trends Data, 2015). Travis et al. (2016) had to scale down the NEI NO<sub>x</sub> emissions in GEOS-Chem by 40% to reproduce the SEAC<sup>4</sup>RS NO<sub>x</sub> observations, but we do not do this in our simulations as it leads to an underestimate of NO<sub>x</sub> in other seasons (Jaeglé et al., 2018; Silvern et al., 2019). Open fire NO<sub>x</sub> emissions are from the GFEDv4 inventory (Giglio et al., 2013). Ship NO<sub>x</sub> emissions are from CEDS and are processed using the PARAMetrization of emitted NOX (PARANOX) model to account for fast in-plume NO<sub>x</sub> oxidation (Vinken et al., 2011; Holmes et al., 2014). Aircraft NO<sub>x</sub> emissions are from the Aviation Emissions Inventory Code (AEIC) inventory (Stettler et al., 2011; Simone et al., 2013), and are updated here with flight traffic data for 2015. Lightning NO<sub>x</sub> emissions follow Murray et al. (2012), with lightning flash rates calculated as a function of the cloud top height and scaled to match the observed climatology from satellite data. Emissions are computed at the native MERRA-2 resolution (0.5°×0.625°). NO yields of 500 moles per flash are used for the northern midlatitudes (>35°N) and 260 moles per flash elsewhere. Emissions are distributed in the vertical following Ott et al.

(2010). Soil and fertilizer  $\text{NO}_x$  emissions are from Hudman et al. (2012) and are computed at  $0.5^\circ \times 0.625^\circ$  resolution (Weng et al., 2020).

GEOS-Chem includes a detailed representation of  $\text{NO}_x$ - $\text{HO}_x$ -VOC-aerosol-halogen chemistry (Mao et al., 2013; Travis et al., 2016; Holmes et al., 2019; Wang et al., 2021; McDuffie et al., 2021; Pai et al., 2020). Recent improvements to the model's  $\text{NO}_x$  chemistry include addition of detailed tropospheric halogen chemistry (Wang et al., 2021), addition of methyl, ethyl, and propyl nitrate emissions and chemistry (Fisher et al., 2018), and updates to the heterogeneous  $\text{NO}_x$  reactions in aerosols and cloud droplets (Holmes et al., 2019; McDuffie et al., 2021). Here we follow Schmidt et al. (2016) and exclude bromine release from sea salt aerosol debromination because it leads to excessive model BrO in the marine boundary layer (MBL). Equilibrium partitioning of  $\text{HNO}_3$  to  $\text{pNO}_3^-$  on fine mode aerosols is calculated using ISORROPIA II (Fountoukis and Nenes, 2007; Wang et al., 2019). The fine mode aerosols are treated as internal mixtures of sulfate, nitrate, ammonium, and sea salt components, representing well-aged particles that have undergone coagulation and cloud processing (Fridlind and Jacobson, 2000). The model also includes the formation and uptake of sulfate and nitrate in alkaline sea salt aerosols (Wang et al., 2019). Uptake of  $\text{HNO}_3$  as  $\text{pNO}_3^-$  on coarse sea salt aerosols is treated as a kinetic process, following Wang et al. (2019). Sea salt aerosol emissions follow Jaeglé et al. (2011) and are calculated at  $0.5^\circ \times 0.625^\circ$  resolution (Weng et al., 2020). Our simulation does not include  $\text{HNO}_3$  uptake on alkaline dust particles, which could be important in dust plumes over the ocean (Fairlie et al., 2010; Karydis et al., 2016). Photolysis frequencies in the model are calculated using Fast-JX (Wild and Prather, 2000; Eastham et al., 2014).

Previous studies examining the GEOS-Chem NO simulation for the ATom campaign showed underestimates in the lower troposphere (Fisher et al., 2018; Travis et al., 2020; Guo et al., 2021a). Measurements in the marine atmosphere indicate elevated levels of HONO that originate likely from  $\text{pNO}_3^-$  photolysis (Ye et al., 2016b; Andersen et al., 2022) and would provide a fast source of  $\text{NO}_x$  missing from the model. We address this by including  $\text{pNO}_3^-$  photolysis in our simulation, following the implementation of this reaction in GEOS-Chem by Kasibhatla et al. (2018). The photolysis frequency of  $\text{pNO}_3^-$  is calculated by scaling the photolysis frequency of  $\text{HNO}_3$  by an enhancement factor (EF). There is high uncertainty in the EF, with laboratory studies in the range of 1–1000 (Ye et al., 2016a; Bao et al., 2018; Gen et al., 2019; Shi et al., 2021). Field and modeling studies find that EFs of 10–500 are needed to explain the  $\text{NO}_x$  and HONO observations over the oceans (Ye et al., 2016b, 2017a; Reed et al., 2017; Kasibhatla et al., 2018; Zhu et al., 2022; Andersen et al., 2022), with higher values for  $\text{pNO}_3^-$  in sea salt aerosols (Andersen et al., 2022). In consistency with these studies, we find that we can match the ATom NO observations by using an EF of 100 for  $\text{pNO}_3^-$  in sea salt aerosol. In our model, coarse mode  $\text{pNO}_3^-$  is only present in sea salt aerosols and has an EF of 100, but fine mode  $\text{pNO}_3^-$  is internally mixed with sulfate, ammonium, and sea salt aerosol and so we decrease the EF of fine mode  $\text{pNO}_3^-$  depending on the relative amounts of  $\text{pNO}_3^-$  and sea salt aerosol:



$$EF = \max\left(100 \times \frac{1}{1 + \frac{[pNO_3^-]}{[SSA]}}, 10\right) \quad (1)$$

255 Here  $[pNO_3^-]$  and  $[SSA]$  are the molar concentrations in air of fine mode  $pNO_3^-$  and sea salt aerosol. The molar concentration of sea salt is taken as  $[SSA] = 2.39[Na^+]$  based on the fraction of  $Na^+$  in seawater (Millero et al., 2008), and where  $Na^+$  is the chemically inert sea salt aerosol species simulated by GEOS-Chem. We choose a lower limit of 10 for the EF based on the results of Romer et al. (2018), who estimated EF values for non-sea-salt  $pNO_3^-$  aerosols in the range 1–30 from observations over South Korea. The relative yields of  $HONO:NO_2$  from  $pNO_3^-$  photolysis are taken as 2:1 (Ye et al., 2017b; Kasibhatla et al., 2018). We will discuss the effect of  $pNO_3^-$  photolysis on remote  $NO_x$  concentrations in more detail in Section 3.2.

## 2.3 Other models

In addition to GEOS-Chem simulations, we analyze results from three other global atmospheric chemistry models: the Global Modeling Initiative (GMI) model, the Tracer Model version 5's "massively parallel" version (TM5-MP), and the Copernicus  
 265 Atmosphere Monitoring Service (CAMS) reanalysis product. The GMI model simulates tropospheric and stratospheric chemistry (Duncan et al., 2007; Strahan et al., 2007; Strode et al., 2015) using meteorological fields from NASA GMAO's MERRA-2 reanalysis. GMI  $NO_2$  vertical profiles are used to specify shape factors in the OMI  $NO_2$  retrievals (Krotkov et al., 2017; Lamsal et al., 2021). The version used here has a horizontal resolution of  $1^\circ \times 1.25^\circ$ . Strode et al. (2021) describe the GMI model simulations for the ATom campaign. The TM5-MP model is a high resolution ( $1^\circ \times 1^\circ$ ) version of the TM5 global  
 270 atmospheric chemistry model developed specifically for application to satellite retrievals (Williams et al., 2017; Huijnen et al., 2010). It is driven by assimilated meteorology from the European Centre for Medium-Range Weather Forecasts (ECMWF) ERA-Interim reanalysis. The TM5  $NO_2$  profiles are used in the Quality Assurance for Essential Climate Variables (QA4ECV) OMI and TROPOMI  $NO_2$  retrievals (Boersma et al., 2018; van Geffen et al., 2022). CAMS provides a global reanalysis of atmospheric composition at a horizontal resolution of 80 km (T255) for the period 2003 onwards (Inness et al., 2019). It is  
 275 based on ECMWF's Integrated Forecast System (IFS) and uses 4D-Var data assimilation of satellite retrievals of  $NO_2$ ,  $O_3$ , CO, and aerosol optical depth. The CAMS  $NO_2$  profiles are planned for use in  $NO_2$  retrievals from the European Sentinel-4 geostationary satellite (ESA Sentinel-4 Data Products, 2022). The TM5 and CAMS output along the ATom flight tracks was available only for the first ATom deployment (July–Aug 2016).

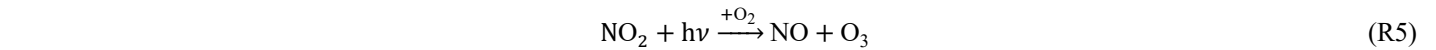
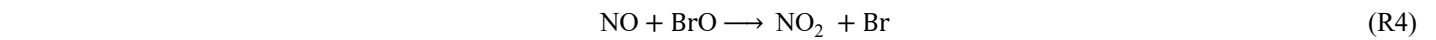
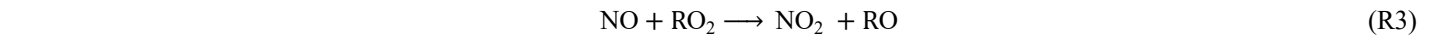
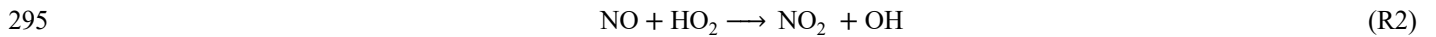
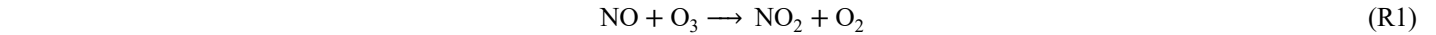
## 3 Results and discussion

### 280 3.1 Vertical distribution of $NO_x$ over the US

Figure 1 compares the median vertical profiles of the observed and GEOS-Chem NO and  $NO_2$  concentrations for the SEAC<sup>4</sup>RS and DC3 aircraft campaigns. For both campaigns, the observed and GEOS-Chem NO concentrations peak in the boundary layer, and again in the upper troposphere because of lightning and aircraft emissions, convective lifting of surface emissions,

long NO<sub>x</sub> lifetime (except near fresh convection), and shift of the daytime NO/NO<sub>2</sub> ratio toward NO at low temperatures (Jaeglé et al., 1998a; Bertram et al., 2007; Hudman et al., 2007; Nault et al., 2017). The GEOS-Chem NO<sub>2</sub> profiles are similar to the LIF NO<sub>2</sub> profiles below 10 km but differ in the upper troposphere, as previously noted by Travis et al. (2016). LIF NO<sub>2</sub> concentrations in SEAC<sup>4</sup>RS increase from 20 pptv at 9 km to 120 pptv at 12 km, but GEOS-Chem NO<sub>2</sub> concentrations remain below 30 pptv. The difference between GEOS-Chem and the P-CL NO<sub>2</sub> observations in the upper troposphere during DC3 is even larger.

Travis et al. (2016) and Silvern et al. (2018) showed that the difference between the measured and GEOS-Chem NO<sub>2</sub> in the upper troposphere in SEAC<sup>4</sup>RS can be explained by the departure of the measured NO/NO<sub>2</sub> ratio from that expected from calculated PSS between NO and NO<sub>2</sub>. In daytime, NO and NO<sub>2</sub> interconvert rapidly through the following main reactions:



Here RO<sub>2</sub> represents the ensemble of organic peroxy radicals. At PSS, the NO/NO<sub>2</sub> ratio is given by:

$$\text{PSS} = \frac{[\text{NO}]}{[\text{NO}_2]} = \frac{j_{\text{NO}_2}}{k_1[\text{O}_3] + k_2[\text{HO}_2] + k_3[\text{RO}_2] + k_4[\text{BrO}]} \quad (2)$$

where  $j_{\text{NO}_2}$  is the NO<sub>2</sub> photolysis frequency and  $k_i$  is the rate constant of reaction  $i$ . We calculate the PSS NO/NO<sub>2</sub> ratio for the SEAC<sup>4</sup>RS and DC3 data using concurrent aircraft measurements and GEOS-Chem simulated values along the flight path for quantities that were not measured. [O<sub>3</sub>] and  $j_{\text{NO}_2}$  were measured in both campaigns. [HO<sub>2</sub>] was measured only in DC3, but H<sub>2</sub>O<sub>2</sub> concentrations measured in SEAC<sup>4</sup>RS are consistent with GEOS-Chem (Silvern et al., 2018), which provides support for the model [HO<sub>2</sub>]. Rate constants are as recommended by the JPL evaluation (Burkholder et al., 2020) and adjusted for temperature and pressure. We take the NO + CH<sub>3</sub>O<sub>2</sub> reaction rate constant as  $k_3$ . [RO<sub>2</sub>] and [BrO] are taken from GEOS-Chem but make only small contributions. In the free troposphere, NO-NO<sub>2</sub> PSS is largely governed by the NO + O<sub>3</sub> reaction (Bradshaw et al., 1999; Silvern et al., 2018). Thus, the PSS NO/NO<sub>2</sub> ratio depends mainly on observed quantities and on relatively well-established kinetics (Silvern et al., 2018). We estimate the uncertainty in the PSS NO/NO<sub>2</sub> ratio at 1 Hz of about ±20%, based on uncertainties in the [O<sub>3</sub>], [HO<sub>2</sub>], and  $j_{\text{NO}_2}$  measurements (Table 1), rate constants (10%; Burkholder et al., 2020), and model [RO<sub>2</sub>] and [BrO] (assumed to be 50%).

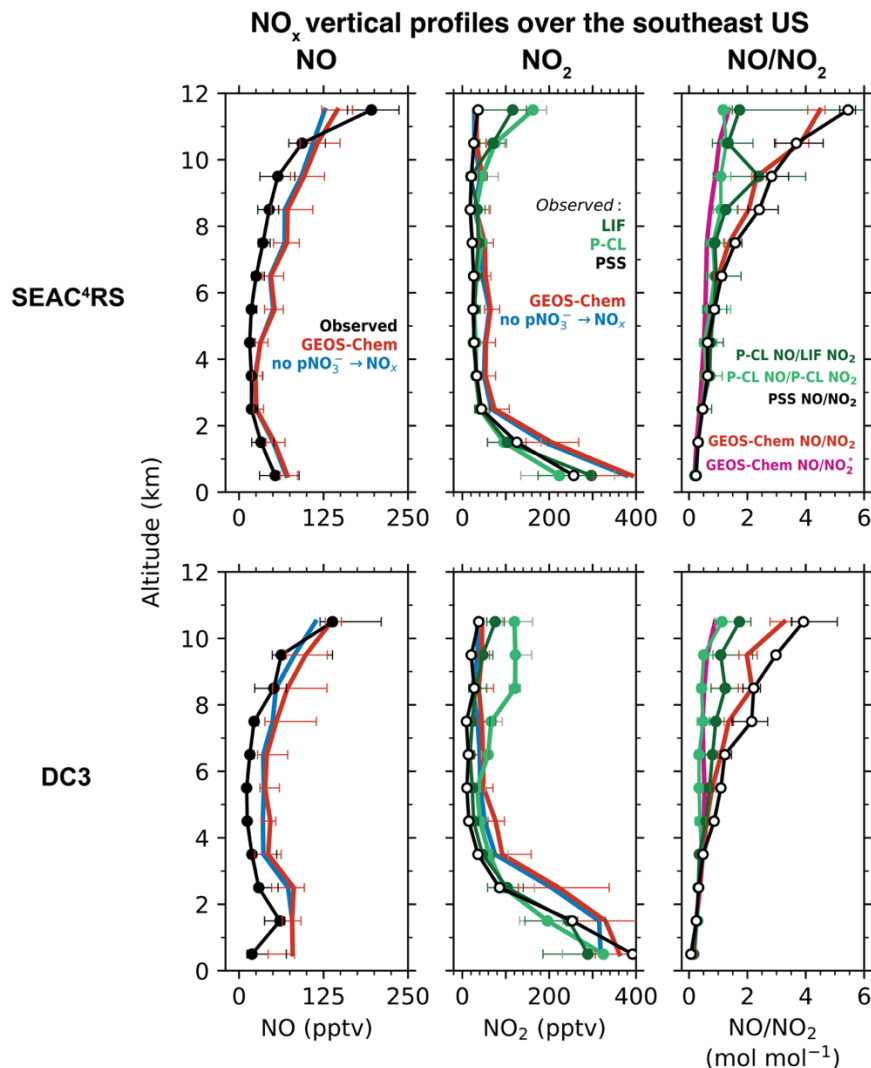


Figure 1. Median vertical profiles of observed and GEOS-Chem simulated NO and NO<sub>2</sub> concentrations, and NO/NO<sub>2</sub> molar ratios, during the SEAC<sup>4</sup>RS (Aug–Sep 2013) and DC3 (Apr–May 2012) aircraft campaigns over the southeastern US. The NO measurements are from the NOAA P-CL instrument. NO<sub>2</sub> was measured by the Berkeley LIF and the NOAA P-CL instruments. The NO/NO<sub>2</sub> ratios at photochemical steady state (PSS; Eq. 2) and the corresponding NO<sub>2</sub> concentrations (Eq. 3) are also shown. The PSS calculation is based mostly on observed quantities but uses modeled values for quantities that were not measured, as described in the text. Also shown are the NO/NO<sub>2</sub>\* (NO<sub>2</sub>\*≡NO<sub>2</sub>+HNO<sub>4</sub>+MPN) ratios from GEOS-Chem. MPN is methyl peroxy nitrate. We exclude measurements in early mornings and late evenings (solar zenith angle >70°) and influenced by fresh NO<sub>x</sub> emissions recent convection, biomass burning, and the stratosphere as described in Sect. 2.1. The horizontal bars show the interquartile ranges of the measurements in each 1-km altitude bin.

Figure 1 compares the vertical profiles of the measured and the PSS NO/NO<sub>2</sub> ratios. The PSS NO/NO<sub>2</sub> ratio increases with altitude because of the slower rate of the NO + O<sub>3</sub> reaction at colder temperatures (Burkholder et al., 2020). There is relatively little change in  $j_{\text{NO}_2}$  with altitude (Silvern et al., 2018). The measured and PSS ratios match below 5 km, but at higher altitudes

the measured ratios are smaller than the PSS ratios. Between 10 and 12 km, the NO/NO<sub>2</sub> ratios using the LIF measurements are in the range of 1 to 2, while the PSS NO/NO<sub>2</sub> ratios are in the range of 3 to 6. The NO/NO<sub>2</sub> ratios using the P-CL measurements at this altitude are close to 1. The GEOS-Chem NO/NO<sub>2</sub> ratios are similar to the PSS ratios throughout the troposphere.

The P-CL NO<sub>2</sub> instrument is known to have interference from dissociation of HNO<sub>4</sub> and MPN (Reed et al., 2016; Nussbaumer et al., 2021; Bourgeois et al., 2022), but the magnitude of the interference has not been quantified. We find that the ratio of NO/NO<sub>2</sub>\* (NO<sub>2</sub>\*≡NO<sub>2</sub>+HNO<sub>4</sub>+MPN) in GEOS-Chem closely matches the NO/NO<sub>2</sub> ratio for the P-CL NO<sub>2</sub> measurements, suggesting that HNO<sub>4</sub> and MPN dissociate completely in the instrument to NO<sub>2</sub>. The LIF NO<sub>2</sub> measurements correct for the thermal dissociation of MPN (there is little thermal dissociation of HNO<sub>4</sub>), but the correction is affected by the high uncertainty in the concentrations and the thermal stability of MPN (Nault et al., 2015). The LIF instrument was modified between DC3 and SEAC<sup>4</sup>RS to shorten the sample residence time and reduce the fraction of MPN dissociating in the instrument (Nault et al., 2015), but we do not find that this improved agreement between the measured and PSS NO/NO<sub>2</sub> (Fig. 1). It is also possible that HNO<sub>4</sub> and MPN (and potentially other labile NO<sub>2</sub> reservoir species) dissociate on the inlet walls, which the correction would not account for. Bradshaw et al. (1999) could achieve agreement of their NO<sub>2</sub> measurements with the PSS concentrations at all altitudes by using an unusually large inlet (10 cm diameter) and a very high flow rate in the instrument to minimize wall collisions.

Silvern et al. (2018) pointed out that the difference between the measured and PSS NO/NO<sub>2</sub> ratios could arise from either an error in the NO-NO<sub>2</sub>-O<sub>3</sub> kinetics or a systematic bias in the NO<sub>2</sub> measurements in the upper troposphere. Here we arbitrate between these two hypotheses by using quasi-Lagrangian observations in the outflow from a dissipating thunderstorm in the upper troposphere deliberately sampled during DC3 (flight RF17). Nault et al. (2016) previously analyzed the evolution of NO<sub>x</sub> and NO<sub>y</sub> (NO<sub>y</sub> ≡ NO<sub>x</sub> + non-radical reservoirs) on this flight to determine NO<sub>x</sub> oxidation rates, and showed a steady decrease with time in the NO and NO<sub>2</sub> concentrations and an increase in the NO<sub>y</sub> oxidation products during the two-hour sampling period. Figure 2a shows the flight path with daytime plume crossings colored by the measured NO<sub>y</sub>/NO molar ratio. The NO<sub>y</sub>/NO ratio increases on each successive plume crossing as NO<sub>x</sub> undergoes oxidation in the outflow, and we use the ratio as a measure of chemical aging in the plume (Kleinman et al., 2008; Hayes et al., 2013). Figure 2b shows the measured NO, NO<sub>2</sub>, and the sum of HNO<sub>4</sub> and MPN concentrations as a function of the NO<sub>y</sub>/NO ratio. NO concentrations decreased from 900 pptv to 400 pptv between the start and the end of the measurement period. But there was relatively little change in the NO<sub>2</sub> concentrations. The mean LIF NO<sub>2</sub> concentrations decreased by 25%, while the mean P-CL NO<sub>2</sub> concentrations increased, likely due to increasing interference from HNO<sub>4</sub> and MPN produced in the plume. Figure 2b also shows the NO<sub>2</sub> concentrations inferred by applying PSS to NO observations:

$$[\text{NO}_2]_{\text{PSS}} = \frac{[\text{NO}]}{\text{PSS}}, \quad (3)$$

360 where PSS is calculated from observations using Eq. (2) and measured  $[\text{O}_3]$ ,  $[\text{HO}_2]$  and  $j_{\text{NO}_2}$ . In this case, we take  $[\text{RO}_2]$  to be equal to the measured  $[\text{HO}_2]$  as an upper limit, instead of using the value from GEOS-Chem, since we do not expect the model to simulate the thunderstorm plume. The PSS  $\text{NO}_2$  concentrations decreased by a factor of 2 between the start and end of the measurement period, in line with the NO concentrations.

365 Figure 2c shows the observed ozone concentrations as a function of the  $\text{NO}_y/\text{NO}$  ratio. Ozone concentrations increase with the age of the plume, reflecting the  $\text{NO}_x$ -limited conditions for ozone production prevalent in the upper troposphere over the central US in summer (Pickering et al., 1990; Jaeglé et al., 1998b; Apel et al., 2015). We compare the observed ozone increase to that computed from the observed  $j_{\text{NO}_2}$  and the observed NO,  $\text{NO}_2$ ,  $\text{HO}_2$ , and OH concentrations. Ozone is produced through the photolysis of  $\text{NO}_2$  (reaction R5), and is lost mainly by reaction with NO (reaction R1), photolysis in the presence of water  
 370 vapor (reaction R6), and oxidation by  $\text{HO}_2$  and OH (reactions R7 and R8):



The instantaneous net ozone production rate is then given as follows:

$$375 \quad \frac{d[\text{O}_3]}{dt} = j_{\text{NO}_2}[\text{NO}_2] - k_{\text{NO}+\text{O}_3}[\text{NO}][\text{O}_3] - k_{\text{O}_3 \rightarrow \text{OH}}[\text{O}_3] - k_{\text{HO}_2+\text{O}_3}[\text{HO}_2][\text{O}_3] - k_{\text{OH}+\text{O}_3}[\text{OH}][\text{O}_3], \quad (4)$$

where

$$k_{\text{O}_3 \rightarrow \text{OH}} = \frac{j_{\text{O}_3 \rightarrow \text{O}(^1\text{D})} k_{\text{O}(^1\text{D})+\text{H}_2\text{O}} [\text{H}_2\text{O}]}{k_{\text{O}(^1\text{D})+\text{M}} [\text{M}]}, \quad (5)$$

and  $j_{\text{O}_3 \rightarrow \text{O}(^1\text{D})}$  is the frequency of  $\text{O}_3$  photolysis channel producing  $\text{O}(^1\text{D})$  and was measured on the flight.  $[\text{H}_2\text{O}]$  and  $[\text{M}]$  are calculated from meteorological observations on the flight. We use Eq. (4) to calculate three estimates for the instantaneous net  
 380 ozone production rate in the plume using  $\text{NO}_2$  from LIF, P-CL, and PSS. The total ozone increase in the plume is calculated by integrating  $\frac{d[\text{O}_3]}{dt}$  over the measurement period.

## NO<sub>x</sub> and O<sub>3</sub> in convective outflow

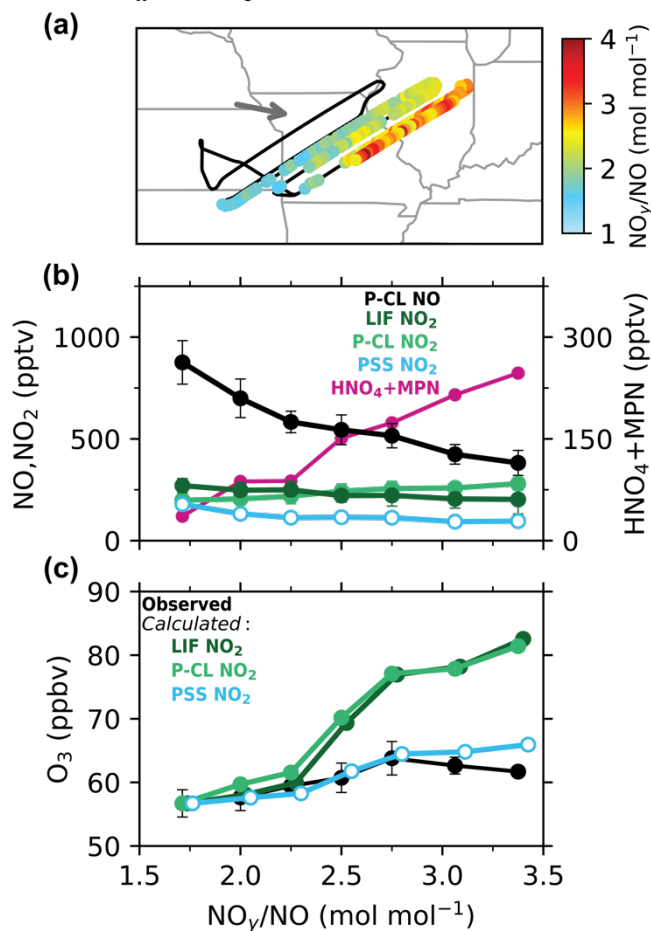


Figure 2. Evolution of NO<sub>x</sub> and O<sub>3</sub> concentrations in a thunderstorm outflow targeted for quasi-Lagrangian sampling by DC3 flight 17 over the central US at 12 km altitude. Panel (a) shows the flight track with data points within the outflow colored by the observed NO<sub>y</sub>/NO ratio as a measure of chemical aging. The arrow shows the mean wind direction. Panel (b) shows the measured concentrations of NO, NO<sub>2</sub> and the sum of HNO<sub>4</sub> and MPN as a function of the NO<sub>y</sub>/NO molar ratio. Also shown are the PSS NO<sub>2</sub> concentrations (Eq. 3). Panel (c) shows the measured ozone concentrations as a function of the NO<sub>y</sub>/NO molar ratio along with the ozone concentrations calculated from Eq. (4) with NO<sub>2</sub> concentrations from LIF, P-CL, or PSS NO<sub>2</sub>. The circles and the error bars in panels (b) and (c) show means and standard deviations for each NO<sub>y</sub>/NO bin.

The observed ozone concentrations increased by 7 ppbv between the start and the end of the measurement period in the plume. In comparison, the ozone increase calculated using the NO<sub>2</sub> measurements from both the LIF and P-CL instruments is 25 ppbv, while that calculated using the PSS NO<sub>2</sub> concentrations is close to the observations. We also examine the effect of potential uncertainties in the NO-NO<sub>2</sub>-O<sub>3</sub> kinetic data by decreasing  $j_{\text{NO}_2}$  by 20% and increasing  $k_{\text{NO}+\text{O}_3}$  by 40% in Eq. (4), following Silvern et al. (2018). We find that the ozone increase calculated using the NO<sub>2</sub> measurements is lowered to 17 ppbv, still much higher than the observed increase, and implying that the difference between the NO<sub>2</sub> measurements and the PSS NO<sub>2</sub>

concentrations cannot be attributed to errors in the NO-NO<sub>2</sub>-O<sub>3</sub> kinetic data. The most likely explanation is that the LIF NO<sub>2</sub> measurements are biased high, as are the P-CL measurements. The median LIF and P-CL NO<sub>2</sub> concentrations in the outflow plume were both 235 pptv, compared to a median PSS NO<sub>2</sub> concentration of 116 pptv. The median measured HNO<sub>4</sub> and MPN concentrations were 44 and 90 pptv, respectively, and can explain the difference between the P-CL and PSS NO<sub>2</sub> concentrations. The LIF NO<sub>2</sub> measurements are thought to have little interference from HNO<sub>4</sub>, and were corrected for the partial dissociation of MPN, but it appears that this correction may have been underestimated. For this flight, the median correction to the NO<sub>2</sub> measurements was just 7%. The correction is affected by high uncertainty in the thermal dissociation rate constant of MPN ( $\pm 30\%$ ) and in the MPN measurements ( $\pm 40\% + 20$  pptv for 1 Hz; Nault et al., 2015). The MPN measurements themselves would be affected by a bias in the NO<sub>2</sub> measurements as they are based on the difference in the NO<sub>2</sub> measured between the heated MPN channel and the NO<sub>2</sub> channel at cabin temperature. Interference from other known non-acyl peroxy nitrates would not be significant (Khan et al., 2020), but there could be other unknown organic NO<sub>2</sub> reservoir species forming in convective outflows (Silvern et al., 2018).

Considering this bias in the LIF and P-CL NO<sub>2</sub> measurements in the upper troposphere, we instead use the NO observations and the related PSS NO<sub>2</sub> concentrations inferred from the NO and other observations (Eq. 3) to evaluate the modeled NO<sub>x</sub> in the free troposphere (Fig. 1). GEOS-Chem reproduces the shape of the NO and the PSS NO<sub>2</sub> profiles throughout the troposphere for SEAC<sup>4</sup>RS and DC3. There is no increase in the modeled or the PSS NO<sub>2</sub> concentrations in the upper troposphere, as higher NO concentrations are compensated by higher NO/NO<sub>2</sub> ratios. GEOS-Chem NO concentrations are about 2 times higher than the observations in the free troposphere, consistent with previous work for SEAC<sup>4</sup>RS (Travis et al., 2016; Silvern et al., 2018). We calculate the NO<sub>2</sub> column density corresponding to the PSS and GEOS-Chem NO<sub>2</sub> profiles by converting the median NO<sub>2</sub> concentrations at each altitude to a partial column density (product of the NO<sub>2</sub> number density and the height of the altitude bin) and summing them from the surface to 12 km. We find that the PSS NO<sub>2</sub> column densities in the free troposphere for the SEAC<sup>4</sup>RS and DC3 profiles in Fig. 1 are  $3.6 \times 10^{14}$  and  $3.8 \times 10^{14}$  molec cm<sup>-2</sup>, respectively, compared to  $6.5 \times 10^{14}$  and  $10.4 \times 10^{14}$  molec cm<sup>-2</sup> in GEOS-Chem. However, the model does not overestimate NO<sub>y</sub> concentrations, suggesting that the model may be missing NO<sub>x</sub> oxidation chemistry, which is likely organic. We find that the median MPN concentration in the free troposphere in GEOS-Chem is about 5 pptv compared to about 40 pptv in the observations, consistent with the findings of Silvern et al. (2018) for SEAC<sup>4</sup>RS. Similarly, median alkyl nitrate concentration in the model is about 12 pptv but 60 pptv in the observations. NO<sub>x</sub> emissions are likely overestimated in the US EPA NEI inventory used in our simulations (Travis et al., 2016), which explains the NO<sub>2</sub> overestimate in the boundary layer, but this would have little effect in the free troposphere, where lightning emissions supply the majority of NO<sub>x</sub>. Finally, we find little difference in the SEAC<sup>4</sup>RS and DC3 NO<sub>x</sub> profiles in the free troposphere between our baseline simulation and the simulation without pNO<sub>3</sub><sup>-</sup> photolysis, indicating that chemical recycling through pNO<sub>3</sub><sup>-</sup> photolysis is a minor source of NO<sub>x</sub> over the US compared to emissions.

Retrieval of NO<sub>2</sub> columns from satellite-based instruments generally involves the following steps: (i) using the observed solar backscatter radiance to calculate a total slant NO<sub>2</sub> column density along the light path, (ii) removal of the stratospheric contribution to calculate the tropospheric slant column density  $\Omega_s$ , and (iii) conversion of the tropospheric slant column density to a tropospheric vertical column density  $\Omega_v$ , using an air mass factor (AMF) that depends on the vertical profile of NO<sub>2</sub> (Palmer et al., 2001; Martin et al., 2002):

$$\frac{\Omega_s}{\Omega_v} = \text{AMF} = \text{AMF}_G \int_0^{z_t} w(z) S(z) dz, \quad (6)$$

where  $\text{AMF}_G$  is the geometric AMF that describes the satellite viewing geometry,  $w(z)$  are the scattering weights that describe the sensitivity of the backscattered radiance to the NO<sub>2</sub> abundance as a function of altitude ( $z$ ),  $S(z)$  is the NO<sub>2</sub> shape factor describing the vertical profile of the NO<sub>2</sub> number density normalized to the NO<sub>2</sub> vertical column density, and  $z_t$  is the tropopause height.  $w(z)$  is computed with radiative transfer modeling, and in clear skies is 3–4 times higher in the upper troposphere than in the boundary layer because of atmospheric scattering (Martin et al., 2002). Here we use scattering weights from the NASA OMI NO<sub>2</sub> retrieval (v4.0; Lamsal et al., 2021), and exclude scenes with cloud fraction greater than 0.1 and surface albedo greater than 0.3.

We use Eq. 6 to calculate AMFs corresponding to PSS and GEOS-Chem NO<sub>2</sub> profiles for SEAC<sup>4</sup>RS and DC3.  $\text{AMF}_G$  over the southeastern US in summer for OMI is about 2.6. The shape factors are calculated by converting the NO<sub>2</sub> concentration profiles (Fig. 1) to number density profiles and normalizing them to the respective NO<sub>2</sub> columns. For SEAC<sup>4</sup>RS, both the PSS and GEOS-Chem NO<sub>2</sub> profiles yield an AMF of 1.0, reflecting the similar shapes of the NO<sub>2</sub> profiles despite the GEOS-Chem overestimate of the NO<sub>2</sub> concentrations. For DC3, the AMFs corresponding to the PSS and GEOS-Chem profiles are 0.91 and 1.03, respectively. These results suggest that using the GEOS-Chem NO<sub>2</sub> profiles as *a priori* in the NO<sub>2</sub> column retrievals over the southeast US would result in an error of 0–10%, compared to the previous error estimate of 30% based on the LIF NO<sub>2</sub> measurements in SEAC<sup>4</sup>RS (Silvern et al., 2018). The sensitivity of satellite retrievals to NO<sub>2</sub> vertical profiles is discussed further in Section 3.5.

### 3.2 NO<sub>x</sub> in the remote troposphere: interpreting the ATom data

We now examine the distribution of NO<sub>x</sub> over the Pacific and Atlantic oceans during the ATom campaign in order to contrast the NO<sub>2</sub> profiles in the remote troposphere to the SEAC<sup>4</sup>RS and DC3 NO<sub>2</sub> profiles over land. Modeled NO<sub>2</sub> over remote regions is often used in the stratospheric-tropospheric separation of satellite NO<sub>2</sub> columns (Bucsela et al., 2013). NO<sub>x</sub> in the remote troposphere is also important for global tropospheric ozone and OH production. Figures 3 and 4 show the median vertical profiles of NO and the PSS NO<sub>2</sub> concentrations over the Pacific and Atlantic Oceans separated by seasons and latitude bands. The PSS NO<sub>2</sub> concentrations in Fig. 4 are inferred from the ATom observations of NO, ozone, HO<sub>2</sub> and  $j_{\text{NO}_2}$  using Eqs. (2) and (3). The observed NO concentrations increase from 10 pptv near the surface to 20–100 pptv in the upper troposphere above 8 km because of the longer NO<sub>x</sub> lifetime and the increase in NO/NO<sub>2</sub> ratios with altitude. The PSS NO<sub>2</sub> profiles show a



decrease in NO<sub>2</sub> concentrations with altitude because of an increase in the NO/NO<sub>2</sub> ratio. PSS NO<sub>2</sub> concentrations in the upper troposphere are generally lower than 10 pptv, except in the northern midlatitudes upper troposphere in August and October, where NO<sub>2</sub> concentrations increase in the upper troposphere. The upper tropospheric NO<sub>x</sub> concentrations over the Atlantic in August are similar to those observed over the southeastern US during SEAC<sup>4</sup>RS and DC3 and reflect the transport of lightning-generated NO<sub>x</sub> from the US to the Atlantic Ocean (Crawford et al., 2000; Cooper et al., 2006; Singh et al., 2007). There is little seasonal variation in NO<sub>x</sub> below 8 km. The column density for PSS NO<sub>2</sub> has a campaign median of  $1.7 \times 10^{14}$  molec cm<sup>-2</sup> and a range of  $1.2\text{--}3.0 \times 10^{14}$  molec cm<sup>-2</sup> for the different seasons and latitude bands, which is similar in magnitude to NO<sub>2</sub> columns retrieved from OMI observations over remote regions (Hains et al., 2010; Lamsal et al., 2021). The free tropospheric PSS NO<sub>2</sub> column density over the northern Atlantic (30–60°N) in August is  $2.1 \times 10^{14}$  molec cm<sup>-2</sup>, about 45% lower than that observed in SEAC<sup>4</sup>RS and DC3.

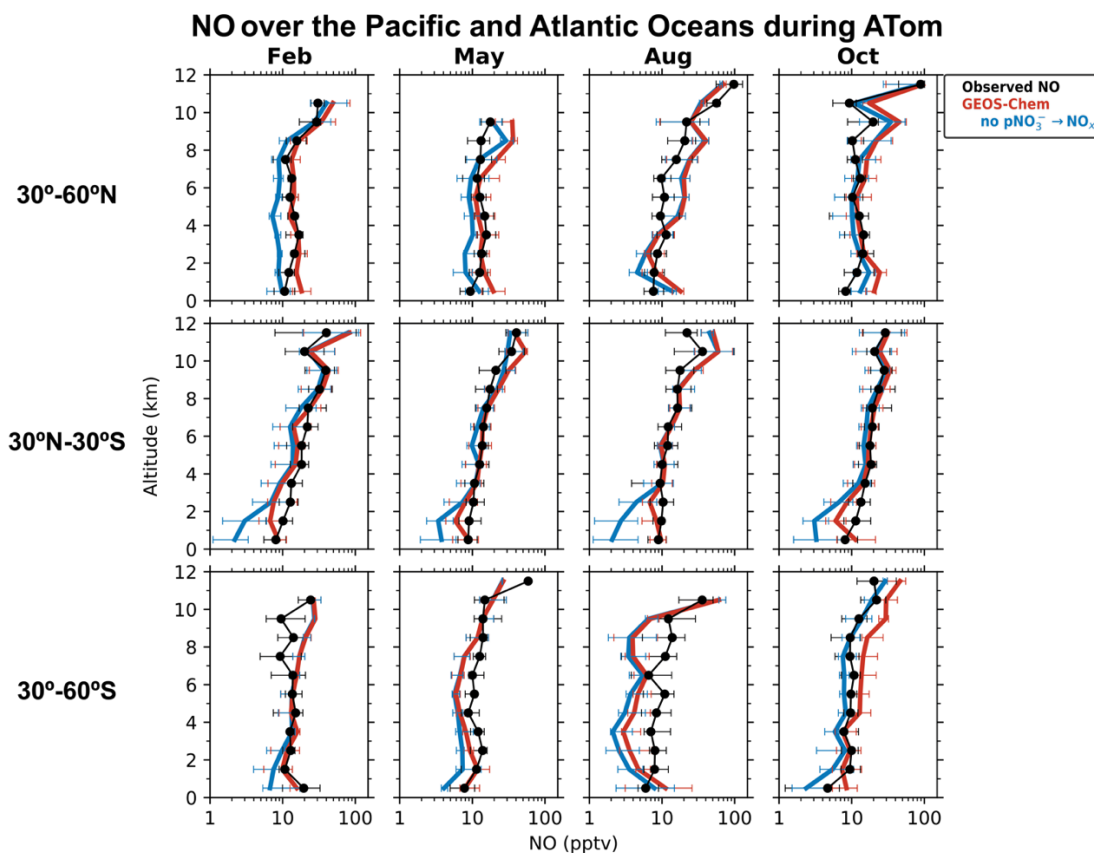


**Figure 3. Median vertical profiles of NO concentrations over the Pacific and Atlantic Oceans during the ATom flight campaigns (2016–18), separated by seasons and latitude bands. Observations (black) are from the NOAA P-CL instrument. The data selection criteria are as described in the caption of Fig. 1. Horizontal bars show the interquartile ranges in 1-km altitude bins. Model results are from our baseline GEOS-Chem simulation and a sensitivity simulation without pNO<sub>3</sub><sup>-</sup> photolysis. The model is sampled along the flight tracks. NO concentrations are plotted on a log scale to show the values in the lower troposphere clearly.**

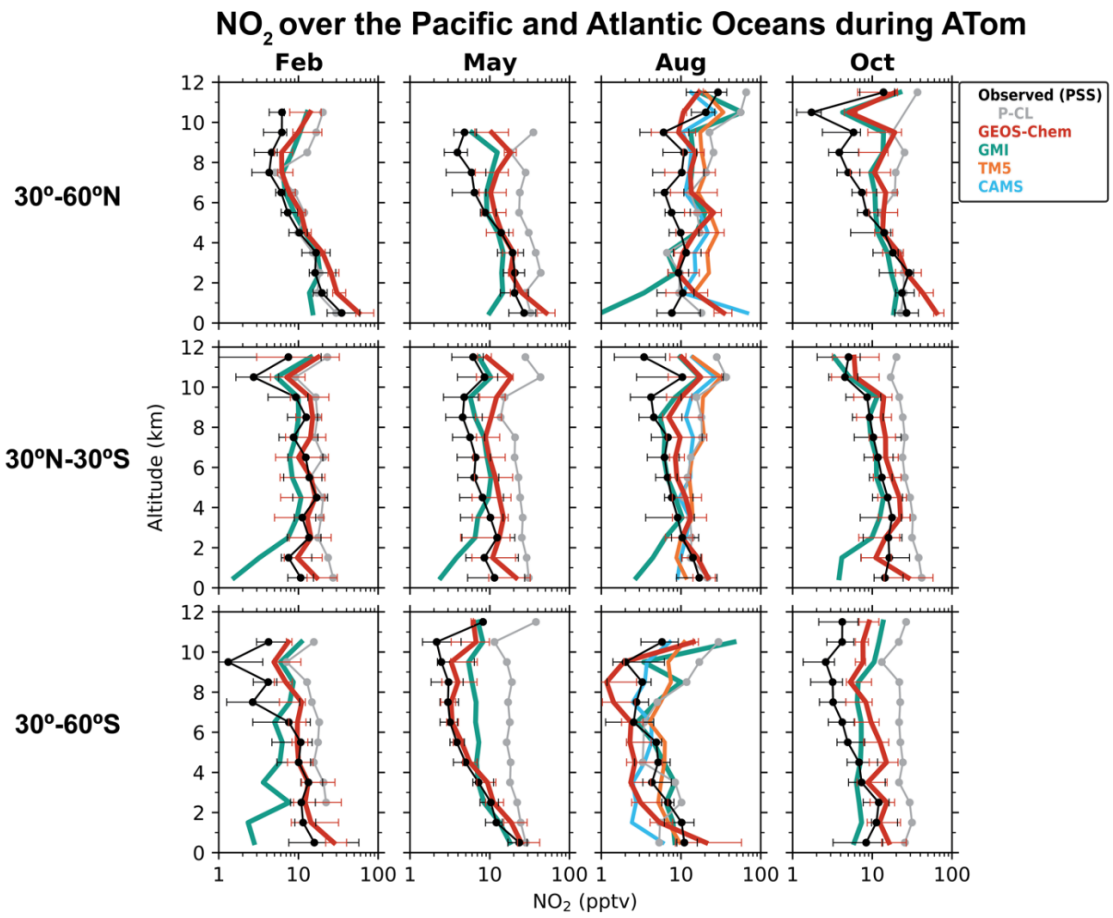
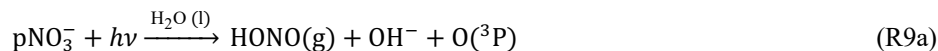


Figure 4. Median vertical profiles of NO<sub>2</sub> concentrations over the Pacific and Atlantic Oceans during the ATom flight campaigns (2016–18), separated by seasons and latitude regions. Observations are based on photochemical steady state (PSS) with local measurements of NO concentrations and other quantities following Eqs. (2) and (3). Horizontal bars show the interquartile ranges in 1-km altitude bins. The data selection criteria are as described in the caption of Fig. 1. NO<sub>2</sub> measurements from the P-CL instrument are also shown for reference. Model results are from our baseline GEOS-Chem simulation (including pNO<sub>3</sub><sup>-</sup> photolysis), GMI, TM5, and CAMS, sampled along the flight tracks. The TM5 and CAMS NO<sub>2</sub> profiles are available only for August. NO<sub>2</sub> concentrations are plotted on a log scale.

Figure 3 compares the NO observations to results from our baseline GEOS-Chem simulation and from a sensitivity simulation without the NO<sub>x</sub> source from pNO<sub>3</sub><sup>-</sup> photolysis. The GEOS-Chem simulation without pNO<sub>3</sub><sup>-</sup> photolysis underestimates NO observations below 6 km by a factor of 2–5 in most cases. The underestimate does not extend to the upper troposphere so it cannot be attributed to errors in lightning or aircraft NO<sub>x</sub> emissions. The underestimate is not related to NO<sub>x</sub> recycling from HNO<sub>3</sub>, PAN, or alkyl nitrates either. GEOS-Chem generally overestimates ATom HNO<sub>3</sub> observations (Fig. S1; Travis et al., 2020; Luo et al., 2020). The model is consistent with the ATom observations of PAN in the tropics and southern midlatitudes

and underestimates it a little in the northern midlatitudes (Fig. S1). GEOS-Chem simulation of methyl, ethyl, and propyl nitrates is generally consistent with the ATom observations (Fisher et al., 2018). Fisher et al. (2018) also considered whether missing oceanic NO emissions in the model could explain the underestimate in NO in the MBL. This source is largely limited to the equatorial region and is estimated to be about  $10^8$  molecules  $\text{cm}^{-2} \text{s}^{-1}$  (Torres and Thompson, 1993; Tian et al., 2020), which is 100 times smaller than that would be required to correct the NO underestimate in the model. The  $\text{NO}_x$  sink from reaction with OH is not overestimated in the model either, considering that GEOS-Chem's OH concentrations are consistent with ATom observations (Travis et al., 2020). There is some uncertainty in the  $\text{NO}_2 + \text{OH} + \text{M} \rightarrow \text{HNO}_3 + \text{M}$  rate constant used in models, as reported in laboratory (Mollner et al., 2010; Burkholder et al., 2020) and field studies (Henderson et al., 2011; Seltzer et al., 2015; Nault et al., 2016), but not large enough to explain the NO underestimate. The representation of heterogeneous  $\text{NO}_x$  chemistry in the model reflects current knowledge and includes an empirical parameterization for the  $\text{N}_2\text{O}_5$  reaction probability derived from aircraft observations (Jaeglé et al., 2018; McDuffie et al., 2018; Holmes et al., 2019). These processes are not well-constrained, but they are important mainly in the extratropical latitudes in winter and spring (Alexander et al., 2020).

Recent studies suggest that photolysis of  $\text{pNO}_3^-$  could be much faster than photolysis of gas-phase  $\text{HNO}_3$  and contribute an important source of  $\text{NO}_x$  over the oceans (Ye et al., 2016a, b; Reed et al., 2017; Kasibhatla et al., 2018).  $\text{pNO}_3^-$  photolysis produces  $\text{NO}_2$  and HONO (Scharko et al., 2014; Ye et al., 2017b), and HONO photolyzes further to produce NO:



In bulk solution, the absorption cross-section of  $\text{NO}_3^-$  is about 100 times larger than that of  $\text{HNO}_3$  (Burley and Johnston, 1992) but the effective quantum yields for Reactions (R9a) and (R9b) are low ( $\sim 1\%$ ) (Warneck and Wurzinger, 1988; Benedict et al., 2017), because the products are surrounded by water molecules and recombine before they can escape to the gas phase (Nissenson et al., 2010; Richards-Henderson et al., 2015). However, the photolysis of  $\text{NO}_3^-$  on aerosols is thought to be much more efficient than that in the gas and bulk aqueous phases. Field studies trying to explain the observed HONO and  $\text{NO}_x$  concentrations over the oceans postulate enhancement factors (EF) for  $\text{pNO}_3^-$  photolysis rate relative to that of  $\text{HNO}_3$  of 10–500 (Ye et al., 2016b, 2017a; Reed et al., 2017; Kasibhatla et al., 2018; Zhu et al., 2022; Andersen et al., 2022). Similar EFs have also been observed in laboratory studies of photolysis of  $\text{pNO}_3^-$  in ambient aerosols from urban and remote areas (Ye et al., 2017b; Bao et al., 2018; Gen et al., 2019). The high EFs could reflect the higher absorption cross-sections and quantum yields for  $\text{NO}_3^-$  molecules at the surface of the particles (Zhu et al., 2008, 2010; Du and Zhu, 2011; Nissenson et al., 2010). The fraction of  $\text{NO}_3^-$  at the surface is larger in the presence of halides as found in sea salt aerosols (Wingen et al., 2008; Richards-Henderson et al., 2013; Zhang et al., 2020). Other factors that could contribute to higher EFs include high aerosol

530  $[H^+]$  (Scharko et al., 2014; Mora Garcia et al., 2021) and the presence of organic species that can act as photosensitizers, H-donors, electron donors, or promote secondary reactions (Ye et al., 2019; Mora Garcia et al., 2021). Laboratory studies on  $NaNO_3$  and  $NH_4NO_3$  particles find EFs of less than 10 (Shi et al., 2021), suggesting that aerosol composition is an important factor in the photolysis rate of  $pNO_3^-$ . The relative yields of HONO:NO<sub>2</sub> in Reactions (R9a) and (R9b) also vary substantially in laboratory results. Ye et al. (2016) found relative yields for HONO:NO<sub>2</sub> ranging from 1:1 to 30:1, with lower values for  
535 marine aerosol samples and higher values for urban samples. Bao et al. (2018) found median relative yields for HONO:NO<sub>2</sub> of 3.5:1 for aerosol samples from Beijing.

Our baseline simulation assumes EFs of 10–100 depending on the relative amount of  $pNO_3^-$  and sea salt aerosols (Eq. 1), and a HONO:NO<sub>2</sub> yield of 2:1 following Kasibhatla et al. (2018). Figure 5 shows the spatial distribution of EFs at the surface and  
540 as a function of altitude. The simulated EF decrease from 100 in the MBL to less than 30 over the continents, where much of the  $pNO_3^-$  is present as  $NH_4NO_3$ . The values over the oceans are consistent with EFs required to explain high daytime HONO concentrations (more than 10 pptv) observed over the oceans (Ye et al., 2016b; Andersen et al., 2022). Kasibhatla et al. (2018) found that an EF of 100 and a HONO:NO<sub>2</sub> yield of 15:1 were needed in GEOS-Chem to reproduce the observed diurnal cycle of HONO at Cape Verde, although EFs of 25–50 and HONO:NO<sub>2</sub> yield of 2:1 were sufficient to explain the NO<sub>x</sub> observations.  
545 Romer et al. (2018) suggested an upper limit for the EF of 30, arguing that higher values would lead to inconsistency between the calculated steady state NO<sub>x</sub>/HNO<sub>3</sub> ratios and observations from seven aircraft campaigns. Most of these campaigns were over or near continents in the northern midlatitudes, where EFs in our simulation are also generally low. In the northern midlatitudes, EFs decrease with altitude reflecting the increase in the fraction of  $pNO_3^-$  present as  $NH_4NO_3$  relative to that present on sea salt aerosols. There is little change in the EFs with altitude elsewhere.

550  $pNO_3^-$  concentrations were measured by the AMS and SAGA instruments during ATom and were found to be very low (Fig. S1). The AMS measures total (inorganic and organic) nitrate in non-refractory particles smaller than 1  $\mu m$  diameter, while SAGA measures water-soluble  $NO_3^-$  ions in particles smaller than about 4  $\mu m$  diameter. Almost all of the nitrate measured by the AMS was organic (Nault et al., 2021; Hodzic et al., 2020; Guo et al., 2021b), and (inorganic)  $pNO_3^-$  concentrations were  
555 less than 1  $ng\ sm^{-3}$ . The median SAGA measured  $pNO_3^-$  concentration was 44  $ng\ sm^{-3}$ . In comparison, the median  $pNO_3^-$  concentrations in GEOS-Chem were 2.1  $ng\ sm^{-3}$  in the fine mode and 1.8  $ng\ sm^{-3}$  in the coarse mode. GEOS-Chem overestimated the observed  $pNO_3^-$  concentrations in the northern midlatitudes (Fig. S1), likely reflecting the overestimate in HNO<sub>3</sub> concentrations and aerosol pH compared to the ATom measurements (Travis et al., 2020; Luo et al., 2020; Nault et al., 2021), but the effect on the NO<sub>x</sub> source from  $pNO_3^-$  photolysis is dampened because the EF for fine mode  $pNO_3^-$  photolysis  
560 decreases at higher  $pNO_3^-$  concentrations (Eq. 1). GEOS-Chem  $pNO_3^-$  concentrations are lower compared to the SAGA observations in 30°N–30°S, but much of the  $pNO_3^-$  measured there is associated with dust, and probably has a lower EF than that of  $pNO_3^-$  on sea salt aerosols (Andersen et al., 2022).

# **pNO<sub>3</sub><sup>-</sup> photolysis enhancement factors**

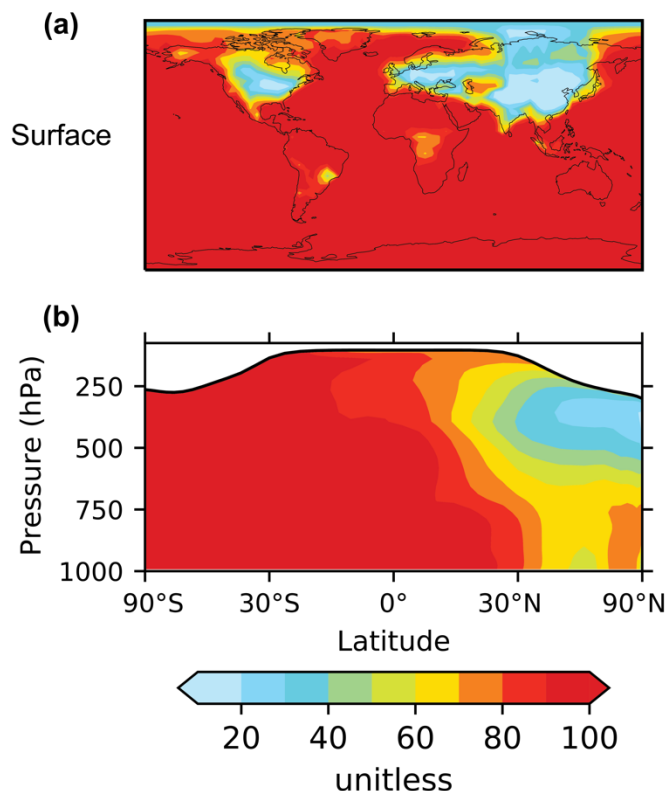


**Figure 5. Annual mean (2015) enhancement factors (EFs) for the photolysis frequency of pNO<sub>3</sub><sup>-</sup> with respect to the photolysis frequency of HNO<sub>3</sub> in our baseline simulation. Panel (a) shows EFs at the surface and panel (b) shows the zonal mean EFs. The EF for fine pNO<sub>3</sub><sup>-</sup> varies from 10 to 100 according to Eq. (1) and that for coarse pNO<sub>3</sub><sup>-</sup> is set at 100. The values shown here are the concentration weighted average EFs for total (fine + coarse) pNO<sub>3</sub><sup>-</sup>. The zonal mean EFs are calculated as pNO<sub>3</sub><sup>-</sup> concentration weighted averages for the band of grid cells in each altitude and latitude bin. The white shading in the zonal mean plots denotes the stratosphere.**

Including pNO<sub>3</sub><sup>-</sup> photolysis in the model significantly increases modeled NO<sub>x</sub> concentrations below 6 km and improves agreement with the NO observations (Fig. 3) and with the PSS NO<sub>2</sub> concentrations inferred from NO observations (Fig. 4). The largest increase is in the tropics (30°S–30°N), where pNO<sub>3</sub><sup>-</sup> photolysis is faster because of high actinic flux and high EFs, and because the NO<sub>x</sub> source from PAN decomposition is small there (Moxim et al., 1996; Fischer et al., 2014). The effect of pNO<sub>3</sub><sup>-</sup> photolysis is generally smaller above 6 km because of lower pNO<sub>3</sub><sup>-</sup> concentrations, except in the midlatitudes in spring when pNO<sub>3</sub><sup>-</sup> concentrations are high and there is sufficient actinic flux. GEOS-Chem NO<sub>2</sub> concentrations are slightly higher than the PSS NO<sub>2</sub> concentrations in the upper troposphere, because of higher NO concentrations and higher ozone concentrations driving down the NO/NO<sub>2</sub> ratios in the model. The ozone concentrations in the upper troposphere in the model

are on average 20 ppbv higher than the ATom observations. Travis et al. (2020) had also reported a similar overestimate in ozone concentrations in GEOS-Chem in the upper troposphere for ATom.

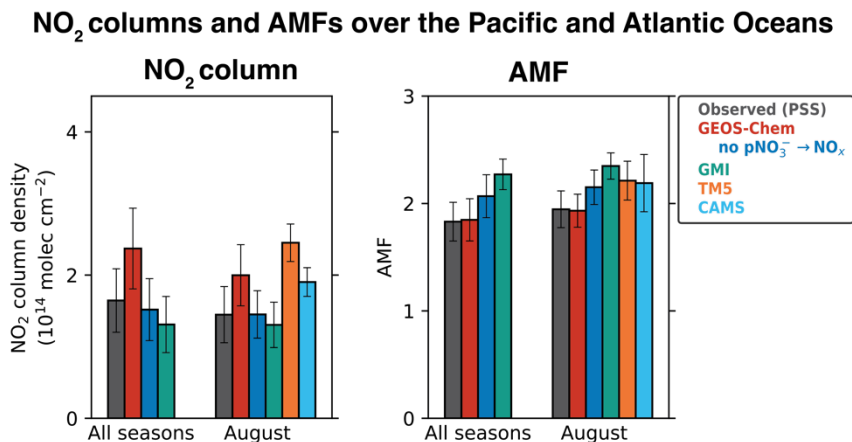


**Figure 6. Tropospheric NO<sub>2</sub> column densities and NO<sub>2</sub> air mass factors (AMFs) over the Pacific and Atlantic Oceans during ATom.** The observed values are based on the median NO<sub>2</sub> vertical profiles calculated using the photochemical steady state (PSS) with local measurements of NO concentrations and other quantities following Eqs. (2) and (3). Model results are from our baseline GEOS-Chem simulation, GEOS-Chem simulation without pNO<sub>3</sub><sup>-</sup> photolysis, GMI, TM5, and CAMS, sampled along the flight tracks. Values shown are medians for all four ATom deployments and for the August deployment, as the TM5 and CAMS NO<sub>2</sub> profiles are available only for August. AMFs are calculated using the NASA OMI NO<sub>2</sub> v4.0 scattering weights following Eq. (6), with geometric AMF (AMF<sub>G</sub>) values of 2.6 for 30°S–30°N and 3.7 for 30°S–60°S and 30°N–60°N. Error bars show the standard deviations of the medians and are calculated using jackknife resampling.

Figure 4 also shows the NO<sub>2</sub> profiles simulated by the GMI, TM5, and CAMS models, and Figure 6 compares the NO<sub>2</sub> column density and AMFs for the PSS and the modeled NO<sub>2</sub> profiles. The TM5 and CAMS results are available only for August, so the NO<sub>2</sub> column density and AMFs for August are shown separately. The NO<sub>2</sub> column densities and AMFs are calculated from the median PSS and modeled NO<sub>2</sub> profiles for the campaign, with the AMF calculation further assuming AMF<sub>G</sub> values of 2.6 for tropics (0°–30°) and 3.7 for midlatitudes (30°–60°), and a scattering weight profile from the NASA OMI NO<sub>2</sub> retrieval (v4.0) for scenes with cloud fraction < 0.1 and surface albedo < 0.3. The campaign median (all seasons) NO<sub>2</sub> column density is  $2.4 \times 10^{14}$  molec cm<sup>-2</sup> in our baseline GEOS-Chem simulation compared to  $1.7 \pm 0.44 \times 10^{14}$  molec cm<sup>-2</sup> for PSS NO<sub>2</sub>, and the corresponding AMFs are about equal (1.8). The NO<sub>2</sub> column density in the simulation without pNO<sub>3</sub><sup>-</sup> photolysis is  $1.5 \times 10^{14}$  molec cm<sup>-2</sup>. GMI NO<sub>2</sub> concentrations are much lower than the PSS NO<sub>2</sub> concentrations below 4 km, similar to the GEOS-Chem simulation without the pNO<sub>3</sub><sup>-</sup> photolysis source, and generally higher than the PSS NO<sub>2</sub> concentrations in the upper troposphere. The campaign average NO<sub>2</sub> column density in GMI is  $1.4 \times 10^{14}$  molec cm<sup>-2</sup> and the AMF is 2.2. GMI NO<sub>2</sub> concentrations are consistent with PSS NO<sub>2</sub> in the northern midlatitudes in February and in the southern midlatitudes in August, even though GMI does not include NO<sub>x</sub> formation from pNO<sub>3</sub><sup>-</sup> photolysis. This is likely because GMI does not include NO<sub>x</sub> loss through the hydrolysis of NO<sub>3</sub> and N<sub>2</sub>O<sub>5</sub> in clouds (Holmes et al., 2019) or the formation of halogen nitrates (Wang et al.,

2021). The TM5 and CAMS models slightly overestimate the PSS NO<sub>2</sub> columns. Overall, the difference in NO<sub>2</sub> column densities among the four models is  $\sim 1 \times 10^{14}$  molec cm<sup>-2</sup>. In comparison, the uncertainty in the NO<sub>2</sub> retrievals from using modeled NO<sub>2</sub> tropospheric columns over clean areas for stratosphere-troposphere separation is estimated to be  $2 \times 10^{14}$  molec cm<sup>-2</sup> (Bucsela et al., 2013; Boersma et al., 2018). The difference among the models in the AMFs is  $\sim 20\%$ , which is higher than the assumed uncertainty of 10% in the QA4ECV NO<sub>2</sub> column retrievals associated with the *a priori* profiles (Boersma et al., 2018). The uncertainty associated with NO<sub>2</sub> spectral fitting and stratosphere-troposphere separation in remote regions is large for single-pixel retrievals ( $\sim 100\%$ ), but this reduces when averaging spatially and temporally (Boersma et al., 2018).

### 3.3 Effect of pNO<sub>3</sub><sup>-</sup> photolysis on global NO<sub>x</sub>, OH, and ozone concentrations

Figure 7 shows the change in the annual mean NO<sub>x</sub>, OH, and ozone concentrations at the surface and zonally between our baseline simulation and the sensitivity simulation without pNO<sub>3</sub><sup>-</sup> photolysis. pNO<sub>3</sub><sup>-</sup> photolysis increases NO<sub>x</sub>, OH and ozone tropospheric masses in the model by 9%, 19%, and 10%, respectively, but there are much larger changes in certain areas (Fig. 7). In comparison, Kasibhatla et al. (2018) found increases in the NO<sub>x</sub>, OH, and ozone tropospheric masses of 1–3% in simulations that included photolysis of only coarse mode pNO<sub>3</sub><sup>-</sup> at an EF of 100 and increases of 3–6% when fine mode pNO<sub>3</sub><sup>-</sup> photolysis was also included at an EF of 25. We find that NO<sub>x</sub> concentrations increase by a factor of 2 on average in the MB though there is little increase in the northern extratropical MBL, as PAN concentrations are high (Fig. S1) and provide the main source of NO<sub>x</sub> in the region. There is little change in surface NO<sub>x</sub> concentrations over continents as local emissions dominate the NO<sub>x</sub> source. NO<sub>x</sub> concentrations decrease slightly over some regions because the increase in OH concentrations resulting from HONO photolysis shortens the NO<sub>x</sub> lifetime. The increase in NO<sub>x</sub> concentrations in the tropics and subtropics is limited mostly to the MBL, since pNO<sub>3</sub><sup>-</sup> concentrations are low at higher altitudes. In the free troposphere of the northern midlatitudes, pNO<sub>3</sub><sup>-</sup> photolysis increases NO<sub>x</sub> concentrations by just 20%, because pNO<sub>3</sub><sup>-</sup> concentrations and EFs for pNO<sub>3</sub><sup>-</sup> photolysis are generally low (Fig. 5). The effect of pNO<sub>3</sub><sup>-</sup> photolysis is larger in spring, when there is a seasonal peak in pNO<sub>3</sub><sup>-</sup> concentrations in the model. There is a large increase in NO<sub>x</sub> concentrations over Antarctica, as there are few other NO<sub>x</sub> sources in the region in the model. Our simulations do not include snow NO<sub>3</sub><sup>-</sup> photolysis, which is an important source of NO<sub>x</sub> in the region (Zatko et al., 2016).

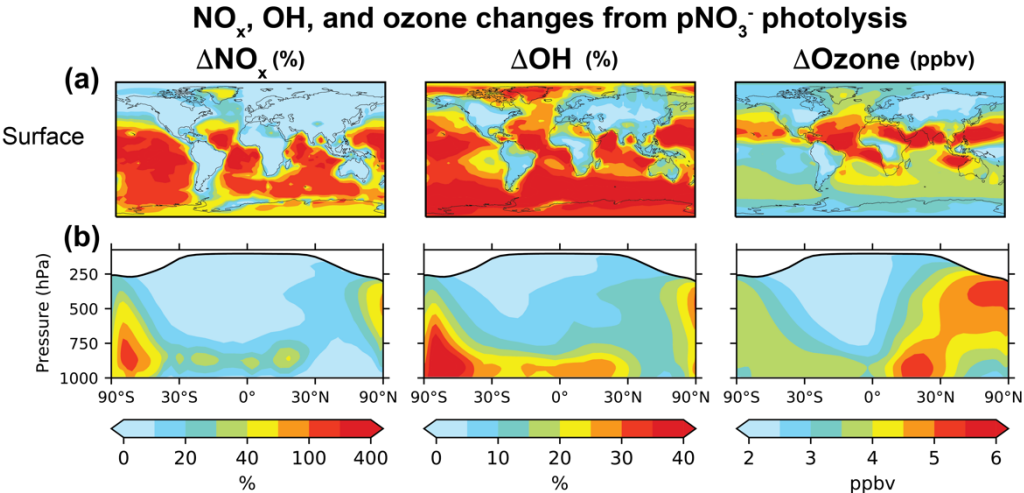
pNO<sub>3</sub><sup>-</sup> photolysis increases the production of OH and ozone because of the increase in NO<sub>x</sub> concentrations in low-NO<sub>x</sub> regions, where OH and ozone production are most sensitive to NO<sub>x</sub> concentrations. OH is also produced by the photolysis of HONO released to the gas phase during pNO<sub>3</sub><sup>-</sup> photolysis (Reaction R10), which would be an important source of OH in winter when OH production from Reaction (R6) is slow (Elshorbany et al., 2012). The increase in OH concentrations is particularly large ( $\sim 30\%$ ) in the MBL. Travis et al. (2020) showed that the GEOS-Chem OH concentrations from a simulation without pNO<sub>3</sub><sup>-</sup> photolysis are consistent with the ATom observations, but they also found an underestimate in the modeled OH reactivity in the lower troposphere due to missing VOCs in the model. The source of these VOCs is likely oceanic and would depress model OH (Thames et al., 2020). The OH source from pNO<sub>3</sub><sup>-</sup> photolysis could then compensate for the increase in OH reactivity. The

OH increase implied by  $\text{pNO}_3^-$  recycling decreases the global atmospheric methane lifetime from 8.0 years to 7.0 years, reducing the agreement with the value of  $9.1 \pm 0.9$  years inferred from the methylchloroform proxy (Prather et al., 2012), but again this could be compensated by an increase in the model OH reactivity (Travis et al., 2020; Kim et al., 2022).

645

$\text{pNO}_3^-$  photolysis increases surface ozone concentrations by  $3.6 \pm 0.94$  ppbv on average at the surface, and up to 8 ppbv in the tropics and subtropics. In the northern extratropics, the ozone increase is small at the surface, but about 5 ppbv in the free troposphere, reflecting the spatial pattern of increase in  $\text{NO}_x$  concentrations. Wang et al. (2021) recently evaluated the GEOS-Chem ozone simulation with ozonesonde observations and found an underestimate in simulated free tropospheric ozone of 5–15 ppbv in the northern hemisphere and up to 5 ppbv in the southern hemisphere, depending on whether halogen chemistry was included or not. Including the  $\text{NO}_x$  source from  $\text{pNO}_3^-$  photolysis improves GEOS-Chem’s ozone simulation. We will examine this further in a future publication.

650



655

**Figure 7. Annual mean (2015) changes in  $\text{NO}_x$ , OH, and ozone concentrations from including  $\text{pNO}_3^-$  photolysis in GEOS-Chem. Panel (a) shows changes at the surface and panel (b) shows the zonal means. Changes in  $\text{NO}_x$  and OH are shown as percent change of concentrations in our baseline simulation relative to that in the sensitivity simulation without  $\text{pNO}_3^-$  photolysis, and changes in ozone are shown as differences in concentrations (in ppbv) between the two simulations. The white shading in the zonal mean plots denotes the stratosphere.**

660

### 3.4 Primary sources of $\text{NO}_x$ in the free troposphere

$\text{NO}_x$  in the free troposphere originates from a variety of primary sources with differing spatial and seasonal characteristics. The sources include in situ emissions from lightning and aircraft, uplifting of  $\text{NO}_x$  emitted from surface sources, and downwelling of stratospheric  $\text{NO}_y$  produced from the photolysis of  $\text{N}_2\text{O}$ . Lightning is the main in situ source of  $\text{NO}_x$  in the

665



free troposphere globally (Table 2), but it is concentrated over continents and has a strong seasonality in the midlatitudes. Aircraft emissions are largest in the northern midlatitudes, and while most of the aircraft emissions are over land, there are significant emissions over the northern Atlantic and Pacific oceans (Simone et al., 2013). Surface emissions are widely distributed over the tropics and the northern midlatitudes, but their transport to the free troposphere would vary seasonally.

670 Here we use GEOS-Chem to determine the relative importance of these primary sources for NO<sub>x</sub> in the free troposphere.

Figure 8 shows the vertical profiles of NO<sub>x</sub> over the Pacific and Atlantic Oceans and the contiguous US for February and August separately for surface emissions (fuel combustion, fires, and soils and fertilizer use), aircraft emissions, and lightning emissions. We focus on the tropospheric sources and exclude the stratospheric NO<sub>y</sub> source from N<sub>2</sub>O because it is small in the global troposphere, although it could be important in the upper troposphere in the high latitudes in summer (Levy et al., 1999). The source contributions are derived from three sensitivity simulations with small (20%) perturbation to each source in turn and are calculated as  $([\text{NO}_x]_0 - [\text{NO}_x]_i) / \sum_{i=1}^3 ([\text{NO}_x]_0 - [\text{NO}_x]_i)$ , where  $[\text{NO}_x]_0$  is the NO<sub>x</sub> concentrations in the baseline simulation and  $[\text{NO}_x]_i$  is the NO<sub>x</sub> concentration in the sensitivity simulation  $i$ . The source contributions for the northern midlatitudes are shown separately for February and August, but for the tropics and southern midlatitudes the February and

675  
680 August average is shown.

Over the northern midlatitude oceans, in February, most of the NO<sub>x</sub> in the free troposphere is supplied by surface and aircraft sources. Both sources contribute equally (42%) to the free tropospheric NO<sub>x</sub> column, but surface emissions are dominant below 6 km and aircraft emissions above 6 km. In August, lightning is the dominant source of NO<sub>x</sub>, supplying 55% of the NO<sub>x</sub> column in the free troposphere. Aircraft emissions contribute 33% but are the major source of NO<sub>x</sub> between 10 and 12 km. Aircraft emissions account for the higher NO<sub>x</sub> concentrations in the upper troposphere over the northern midlatitudes than over the tropics and southern midlatitudes. Lightning is the dominant source of NO<sub>x</sub> in the tropics and the southern midlatitudes, supplying 62–68% of the free tropospheric NO<sub>x</sub> column, with surface sources supplying 18–30% of NO<sub>x</sub>. However, Bourgeois et al. (2021) found that models tend to underestimate the contribution of biomass burning emissions to NO<sub>x</sub> over the remote

685  
690 oceans.

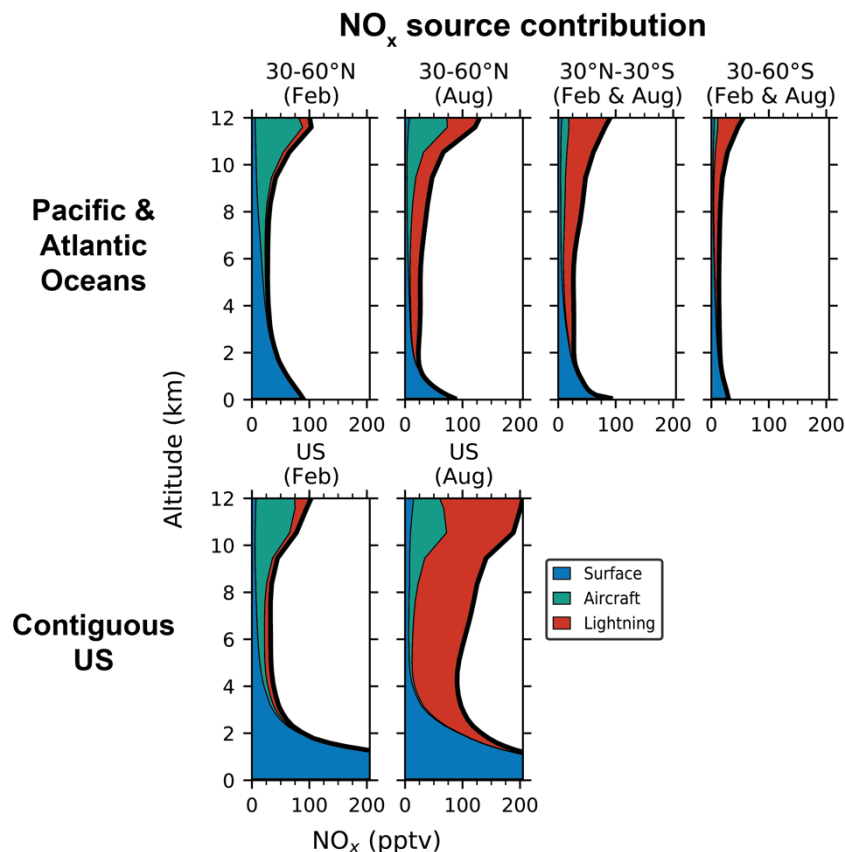


Figure 8. Vertical profiles of  $\text{NO}_x$  concentrations from three primary source categories over the Pacific and Atlantic oceans and over the contiguous US in GEOS-Chem. The source categories include surface emissions (fuel combustion, soil, fertilizer use, and fires), aircraft emissions, and lightning emissions. The profiles for the Pacific and Atlantic Oceans are means for the regions sampled in ATom (160°E–160°W and 25°–50°W in the northern hemisphere and 160°E–160°W and 0°–30°W in the southern hemisphere) and are separated into three latitude bands. The northern midlatitude (30°–60°N) profiles are further separated by month (February and August), while the other profiles are averages for the two months. The profiles for the contiguous US (defined as 25°–50°N and 65°–130°W) are shown separately for February and August.

Comparing the  $\text{NO}_x$  source contributions over the northern midlatitude oceans to those over the contiguous US, we find that the  $\text{NO}_x$  sources over the oceans and the US are similar in winter. Surface and aircraft sources each supply about 40% of  $\text{NO}_x$  in the free troposphere in February over the US, with surface sources dominating below 4 km and aircraft sources in the upper troposphere. In August, lightning emissions supply 73% of the  $\text{NO}_x$  in the free troposphere over the US, much more than in winter and over the oceans. Previous modeling studies have also found lightning to be the main source of  $\text{NO}_x$  in the tropics and southern midlatitudes, and a seasonal change in the main source in the northern midlatitudes from lightning in summer to surface and aircraft emissions in winter (Lamarque et al., 1996; Levy et al., 1999). But the contribution of aircraft emissions

to free tropospheric NO<sub>x</sub> in our simulation is higher than in these previous studies, reflecting a nearly two-fold increase in  
710 global aircraft NO<sub>x</sub> emissions in the past three decades (Hoesly et al., 2018).

### 3.5 Implications for the retrieval and interpretation of satellite NO<sub>2</sub> data

We showed that the previously reported model underestimate of NO<sub>2</sub> concentrations in the upper troposphere over the US can  
be attributed to interference in the NO<sub>2</sub> measurements, and that when compared with the measured NO and PSS NO<sub>2</sub> profiles,  
the modeled NO<sub>2</sub> profiles in the free troposphere are consistent with the SEAC<sup>4</sup>RS, DC3, and ATom observations. This  
715 increases our confidence in the modeled NO<sub>2</sub> profiles and here we use them to examine the importance of the free troposphere  
in the retrieval and interpretation of satellite NO<sub>2</sub> data over the US. Figure 9 shows the GEOS-Chem vertical profiles of the  
NO<sub>2</sub> number density in the early afternoon (OMI and TROPOMI overpass time) over the contiguous US for summer and  
winter of 2015. The results are from our baseline simulation, but there is little difference in the NO<sub>2</sub> profiles between our  
baseline simulation and the simulation without pNO<sub>3</sub><sup>-</sup> photolysis over the US (Fig. 1), except in spring when the NO<sub>2</sub>  
720 concentrations in the free troposphere are about 10% higher due to the pNO<sub>3</sub><sup>-</sup> photolysis source.

In summer, simulated NO<sub>2</sub> partial columns in the boundary layer and the free troposphere are  $6.9 \times 10^{14}$  molec cm<sup>-2</sup> and  
 $5.8 \times 10^{14}$  molec cm<sup>-2</sup>, respectively. In comparison, the simulated wintertime NO<sub>2</sub> partial columns are  $15.4 \times 10^{14}$  molec cm<sup>-2</sup>  
and  $1.9 \times 10^{14}$  molec cm<sup>-2</sup> in the boundary layer and the free troposphere. The boundary layer NO<sub>2</sub> column is higher in winter  
725 because of longer NO<sub>x</sub> chemical lifetimes (Kenagy et al., 2018; Shah et al., 2020) and slower ventilation to the free troposphere,  
while the free troposphere NO<sub>2</sub> column is higher in summer because of lightning emissions (Fig. 7). The GEOS-Chem  
summertime NO<sub>2</sub> column density in the free troposphere over the US is about three times higher than the PSS-inferred NO<sub>2</sub>  
column over the oceans during ATom. In winter, by contrast, the free tropospheric NO<sub>2</sub> column over the US is similar to that  
over the oceans, indicating little contrast in free tropospheric NO<sub>2</sub> between the US and surrounding oceans as was previously  
730 discussed in the context of Fig. 8. The similarity in free tropospheric NO<sub>2</sub> between the US and the oceans in winter reflects the  
longer lifetime of NO<sub>x</sub> and higher pNO<sub>3</sub><sup>-</sup> concentrations over the ocean. It also implies that ATom observations over the  
northern midlatitudes in February could be used to estimate the free tropospheric NO<sub>2</sub> concentrations over the US in winter,  
in the absence of aircraft observations over land that probe the full height of the winter troposphere. Marais et al. (2018) had  
compared the GEOS-Chem NO<sub>2</sub> concentrations at 6–10 km with those derived from the OMI cloud-sliced product (Choi et  
735 al., 2014) for 2005–07 and found that GEOS-Chem underestimates NO<sub>2</sub> concentrations over North America in winter by about  
a factor of 3. The successful simulation of the measured NO and the PSS NO<sub>2</sub> concentrations over the northern midlatitudes  
in winter during ATom suggests that there is little bias in the free tropospheric NO<sub>2</sub> concentrations in the model, and that the  
underestimate with respect to the OMI observations likely reflects uncertainties in the cloud-slicing technique.

## Scattering weight and NO<sub>2</sub> profiles over the US

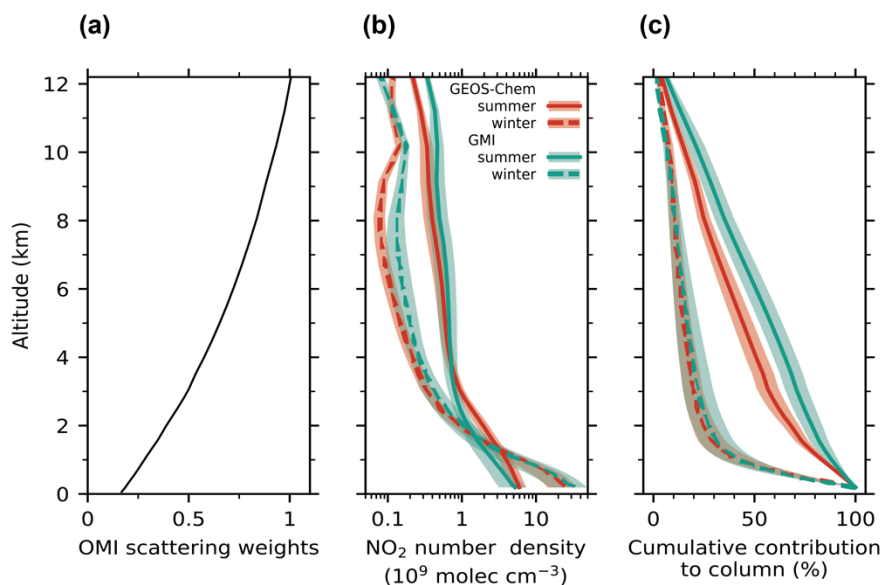


**Figure 9.** Seasonal mean vertical profiles of sensitivity (scattering weights) of the OMI satellite instrument, NO<sub>2</sub> number density, and cumulative percent contributions to tropospheric NO<sub>2</sub> columns as would be observed by OMI over the contiguous US. Panel (a) shows the mean profile of the scattering weights from the NASA OMI NO<sub>2</sub> (v4.0) retrievals averaged over summer and winter for scenes with cloud fraction < 0.1 and surface albedo < 0.3. There is little difference in the scattering weight profile between winter and summer. Panel (b) shows the afternoon NO<sub>2</sub> profiles simulated by GEOS-Chem and GMI for summer (June, July, and August) and winter (December, January, and February) for the year 2015. The x-axis is shown on a log scale. Panel (c) shows the cumulative percent contribution from NO<sub>2</sub> at different altitudes to the tropospheric NO<sub>2</sub> columns as measured by OMI for summer and winter. It is calculated using Eq. (7). The shaded areas in panels (b) and (c) depict the standard deviations.

Figure 9b also shows the afternoon NO<sub>2</sub> number density from the GMI model. The GEOS-Chem and GMI profiles have consistent shapes, but there are differences in the free tropospheric NO<sub>2</sub> concentrations because of differences in NO<sub>x</sub> oxidation chemistry and lightning and aircraft NO<sub>x</sub> emissions. The NO<sub>x</sub> lifetime is longer in GMI compared to GEOS-Chem because of lower summertime OH concentrations in GMI and because GMI does not include NO<sub>x</sub> loss through the hydrolysis of NO<sub>3</sub> and N<sub>2</sub>O<sub>5</sub> in clouds and the formation of halogen nitrates. Both models use similar parameterizations for lightning emissions (Allen et al., 2010; Murray et al., 2012), but GMI assumes a higher NO yield over the US (500 moles per flash north of 26°N and 250 moles per flash south of it) than GEOS-Chem (500 moles per flash north of 35°N and 260 moles per flash south of it). Aircraft emissions in GMI are from an older inventory (Duncan et al., 2007) with global NO<sub>x</sub> emissions of 0.56 TgN a<sup>-1</sup> compared to 1.2 TgN a<sup>-1</sup> in our simulation.

We calculate the seasonal AMFs corresponding to the GEOS-Chem and GMI NO<sub>2</sub> profiles (Eq. 6) to determine the effect of different *a priori* profiles on the retrieved NO<sub>2</sub> columns. As before, we use scattering weights from the NASA OMI NO<sub>2</sub>

retrieval (v4.0) and exclude scenes with cloud fraction greater than 0.1 and surface albedo greater than 0.3. The scattering weight profile over the US is shown in Fig. 9a and shows values decreasing by a factor of 5 between the upper troposphere and the surface. The gradient is steeper than that for strictly clear-sky conditions (Martin et al., 2002). There is little seasonal difference in the scattering weight profile because scenes with high cloud fraction and bright surfaces were excluded, but AMF<sub>G</sub> is higher in winter (3.7) than in summer (2.6) because of higher solar zenith angles. In summer, the AMF calculated using the GEOS-Chem profile is  $1.14 \pm 0.11$ , compared to  $1.33 \pm 0.20$  calculated with the GMI profile. In winter, the AMFs from the two models are nearly identical (about 1.0). The AMFs are lower in winter than in summer because of higher NO<sub>2</sub> concentrations in winter in the boundary layer where satellite measurements are less sensitive. GEOS-Chem NO concentrations in the free troposphere were about 2 times higher than the measurements during SEAC<sup>4</sup>RS and DC3 (Fig. 1). If we decrease the GEOS-Chem NO<sub>2</sub> number density in the free troposphere by half in summer, then the AMF decreases to 0.98. Decreasing the NO<sub>2</sub> number density by half in the free troposphere and the boundary layer would have no effect on the AMF, since the shape factor (Eq. 6) would remain the same. Boersma et al. (2018) estimated a single-pixel uncertainty in the QA4ECV retrieval AMFs over the US of 20% in summer and 25% in winter, attributing about half (10%) of it to NO<sub>2</sub> profile uncertainty and the remaining to uncertainties in surface albedo and cloud properties. However, we find that the uncertainty in AMFs from errors in the *a priori* NO<sub>2</sub> profiles in summer is larger than 10%.

Figure 9c shows the cumulative contribution from different altitudes to the tropospheric NO<sub>2</sub> columns as would be measured by OMI. It is calculated as:

$$\Gamma(z) = 100 \times \frac{\int_z^{z_t} w(z) n(z) dz}{\int_0^{z_t} w(z) n(z) dz}, \quad (7)$$

where  $\Gamma(z)$  is the percent contribution to the tropospheric NO<sub>2</sub> column from NO<sub>2</sub> at and above altitude  $z$ ,  $z_t$  is the tropopause altitude, and  $w(z)$  and  $n(z)$  are the vertical profiles of scattering weight and NO<sub>2</sub> number density. The contribution of the free troposphere to NO<sub>2</sub> columns is significantly higher in summer than in winter. In summer, the free troposphere contributes  $65 \pm 9\%$  of the tropospheric NO<sub>2</sub> column over the US in GEOS-Chem ( $75 \pm 10\%$  in GMI), whereas in winter,  $75 \pm 11\%$  of the NO<sub>2</sub> column resides below 2 km. The free tropospheric contribution decreases to 55% if we halve the GEOS-Chem NO<sub>2</sub> column in the free troposphere in summer. Travis et al. (2016) had also calculated a free troposphere contribution of 70–75% from the GEOS-Chem NO<sub>2</sub> profiles in SEAC<sup>4</sup>RS.

The large contribution of the free troposphere to NO<sub>2</sub> columns affects the interpretation of satellite data in terms of NO<sub>x</sub> emissions. It greatly diminishes the sensitivity of the summertime NO<sub>2</sub> columns to changes in surface NO<sub>x</sub> emissions over the US. The free tropospheric contribution would be relatively smaller over major cities, where summertime NO<sub>2</sub> columns exceed  $3 \times 10^{15}$  molec cm<sup>-2</sup> (Lamsal et al., 2021), but it still needs to be accounted for. Urban NO<sub>x</sub> emissions and their trends are commonly derived by fitting an exponential decay function to satellite NO<sub>2</sub> columns downwind of the source (e.g., Beirle et al., 2011; Lorente et al., 2019; Goldberg et al., 2021). The fitting function includes a background offset term and thus implicitly accounts for the free tropospheric contribution. The free tropospheric contribution is also accounted for when models that

include lightning and aircraft NO<sub>x</sub> emissions are used to relate NO<sub>2</sub> columns to NO<sub>x</sub> emissions, but there is substantial uncertainty in the magnitude and distribution of lightning NO<sub>x</sub> emissions (Schumann and Huntrieser, 2007; Murray, 2016), which is the main source of NO<sub>2</sub> in the free troposphere in summer. Missing organic NO<sub>x</sub> chemistry in summer would also contribute to model errors in the free tropospheric NO<sub>2</sub>, as suggested by our SEAC<sup>4</sup>RS and DC3 analysis. Wintertime NO<sub>2</sub> columns will respond more strongly to changes in NO<sub>x</sub> emissions, but the uncertainty in the NO<sub>2</sub> retrievals associated with surface albedo and clouds is larger in winter (Boersma et al., 2018). Better observational constraints on free tropospheric NO<sub>2</sub> concentrations are needed.

#### 4. Conclusions

We used aircraft measurements from the SEAC<sup>4</sup>RS, DC3, and ATom campaigns to evaluate the vertical distribution of NO<sub>x</sub> in the free troposphere in the GEOS-Chem, GMI, TM5, and CAMS atmospheric chemistry models in the context of their use for retrieval and interpretation of satellite NO<sub>2</sub> column measurements. We first examined the accuracy of the in situ NO<sub>2</sub> measurements in the upper troposphere using observations made in a thunderstorm outflow during the DC3 campaign. We found that the laser induced fluorescence (LIF) and the photolysis-chemiluminescence (P-CL) NO<sub>2</sub> measurements were significantly higher than the NO<sub>2</sub> concentrations calculated using the NO measurements and the NO-NO<sub>2</sub> photochemical steady state (PSS), and that the ozone production expected based on these NO<sub>2</sub> measurements was much higher than the observed ozone production. This indicates a positive interference in the NO<sub>2</sub> measurements, presumably from dissociation of non-radical NO<sub>y</sub> species such as HNO<sub>4</sub> and methyl peroxy nitrate (MPN), even though the LIF measurements include a correction for the thermal dissociation of MPN. The underestimate in modeled NO<sub>2</sub> concentrations relative to the LIF measurements in the upper troposphere reported previously (Travis et al., 2016; Silvern et al., 2018) is likely due to the interference in the NO<sub>2</sub> measurements. There is a need to improve NO<sub>2</sub> measurements in the free troposphere. At present, NO<sub>2</sub> concentrations inferred by applying PSS to NO and other measurements provide a better estimate of free tropospheric NO<sub>2</sub> than the direct measurements, and we use them as basis for evaluating the models.

GEOS-Chem reproduces the shapes of the vertical profiles of the NO observations and the PSS-inferred NO<sub>2</sub> concentrations during SEAC<sup>4</sup>RS and DC3 over the southeastern US in summer. The NO<sub>2</sub> air mass factors (AMFs) calculated using the measured (PSS) and the GEOS-Chem NO<sub>2</sub> vertical profiles combined with scattering weights from the NASA OMI NO<sub>2</sub> v4.0 retrievals differ by less than 10%. However, GEOS-Chem overestimates NO<sub>2</sub> concentrations in the free troposphere for SEAC<sup>4</sup>RS and DC-3 by about a factor of 2, and underestimates concentrations of MPN and alkyl nitrates, suggesting missing organic NO<sub>x</sub> chemistry in the model that needs further examination.

The NO concentrations measured over the Pacific and Atlantic Oceans were reproduced by GEOS-Chem when pNO<sub>3</sub><sup>-</sup> photolysis was included in the model with photolysis frequencies 10–100 times higher than that of gas-phase HNO<sub>3</sub>, as

suggested by laboratory studies of  $\text{pNO}_3^-$  photolysis and field studies of HONO sources in the marine atmosphere (Ye et al., 2016a, 2017b; Andersen et al., 2022). The median  $\text{NO}_2$  column density for the ATom campaign was  $1.7 \pm 0.44 \times 10^{14}$  molec  $\text{cm}^{-2}$  for the observed PSS  $\text{NO}_2$  concentrations, and  $2.4 \times 10^{14}$  molec  $\text{cm}^{-2}$  for GEOS-Chem with  $\text{pNO}_3^-$  photolysis and  $1.5 \times 10^{14}$  molec  $\text{cm}^{-2}$  without. The  $\text{NO}_2$  column density for the GMI, TM5, and CAMS models was between  $1.4$  and  $2.5 \times 10^{14}$  molec  $\text{cm}^{-2}$  and the  $\text{NO}_2$  AMFs calculated using the PSS  $\text{NO}_2$  profiles and the simulated  $\text{NO}_2$  profiles differed by less than 20%. We conclude that model errors in the tropospheric  $\text{NO}_2$  profiles over the remote oceans are not a major source of uncertainty in the satellite  $\text{NO}_2$  retrievals. We calculated the contribution of surface, aircraft, and lightning emissions to  $\text{NO}_x$  columns over the Pacific and Atlantic Oceans and over the US in GEOS-Chem, and found that lightning is the main  $\text{NO}_x$  source over the tropics and southern midlatitudes, and over the US in the summer, contributing 62–73% of the  $\text{NO}_x$  columns in the free troposphere. However, aircraft emissions are the main source of free tropospheric  $\text{NO}_x$  in the northern mid-latitudes in winter and in summer over the oceans.

$\text{pNO}_3^-$  photolysis increases the global tropospheric mass of  $\text{NO}_x$ , OH and ozone in GEOS-Chem by 9%, 19%, and 10%, respectively.  $\text{NO}_x$  concentrations increase most in the tropical MBL where  $\text{NO}_x$  sources from PAN are small. There is a small increase in  $\text{NO}_x$  concentrations in the free troposphere over the continents, particularly in spring when the  $\text{pNO}_3^-$  concentration is highest. The increase in OH concentrations would degrade the model performance relative to OH measurements in ATom, but the ATom observations also indicate an underestimate in the modeled OH reactivity in the lower troposphere (Travis et al., 2020) implying missing OH sinks in the model.  $\text{pNO}_3^-$  photolysis increases ozone concentrations by up to 8 ppbv at the surface in the tropics and subtropics, and by 5 ppbv in the free troposphere over the northern extratropics, which would largely correct the low model bias relative to ozonesonde observations (Wang et al., 2021).

The seasonal GEOS-Chem and GMI afternoon  $\text{NO}_2$  profiles over the contiguous US are largely consistent with each other and show higher boundary layer  $\text{NO}_2$  columns in winter than in summer because of longer  $\text{NO}_x$  chemical lifetimes and slower ventilation to the free troposphere, but higher free tropospheric  $\text{NO}_2$  columns in summer because of lightning emissions. In winter, the free troposphere contributes  $25 \pm 11$  % of the  $\text{NO}_2$  columns that would be observed by satellite instruments over the contiguous US, but in summer this increases to 65–75%, and weakens the sensitivity of the summertime  $\text{NO}_2$  columns to changes in surface  $\text{NO}_x$  emissions. This is less of a problem for urban areas where boundary layer  $\text{NO}_2$  columns are generally much larger than the free tropospheric columns.

*Data availability:* The SEAC<sup>4</sup>RS aircraft measurements are available at <https://doi.org/10.5067/Aircraft/SEAC4RS/Aerosol-TraceGas-Cloud> (last access: 1 July 2021, SEAC<sup>4</sup>RS Science Team, 2014), DC3 at <https://doi.org/10.5067/Aircraft/DC3/DC8/Aerosol-TraceGas> (last access: 1 July 2021, DC3 Science Team, 2013), and ATom at <https://doi.org/10.3334/ORNLDAAAC/1925> (last access: 1 July 2022, Wofsy et al., 2021). The GMI model results for ATom are available at <https://doi.org/10.3334/ORNLDAAAC/1897> (last access: 1 July 2021, Strode et al., 2021). All other model results are available on request from the corresponding author.

865 *Author contributions:* VS and DJJ designed the study and led the analysis. RD helped with interpreting the GEOS-Chem results. LNL, SAS, and SDS provided the GMI simulation results and KFB provided the TM5 and CAMS results. SDE and TMF provided the updated AEIC inventory. CT, JP, IB, IP, BAN, RCC, PCJ, and JLJ made the NO, NO<sub>2</sub>, NO<sub>y</sub>, ozone, and pNO<sub>3</sub><sup>-</sup> measurements during the SEAC<sup>4</sup>RS, DC3, and ATom campaigns. STA, LJC, TS, and MJE helped with the pNO<sub>3</sub><sup>-</sup> photolysis simulation. VS and DJJ wrote the paper with input from all authors.

870 *Competing interests:* The authors declare that they have no conflict of interest.

*Acknowledgements:* We are grateful to the instrument teams of the SEAC<sup>4</sup>RS, DC3 and ATom campaigns for making their data freely available. We thank Tom Ryerson (NOAA) for contributing to the NO, NO<sub>2</sub>, NO<sub>y</sub>, and O<sub>3</sub> measurements in the three campaigns, and Eloïse Marais (U. College London) and Sunny Choi (NASA GSFC) for helpful discussions. This  
875 product/document has been created with or contains elements of Base of Aircraft Data (BADA) Family Release which has been made available by EUROCONTROL to MIT. EUROCONTROL has all relevant rights to BADA. ©2019 The European Organisation for the Safety of Air Navigation (EUROCONTROL). All rights reserved. EUROCONTROL shall not be liable for any direct, indirect, incidental, or consequential damages arising out of or in connection with this product or document, including with respect to the use of BADA. GMI is supported by the NASA Modeling, Analysis, and Prediction (MAP)  
880 program. GMI simulations used computational resources from the NASA High-End Computing (HEC) Program through the NASA Center for Climate Simulation (NCCS). JLJ and PCJ were supported by NASA Grant 80NSSC21K1451.

*Financial support:* This work was supported by the NASA Aura Science Team and by the US EPA Science To Achieve Results (STAR) program.

## 885 **References**

- Alexander, B., Sherwen, T., Holmes, C. D., Fisher, J. A., Chen, Q., Evans, M. J., and Kasibhatla, P.: Global inorganic nitrate production mechanisms: comparison of a global model with nitrate isotope observations, *Atmos. Chem. Phys.*, 20, 3859–3877, <https://doi.org/10.5194/acp-20-3859-2020>, 2020.
- Allen, D., Pickering, K., Duncan, B., and Damon, M.: Impact of lightning NO emissions on North American photochemistry as determined using the Global Modeling Initiative (GMI) model, *J. Geophys. Res.*, 115, D22301, <https://doi.org/10.1029/2010JD014062>, 2010.
- Allen, H. M., Crounse, J. D., Kim, M. J., Teng, A. P., and Wennberg, P. O.: Atmospheric Tomography Mission (ATom): L2 In Situ Data from Caltech Chemical Ionization Mass Spectrometer (CIT-CIMS), <https://doi.org/10.3334/ORNLDAAAC/1713>, 2019.
- 895 Andersen, S. T., Carpenter, L. J., Reed, C., Lee, J. D., Chance, R., Sherwen, T., Vaughan, A. R., Bloss, W. J., Sommariva, R., Nott, G., Neves, L., Read, K., Heard, D. E., Seakins, P. W., Whalley, L. K., Boustead, Fleming, L. T., Stone, D., and Fomba, K. W.: Extensive field evidence for the release of HONO from the photolysis of nitrate aerosols, *Sci Adv* (in review), 2022.
- Apel, E. C., Hornbrook, R. S., Hills, A. J., Blake, N. J., Barth, M. C., Weinheimer, A., Cantrell, C., Rutledge, S. A., Basarab, B., Crawford, J., Diskin, G., Homeyer, C. R., Campos, T., Flocke, F., Fried, A., Blake, D. R., Brune, W., Pollack, I. B., Peischl, J., Ryerson, T., Wennberg, P. O., Crounse, J. D., Wisthaler, A., Mikoviny, T., Huey, G., Heikes, B., O’Sullivan, D., and Riemer, D. D.: Upper tropospheric ozone production from lightning NO<sub>x</sub>-impacted convection: Smoke ingestion case study from the DC3 campaign, *J. Geophys. Res. Atmos.*, 120, 2505–2523, <https://doi.org/10.1002/2014JD022121>, 2015.
- 900 Baidar, S., Oetjen, H., Coburn, S., Dix, B., Ortega, I., Sinreich, R., and Volkamer, R.: The CU Airborne MAX-DOAS instrument: vertical profiling of aerosol extinction and trace gases, *Atmos. Meas. Tech.*, 6, 719–739, <https://doi.org/10.5194/amt-6-719-2013>, 2013.



- Bao, F., Li, M., Zhang, Y., Chen, C., and Zhao, J.: Photochemical Aging of Beijing Urban PM<sub>2.5</sub>: HONO Production, *Environ. Sci. Technol.*, 52, 6309–6316, <https://doi.org/10.1021/acs.est.8b00538>, 2018.
- Barth, M. C., Cantrell, C. A., Brune, W. H., Rutledge, S. A., Crawford, J. H., Huntrieser, H., Carey, L. D., MacGorman, D., Weisman, M., Pickering, K. E., Bruning, E., Anderson, B., Apel, E., Biggstaff, M., Campos, T., Campuzano-Jost, P., Cohen, R., Crounse, J., Day, D. A., Diskin, G., Flocke, F., Fried, A., Garland, C., Heikes, B., Honomichl, S., Hornbrook, R., Huey, L. G., Jimenez, J. L., Lang, T., Lichtenstern, M., Mikoviny, T., Nault, B., O’Sullivan, D., Pan, L. L., Peischl, J., Pollack, I., Richter, D., Riemer, D., Ryerson, T., Schlager, H., St. Clair, J., Walega, J., Weibring, P., Weinheimer, A., Wennberg, P., Wisthaler, A., Wooldridge, P. J., and Ziegler, C.: The Deep Convective Clouds and Chemistry (DC3) Field Campaign, *Bull. Amer. Meteor. Soc.*, 96, 1281–1309, <https://doi.org/10.1175/BAMS-D-13-00290.1>, 2015.
- 910 Beirle, S., Boersma, K. F., Platt, U., Lawrence, M. G., and Wagner, T.: Megacity Emissions and Lifetimes of Nitrogen Oxides Probed from Space, *Science*, 333, 1737–1739, <https://doi.org/10.1126/science.1207824>, 2011.
- Belmonte Rivas, M., Veeffkind, P., Eskes, H., and Levelt, P.: OMI tropospheric NO<sub>2</sub> profiles from cloud slicing: constraints on surface emissions, convective transport and lightning NO<sub>x</sub>, *Atmos. Chem. Phys.*, 15, 13519–13553, <https://doi.org/10.5194/acp-15-13519-2015>, 2015.
- 920 Benedict, K. B., McFall, A. S., and Anastasio, C.: Quantum Yield of Nitrite from the Photolysis of Aqueous Nitrate above 300 nm, *Environ. Sci. Technol.*, 51, 4387–4395, <https://doi.org/10.1021/acs.est.6b06370>, 2017.
- Bertram, T. H., Perring, A. E., Wooldridge, P. J., Crounse, J. D., Kwan, A. J., Wennberg, P. O., Scheuer, E., Dibb, J., Avery, M., Sachse, G., Vay, S. A., Crawford, J. H., McNaughton, C. S., Clarke, A., Pickering, K. E., Fuelberg, H., Huey, G., Blake, D. R., Singh, H. B., Hall, S. R., Shetter, R. E., Fried, A., Heikes, B. G., and Cohen, R. C.: Direct Measurements of the Convective Recycling of the Upper Troposphere, *Science*, 315, 816–820, <https://doi.org/10.1126/science.1134548>, 2007.
- 925 Bey, I., Jacob, D. J., Yantosca, R. M., Logan, J. A., Field, B. D., Fiore, A. M., Li, Q., Liu, H. Y., Mickley, L. J., and Schultz, M. G.: Global modeling of tropospheric chemistry with assimilated meteorology: Model description and evaluation, *J. Geophys. Res. Atmos.*, 106, 23073–23095, <https://doi.org/10.1029/2001JD000807>, 2001.
- Boersma, K. F., Jacob, D. J., Bucsela, E. J., Perring, A. E., Dirksen, R., van der A, R. J., Yantosca, R. M., Park, R. J., Wenig, M. O., and Bertram, T. H.: Validation of OMI tropospheric NO<sub>2</sub> observations during INTEX-B and application to constrain NO<sub>x</sub> emissions over the eastern United States and Mexico, *Atmos. Environ.*, 42, 4480–4497, <https://doi.org/10.1016/j.atmosenv.2008.02.004>, 2008.
- 930 Boersma, K. F., Eskes, H. J., Richter, A., De Smedt, I., Lorente, A., Beirle, S., van Geffen, J. H. G. M., Zara, M., Peters, E., Van Roozendaal, M., Wagner, T., Maasakkers, J. D., van der A, R. J., Nightingale, J., De Rudder, A., Irie, H., Pinardi, G., Lambert, J.-C., and Compernelle, S. C.: Improving algorithms and uncertainty estimates for satellite NO<sub>2</sub> retrievals: results from the quality assurance for the essential climate variables (QA4ECV) project, *Atmos Meas. Tech.*, 11, 6651–6678, <https://doi.org/10.5194/amt-11-6651-2018>, 2018.
- 935 Bourgeois, I., Peischl, J., Thompson, C. R., Aikin, K. C., Campos, T., Clark, H., Commane, R., Daube, B., Diskin, G. W., Elkins, J. W., Gao, R.-S., Gaudel, A., Hints, E. J., Johnson, B. J., Kivi, R., McKain, K., Moore, F. L., Parrish, D. D., Querel, R., Ray, E., Sánchez, R., Sweeney, C., Tarasick, D. W., Thompson, A. M., Thouret, V., Witte, J. C., Wofsy, S. C., and Ryerson, T. B.: Global-scale distribution of ozone in the remote troposphere from the ATom and HIPPO airborne field missions, *Atmos. Chem. Phys.*, 20, 10611–10635, <https://doi.org/10.5194/acp-20-10611-2020>, 2020.
- 940 Bourgeois, I., Peischl, J., Neuman, J. A., Brown, S. S., Thompson, C. R., Aikin, K. C., Allen, H. M., Angot, H., Apel, E. C., Baublitz, C. B., Brewer, J. F., Campuzano-Jost, P., Commane, R., Crounse, J. D., Daube, B. C., DiGangi, J. P., Diskin, G. S., Emmons, L. K., Fiore, A. M., Gkatzelis, G. I., Hills, A., Hornbrook, R. S., Huey, L. G., Jimenez, J. L., Kim, M., Lacey, F.,
- 945

- McKain, K., Murray, L. T., Nault, B. A., Parrish, D. D., Ray, E., Sweeney, C., Tanner, D., Wofsy, S. C., and Ryerson, T. B.: Large contribution of biomass burning emissions to ozone throughout the global remote troposphere, *Proc. Natl. Acad. Sci. U.S.A.*, 118, e2109628118, <https://doi.org/10.1073/pnas.2109628118>, 2021.
- 950 Bourgeois, I., Peischl, J., Neuman, J. A., Brown, S. S., Allen, H. M., Campuzano-Jost, P., Coggon, M. M., DiGangi, J. P., Diskin, G. S., Gilman, J. B., Gkatzelis, G. I., Guo, H., Halliday, H. A., Hanisco, T. F., Holmes, C. D., Huey, L. G., Jimenez, J. L., Lamplugh, A. D., Lee, Y. R., Lindaas, J., Moore, R. H., Nault, B. A., Nowak, J. B., Pagonis, D., Rickly, P. S., Robinson, M. A., Rollins, A. W., Selimovic, V., St. Clair, J. M., Tanner, D., Vasquez, K. T., Veres, P. R., Warneke, C., Wennberg, P. O., Washenfelder, R. A., Wiggins, E. B., Womack, C. C., Xu, L., Zarzana, K. J., and Ryerson, T. B.: Comparison of airborne measurements of NO, NO<sub>2</sub>, HONO, NO<sub>y</sub>, and CO during FIREX-AQ, *Atmos. Meas. Tech.*, 15, 4901–4930, <https://doi.org/10.5194/amt-15-4901-2022>, 2022.
- 955 Bradshaw, J., Davis, D., Crawford, J., Chen, G., Shetter, R., Müller, M., Gregory, G., Sachse, G., Blake, D., Heikes, B., Singh, H., Mastromarino, J., and Sandholm, S.: Photofragmentation two-photon laser-induced fluorescence detection of NO<sub>2</sub> and NO: Comparison of measurements with model results based on airborne observations during PEM-Tropics A, *Geophys. Res. Lett.*, 26, 471–474, <https://doi.org/10.1029/1999GL900015>, 1999.
- 960 Browne, E. C., Perring, A. E., Wooldridge, P. J., Apel, E., Hall, S. R., Huey, L. G., Mao, J., Spencer, K. M., Clair, J. M. St., Weinheimer, A. J., Wisthaler, A., and Cohen, R. C.: Global and regional effects of the photochemistry of CH<sub>3</sub> O<sub>2</sub>NO<sub>2</sub>: evidence from ARCTAS, *Atmos. Chem. Phys.*, 11, 4209–4219, <https://doi.org/10.5194/acp-11-4209-2011>, 2011.
- Brune, W. H., Miller, D.O., and Thames, A.B.: Atmospheric Tomography Mission (ATom): Measurements from Airborne Tropospheric Hydrogen Oxides Sensor (ATHOS), V2, <https://doi.org/10.3334/ORNLDAAAC/1930>, 2021.
- 965 Bucsela, E. J., Perring, A. E., Cohen, R. C., Boersma, K. F., Celarier, E. A., Gleason, J. F., Wenig, M. O., Bertram, T. H., Wooldridge, P. J., Dirksen, R., and Veefkind, J. P.: Comparison of tropospheric NO<sub>2</sub> from in situ aircraft measurements with near-real-time and standard product data from OMI, *J. Geophys. Res.*, 113, D16S31, <https://doi.org/10.1029/2007JD008838>, 2008.
- 970 Bucsela, E. J., Krotkov, N. A., Celarier, E. A., Lamsal, L. N., Swartz, W. H., Bhartia, P. K., Boersma, K. F., Veefkind, J. P., Gleason, J. F., and Pickering, K. E.: A new stratospheric and tropospheric NO<sub>2</sub> retrieval algorithm for nadir-viewing satellite instruments: applications to OMI, *Atmos. Meas. Tech.*, 6, 2607–2626, <https://doi.org/10.5194/amt-6-2607-2013>, 2013.
- Burkholder, J., Sander, S., Abbatt, J., Barker, J., Cappa, C., Crounse, J., Dibble, T., Huie, R., Kolb, C., Kurylo, M., and others: Chemical kinetics and photochemical data for use in atmospheric studies; evaluation number 19, Pasadena, CA: Jet Propulsion Laboratory, National Aeronautics and Space Administration, 2020.
- 975 Burley, J. D. and Johnston, H. S.: Ionic mechanisms for heterogeneous stratospheric reactions and ultraviolet photoabsorption cross sections for NO<sub>2</sub><sup>+</sup>, HNO<sub>3</sub>, and NO<sub>3</sub><sup>-</sup> in sulfuric acid, *Geophys. Res. Lett.*, 19, 1359–1362, <https://doi.org/10.1029/92GL01115>, 1992.
- Chen, H., Karion, A., Rella, C. W., Winderlich, J., Gerbig, C., Filges, A., Newberger, T., Sweeney, C., and Tans, P. P.: Accurate measurements of carbon monoxide in humid air using the cavity ring-down spectroscopy (CRDS) technique, *Atmos. Meas. Tech.*, 6, 1031–1040, <https://doi.org/10.5194/amt-6-1031-2013>, 2013.
- 980 Choi, S., Joiner, J., Choi, Y., Duncan, B. N., Vasilkov, A., Krotkov, N., and Bucsela, E.: First estimates of global free-tropospheric NO<sub>2</sub> abundances derived using a cloud-slicing technique applied to satellite observations from the Aura Ozone Monitoring Instrument (OMI), *Atmos. Chem. Phys.*, 14, 10565–10588, <https://doi.org/10.5194/acp-14-10565-2014>, 2014.

- Choi, S., Lamsal, L. N., Follette-Cook, M., Joiner, J., Krotkov, N. A., Swartz, W. H., Pickering, K. E., Loughner, C. P., Appel, W., Pfister, G., Saide, P. E., Cohen, R. C., Weinheimer, A. J., and Herman, J. R.: Assessment of NO<sub>2</sub> observations during DISCOVER-AQ and KORUS-AQ field campaigns, *Atmos. Meas. Tech.*, 13, 2523–2546, <https://doi.org/10.5194/amt-13-2523-2020>, 2020.
- Cleary, P. A., Wooldridge, P. J., and Cohen, R. C.: Laser-induced fluorescence detection of atmospheric NO<sub>2</sub> with a commercial diode laser and a supersonic expansion, *Appl. Opt.*, 41, 6950, <https://doi.org/10.1364/AO.41.006950>, 2002.
- Cooper, O. R., Stohl, A., Trainer, M., Thompson, A. M., Witte, J. C., Oltmans, S. J., Morris, G., Pickering, K. E., Crawford, J. H., Chen, G., Cohen, R. C., Bertram, T. H., Wooldridge, P., Perring, A., Brune, W. H., Merrill, J., Moody, J. L., Tarasick, D., Nédélec, P., Forbes, G., Newchurch, M. J., Schmidlin, F. J., Johnson, B. J., Turquety, S., Baughcum, S. L., Ren, X., Fehsenfeld, F. C., Meagher, J. F., Spichtinger, N., Brown, C. C., McKeen, S. A., McDermid, I. S., and Leblanc, T.: Large upper tropospheric ozone enhancements above midlatitude North America during summer: In situ evidence from the IONS and MOZAIC ozone measurement network, *J. Geophys. Res.*, 111, D24S05, <https://doi.org/10.1029/2006JD007306>, 2006.
- Crawford, J., Davis, D., Chen, G., Bradshaw, J., Sandholm, S., Gregory, G., Sachse, G., Anderson, B., Collins, J., Blake, D., Singh, H., Heikes, B., Talbot, R., and Rodriguez, J.: Photostationary state analysis of the NO<sub>2</sub>-NO system based on airborne observations from the western and central North Pacific, *J. Geophys. Res.*, 101, 2053–2072, <https://doi.org/10.1029/95JD02201>, 1996.
- Crawford, J., Davis, D., Olson, J., Chen, G., Liu, S., Fuelberg, H., Hannan, J., Kondo, Y., Anderson, B., Gregory, G., Sachse, G., Talbot, R., Viggiano, A., Heikes, B., Snow, J., Singh, H., and Blake, D.: Evolution and chemical consequences of lightning-produced NO<sub>x</sub> observed in the North Atlantic upper troposphere, *J. Geophys. Res.*, 105, 19795–19809, <https://doi.org/10.1029/2000JD900183>, 2000.
- Davis, D. D., Chen, G., Chameides, W., Bradshaw, J., Sandholm, S., Rodgers, M., Schendal, J., Madronich, S., Sachse, G., Gregory, G., Anderson, B., Barrick, J., Shipham, M., Collins, J., Wade, L., and Blake, D.: A photostationary state analysis of the NO<sub>2</sub>-NO system based on airborne observations from the subtropical/tropical North and South Atlantic, *J. Geophys. Res.*, 98, 23501, <https://doi.org/10.1029/93JD02412>, 1993.
- Day, D. A., Wooldridge, P. J., Dillon, M. B., Thornton, J. A., and Cohen, R. C.: A thermal dissociation laser-induced fluorescence instrument for in situ detection of NO<sub>2</sub>, peroxy nitrates, alkyl nitrates, and HNO<sub>3</sub>, *J. Geophys. Res. Atmos.*, 107, ACH 4-1-ACH 4-14, <https://doi.org/10.1029/2001JD000779>, 2002.
- DC3 Science Team: DC3 Field Campaign Data from DC-8 aircraft, <https://doi.org/10.5067/AIRCRAFT/DC3/DC8/AEROSOL-TRACEGAS>, 2013.
- Dibb, J. E.: Atmospheric Tomography Mission (ATom): Measurements of Soluble Acidic Gases and Aerosols (SAGA), <https://doi.org/10.3334/ORNLDAAAC/1748>, 2020.
- Du, J. and Zhu, L.: Quantification of the absorption cross sections of surface-adsorbed nitric acid in the 335–365nm region by Brewster angle cavity ring-down spectroscopy, *Chemical Physics Letters*, 511, 213–218, <https://doi.org/10.1016/j.cplett.2011.06.062>, 2011.
- Duncan, B. N., Strahan, S. E., Yoshida, Y., Steenrod, S. D., and Livesey, N.: Model study of the cross-tropopause transport of biomass burning pollution, *Atmos. Chem. Phys.*, 7, 3713–3736, <https://doi.org/10.5194/acp-7-3713-2007>, 2007.
- Eastham, S. D., Weisenstein, D. K., and Barrett, S. R. H.: Development and Evaluation of the Unified Tropospheric–Stratospheric Chemistry Extension (UCX) for the Global Chemistry-Transport Model GEOS-Chem, *Atmos. Environ.*, 89, 52–63, <https://doi.org/10.1016/j.atmosenv.2014.02.001>, 2014.

Air Pollutant Emissions Inventory: <https://www.canada.ca/en/environment-climate-change/services/pollutants/air-emissions-inventory-overview.html>, last access: 1 January 2017.

- 1025 Elshorbany, Y. F., Steil, B., Brühl, C., and Lelieveld, J.: Impact of HONO on global atmospheric chemistry calculated with an empirical parameterization in the EMAC model, *Atmos. Chem. Phys.*, 12, 9977–10000, <https://doi.org/10.5194/acp-12-9977-2012>, 2012.
- Emmons, L. K., Carroll, M. A., Hauglustaine, D. A., Brasseur, G. P., Atherton, C., Penner, J., Sillman, S., Levy, H., Rohrer, F., Wauben, W. M. F., Van Velthoven, P. F. J., Wang, Y., Jacob, D., Bakwin, P., Dickerson, R., Doddridge, B., Gerbig, C., 1030 Honrath, R., Hübler, G., Jaffe, D., Kondo, Y., Munger, J. W., Torres, A., and Volz-Thomas, A.: Climatologies of NO<sub>x</sub> and NO<sub>y</sub>: A comparison of data and models, *Atmos. Environ.*, 31, 1851–1904, [https://doi.org/10.1016/S1352-2310\(96\)00334-2](https://doi.org/10.1016/S1352-2310(96)00334-2), 1997.
- ESA Sentinel-4 Data Products: <https://sentinel.esa.int/web/sentinel/missions/sentinel-4/data-products>, last access: 15 May 2022.
- 1035 Eskes, H. J. and Boersma, K. F.: Averaging kernels for DOAS total-column satellite retrievals, *Atmos. Chem. Phys.*, 3, 1285–1291, <https://doi.org/10.5194/acp-3-1285-2003>, 2003.
- Fairlie, T. D., Jacob, D. J., Dibb, J. E., Alexander, B., Avery, M. A., van Donkelaar, A., and Zhang, L.: Impact of mineral dust on nitrate, sulfate, and ozone in transpacific Asian pollution plumes, *Atmos. Chem. Phys.*, 10, 3999–4012, <https://doi.org/10.5194/acp-10-3999-2010>, 2010.
- 1040 Faloon, I. C., Tan, D., Leshner, R. L., Hazen, N. L., Frame, C. L., Simpas, J. B., Harder, H., Martinez, M., Di Carlo, P., Ren, X., and Brune, W. H.: A Laser-induced Fluorescence Instrument for Detecting Tropospheric OH and HO<sub>2</sub>: Characteristics and Calibration, *Journal of Atmospheric Chemistry*, 47, 139–167, <https://doi.org/10.1023/B:JOCH.0000021036.53185.0e>, 2004.
- Fan, S.-M., Jacob, D. J., Mauzerall, D. L., Bradshaw, J. D., Sandholm, S. T., Blake, D. R., Singh, H. B., Talbot, R. W., Gregory, G. L., and Sachse, G. W.: Origin of tropospheric NO<sub>x</sub> over subarctic eastern Canada in summer, *J. Geophys. Res.*, 99, 16867, 1045 <https://doi.org/10.1029/94JD01122>, 1994.
- Fischer, E. V., Jacob, D. J., Yantosca, R. M., Sulprizio, M. P., Millet, D. B., Mao, J., Paulot, F., Singh, H. B., Roiger, A., Ries, L., Talbot, R. W., Dzepina, K., and Pandey Deolal, S.: Atmospheric peroxyacetyl nitrate (PAN): a global budget and source attribution, *Atmos. Chem. Phys.*, 14, 2679–2698, <https://doi.org/10.5194/acp-14-2679-2014>, 2014.
- Fisher, J. A., Atlas, E. L., Barletta, B., Meinardi, S., Blake, D. R., Thompson, C. R., Ryerson, T. B., Peischl, J., Tzompa-Sosa, Z. A., and Murray, L. T.: Methyl, Ethyl, and Propyl Nitrates: Global Distribution and Impacts on Reactive Nitrogen in Remote 1050 Marine Environments, *J. Geophys. Res. Atmos.*, 123, 12,429–12,451, <https://doi.org/10.1029/2018JD029046>, 2018.
- Fountoukis, C. and Nenes, A.: ISORROPIA II: a computationally efficient thermodynamic equilibrium model for K<sup>+</sup>–Ca<sup>2+</sup>–Mg<sup>2+</sup>–NH<sub>4</sub><sup>+</sup>–Na<sup>+</sup>–SO<sub>4</sub><sup>2-</sup>–NO<sub>3</sub><sup>-</sup>–Cl<sup>-</sup>–H<sub>2</sub>O aerosols, *Atmos. Chem. Phys.*, 7, 4639–4659, <https://doi.org/10.5194/acp-7-4639-2007>, 2007.
- 1055 Fridlind, A. M. and Jacobson, M. Z.: A study of gas-aerosol equilibrium and aerosol pH in the remote marine boundary layer during the First Aerosol Characterization Experiment (ACE 1), *J. Geophys. Res.*, 105, 17325–17340, <https://doi.org/10.1029/2000JD900209>, 2000.
- Fuchs, H., Ball, S. M., Bohn, B., Brauers, T., Cohen, R. C., Dorn, H.-P., Dubé, W. P., Fry, J. L., Häsel, R., Heitmann, U., Jones, R. L., Kleffmann, J., Mentel, T. F., Müsgen, P., Rohrer, F., Rollins, A. W., Ruth, A. A., Kiendler-Scharr, A., Schlosser, E., Shillings, A. J. L., Tillmann, R., Varma, R. M., Venables, D. S., Villena Tapia, G., Wahner, A., Wegener, R., Wooldridge, 1060

- P. J., and Brown, S. S.: Intercomparison of measurements of NO<sub>2</sub> concentrations in the atmosphere simulation chamber SAPHIR during the NO<sub>3</sub>Comp campaign, *Atmos. Meas. Tech.*, 3, 21–37, <https://doi.org/10.5194/amt-3-21-2010>, 2010.
- van Geffen, J., Eskes, H., Compernelle, S., Pinardi, G., Verhoelst, T., Lambert, J.-C., Sneep, M., ter Linden, M., Ludewig, A., Boersma, K. F., and Veefkind, J. P.: Sentinel-5P TROPOMI NO<sub>2</sub> retrieval: impact of version v2.2 improvements and comparisons with OMI and ground-based data, *Atmos. Meas. Tech.*, 15, 2037–2060, <https://doi.org/10.5194/amt-15-2037-2022>, 2022.
- Gelaro, R., McCarty, W., Suárez, M. J., Todling, R., Molod, A., Takacs, L., Randles, C. A., Darmenov, A., Bosilovich, M. G., Reichle, R., Wargan, K., Coy, L., Cullather, R., Draper, C., Akella, S., Buchard, V., Conaty, A., da Silva, A. M., Gu, W., Kim, G.-K., Koster, R., Lucchesi, R., Merkova, D., Nielsen, J. E., Partyka, G., Pawson, S., Putman, W., Rienecker, M., Schubert, S. D., Sienkiewicz, M., and Zhao, B.: The Modern-Era Retrospective Analysis for Research and Applications, Version 2 (MERRA-2), *J. Climate*, 30, 5419–5454, <https://doi.org/10.1175/JCLI-D-16-0758.1>, 2017.
- Gen, M., Zhang, R., Huang, D. D., Li, Y., and Chan, C. K.: Heterogeneous Oxidation of SO<sub>2</sub> in Sulfate Production during Nitrate Photolysis at 300 nm: Effect of pH, Relative Humidity, Irradiation Intensity, and the Presence of Organic Compounds, *Environ. Sci. Technol.*, 53, 8757–8766, <https://doi.org/10.1021/acs.est.9b01623>, 2019.
- Giglio, L., Randerson, J. T., and van der Werf, G. R.: Analysis of daily, monthly, and annual burned area using the fourth-generation global fire emissions database (GFED4), *J. Geophys. Res. Biogeo.*, 118, 317–328, <https://doi.org/10.1002/jgrg.20042>, 2013.
- Goldberg, D. L., Anenberg, S. C., Lu, Z., Streets, D. G., Lamsal, L. N., McDuffie, E., and Smith, S. J.: Urban NO<sub>x</sub> emissions around the world declined faster than anticipated between 2005 and 2019, *Environ. Res. Lett.*, 16, 115004, <https://doi.org/10.1088/1748-9326/ac2c34>, 2021.
- Gregory, G. L., Hoell, J. M., Torres, A. L., Carroll, M. A., Ridley, B. A., Rodgers, M. O., Bradshaw, J., Sandholm, S., and Davis, D. D.: An intercomparison of airborne nitric oxide measurements: A second opportunity, *J. Geophys. Res.*, 95, 10129–10138, <https://doi.org/10.1029/JD095iD07p10129>, 1990a.
- Gregory, G. L., Hoell, J. M., Carroll, M. A., Ridley, B. A., Davis, D. D., Bradshaw, J., Rodgers, M. O., Sandholm, S. T., Schiff, H. I., Hastie, D. R., Karecki, D. R., Mackay, G. I., Harris, G. W., Torres, A. L., and Fried, A.: An intercomparison of airborne nitrogen dioxide instruments, *J. Geophys. Res.*, 95, 10103–10127, <https://doi.org/10.1029/JD095iD07p10103>, 1990b.
- Guo, H., Flynn, C. M., Prather, M. J., Strode, S. A., Steenrod, S. D., Emmons, L., Lacey, F., Lamarque, J.-F., Fiore, A. M., Correa, G., Murray, L. T., Wolfe, G. M., St. Clair, J. M., Kim, M., Crounse, J., Diskin, G., DiGangi, J., Daube, B. C., Commane, R., McKain, K., Peischl, J., Ryerson, T. B., Thompson, C., Hanisco, T. F., Blake, D., Blake, N. J., Apel, E. C., Hornbrook, R. S., Elkins, J. W., Hints, E. J., Moore, F. L., and Wofsy, S.: Heterogeneity and chemical reactivity of the remote troposphere defined by aircraft measurements, *Atmos. Chem. Phys.*, 21, 13729–13746, <https://doi.org/10.5194/acp-21-13729-2021>, 2021a.
- Guo, H., Campuzano-Jost, P., Nault, B. A., Day, D. A., Schroder, J. C., Kim, D., Dibb, J. E., Dollner, M., Weinzierl, B., and Jimenez, J. L.: The importance of size ranges in aerosol instrument intercomparisons: a case study for the Atmospheric Tomography Mission, *Atmos. Meas. Tech.*, 14, 3631–3655, <https://doi.org/10.5194/amt-14-3631-2021>, 2021b.
- Hains, J. C., Boersma, K. F., Kroon, M., Dirksen, R. J., Cohen, R. C., Perring, A. E., Bucsela, E., Volten, H., Swart, D. P. J., Richter, A., Wittrock, F., Schoenhardt, A., Wagner, T., Ibrahim, O. W., van Roozendaal, M., Pinardi, G., Gleason, J. F., Veefkind, J. P., and Levelt, P.: Testing and improving OMI DOMINO tropospheric NO<sub>2</sub> using observations from the DANDELIONS and INTEx-B validation campaigns, *J. Geophys. Res.*, 115, D05301, <https://doi.org/10.1029/2009JD012399>, 2010.

- 1100 Hall, S. R. and Ullmann, K.: Atmospheric Tomography Mission (ATom): Actinic Flux and Photolysis Frequencies from CAFS Instrument, 2016-2018, V2, <https://doi.org/10.3334/ORNLDAAAC/1933>, 2021.
- Hayes, P. L., Ortega, A. M., Cubison, M. J., Froyd, K. D., Zhao, Y., Cliff, S. S., Hu, W. W., Toohey, D. W., Flynn, J. H., Lefer, B. L., Grossberg, N., Alvarez, S., Rappenglück, B., Taylor, J. W., Allan, J. D., Holloway, J. S., Gilman, J. B., Kuster, W. C., de Gouw, J. A., Massoli, P., Zhang, X., Liu, J., Weber, R. J., Corrigan, A. L., Russell, L. M., Isaacman, G., Worton, D.  
1105 R., Kreisberg, N. M., Goldstein, A. H., Thalman, R., Waxman, E. M., Volkamer, R., Lin, Y. H., Surratt, J. D., Kleindienst, T. E., Offenberg, J. H., Dusanter, S., Griffith, S., Stevens, P. S., Brioude, J., Angevine, W. M., and Jimenez, J. L.: Organic aerosol composition and sources in Pasadena, California, during the 2010 CalNex campaign, *J. Geophys. Res. Atmos.*, 118, 9233–9257, <https://doi.org/10.1002/jgrd.50530>, 2013.
- Heim, E. W., Dibb, J., Scheuer, E., Jost, P. C., Nault, B. A., Jimenez, J. L., Peterson, D., Knote, C., Fenn, M., Hair, J.,  
1110 Beyersdorf, A. J., Corr, C., and Anderson, B. E.: Asian dust observed during KORUS-AQ facilitates the uptake and incorporation of soluble pollutants during transport to South Korea, *Atmospheric Environment*, 224, 117305, <https://doi.org/10.1016/j.atmosenv.2020.117305>, 2020.
- Henderson, B. H., Pinder, R. W., Crooks, J., Cohen, R. C., Hutzell, W. T., Sarwar, G., Goliff, W. S., Stockwell, W. R., Fahr, A., Mathur, R., Carlton, A. G., and Vizuete, W.: Evaluation of simulated photochemical partitioning of oxidized nitrogen in  
1115 the upper troposphere, *Atmos. Chem. Phys.*, 11, 275–291, <https://doi.org/10.5194/acp-11-275-2011>, 2011.
- Hodzic, A., Campuzano-Jost, P., Bian, H., Chin, M., Colarco, P. R., Day, D. A., Froyd, K. D., Heinold, B., Jo, D. S., Katich, J. M., Kodros, J. K., Nault, B. A., Pierce, J. R., Ray, E., Schacht, J., Schill, G. P., Schroder, J. C., Schwarz, J. P., Sueper, D. T., Tegen, I., Tilmes, S., Tsigaridis, K., Yu, P., and Jimenez, J. L.: Characterization of organic aerosol across the global remote troposphere: a comparison of ATom measurements and global chemistry models, *Atmos. Chem. Phys.*, 20, 4607–4635,  
1120 <https://doi.org/10.5194/acp-20-4607-2020>, 2020.
- Hoesly, R. M., Smith, S. J., Feng, L., Klimont, Z., Janssens-Maenhout, G., Pitkanen, T., Seibert, J. J., Vu, L., Andres, R. J., Bolt, R. M., Bond, T. C., Dawidowski, L., Kholod, N., Kurokawa, J., Li, M., Liu, L., Lu, Z., Moura, M. C. P., O&apos;Rourke, P. R., and Zhang, Q.: Historical (1750–2014) anthropogenic emissions of reactive gases and aerosols from the Community Emissions Data System (CEDS), *Geosci. Model Dev.*, 11, 369–408, <https://doi.org/10.5194/gmd-11-369-2018>, 2018.  
1125
- Holmes, C. D., Prather, M. J., and Vinken, G. C. M.: The climate impact of ship NO<sub>x</sub> emissions: an improved estimate accounting for plume chemistry, *Atmospheric Chemistry and Physics*, 14, 6801–6812, <https://doi.org/10.5194/acp-14-6801-2014>, 2014.
- Holmes, C. D., Bertram, T. H., Confer, K. L., Graham, K. A., Ronan, A. C., Wirks, C. K., and Shah, V.: The Role of Clouds  
1130 in the Tropospheric NO<sub>x</sub> Cycle: A New Modeling Approach for Cloud Chemistry and Its Global Implications, *Geophys. Res. Lett.*, 46, 4980–4990, <https://doi.org/10.1029/2019GL081990>, 2019.
- Horowitz, L. W., Walters, S., Mauzerall, D. L., Emmons, L. K., Rasch, P. J., Granier, C., Tie, X., Lamarque, J.-F., Schultz, M. G., Tyndall, G. S., Orlando, J. J., and Brasseur, G. P.: A global simulation of tropospheric ozone and related tracers: Description and evaluation of MOZART, version 2., *J. Geophys. Res.*, 108, 4784, <https://doi.org/10.1029/2002JD002853>,  
1135 2003.
- Hudman, R. C., Jacob, D. J., Turquety, S., Leibensperger, E. M., Murray, L. T., Wu, S., Gilliland, A. B., Avery, M., Bertram, T. H., Brune, W., Cohen, R. C., Dibb, J. E., Flocke, F. M., Fried, A., Holloway, J., Neuman, J. A., Orville, R., Perring, A., Ren, X., Sachse, G. W., Singh, H. B., Swanson, A., and Wooldridge, P. J.: Surface and lightning sources of nitrogen oxides over the United States: Magnitudes, chemical evolution, and outflow, *J. Geophys. Res.*, 112,  
1140 <https://doi.org/10.1029/2006JD007912>, 2007.

- Hudman, R. C., Moore, N. E., Mebust, A. K., Martin, R. V., Russell, A. R., Valin, L. C., and Cohen, R. C.: Steps towards a mechanistic model of global soil nitric oxide emissions: implementation and space based-constraints, *Atmos. Chem. Phys.*, 12, 7779–7795, <https://doi.org/10.5194/acp-12-7779-2012>, 2012.
- Huijnen, V., Williams, J., van Weele, M., van Noije, T., Krol, M., Dentener, F., Segers, A., Houweling, S., Peters, W., de Laat, J., Boersma, F., Bergamaschi, P., van Velthoven, P., Le Sager, P., Eskes, H., Alkemade, F., Scheele, R., Nédélec, P., and Pätz, H.-W.: The global chemistry transport model TM5: description and evaluation of the tropospheric chemistry version 3.0, *Geosci. Model Dev.*, 3, 445–473, <https://doi.org/10.5194/gmd-3-445-2010>, 2010.
- Inness, A., Ades, M., Agustí-Panareda, A., Barré, J., Benedictow, A., Blechschmidt, A.-M., Dominguez, J. J., Engelen, R., Eskes, H., Flemming, J., Huijnen, V., Jones, L., Kipling, Z., Massart, S., Parrington, M., Peuch, V.-H., Razinger, M., Remy, S., Schulz, M., and Suttie, M.: The CAMS reanalysis of atmospheric composition, *Atmos. Chem. Phys.*, 19, 3515–3556, <https://doi.org/10.5194/acp-19-3515-2019>, 2019.
- Jaeglé, L., Jacob, D. J., Wang, Y., Weinheimer, A. J., Ridley, B. A., Campos, T. L., Sachse, G. W., and Hagen, D. E.: Sources and chemistry of NO<sub>x</sub> in the upper troposphere over the United States, *Geophys. Res. Lett.*, 25, 1705–1708, <https://doi.org/10.1029/97GL03591>, 1998a.
- Jaeglé, L., Jacob, D. J., Brune, W. H., Tan, D., Faloona, I. C., Weinheimer, A. J., Ridley, B. A., Campos, T. L., and Sachse, G. W.: Sources of HO<sub>x</sub> and production of ozone in the upper troposphere over the United States, *Geophys. Res. Lett.*, 25, 1709–1712, <https://doi.org/10.1029/98GL00041>, 1998b.
- Jaeglé, L., Quinn, P. K., Bates, T. S., Alexander, B., and Lin, J.-T.: Global distribution of sea salt aerosols: new constraints from in situ and remote sensing observations, *Atmos. Chem. Phys.*, 11, 3137–3157, <https://doi.org/10.5194/acp-11-3137-2011>, 2011.
- Jaeglé, L., Shah, V., Thornton, J. A., Lopez-Hilfiker, F. D., Lee, B. H., McDuffie, E. E., Fibiger, D., Brown, S. S., Veres, P., Sparks, T. L., Ebben, C. J., Wooldridge, P. J., Kenagy, H. S., Cohen, R. C., Weinheimer, A. J., Campos, T. L., Montzka, D. D., Digangi, J. P., Wolfe, G. M., Hanisco, T., Schroder, J. C., Campuzano-Jost, P., Day, D. A., Jimenez, J. L., Sullivan, A. P., Guo, H., and Weber, R. J.: Nitrogen Oxides Emissions, Chemistry, Deposition, and Export Over the Northeast United States During the WINTER Aircraft Campaign, *J. Geophys. Res. Atmos.*, 123, 12,368–12,393, <https://doi.org/10.1029/2018JD029133>, 2018.
- Javed, U., Kubistin, D., Martinez, M., Pollmann, J., Rudolf, M., Parchatka, U., Reiffs, A., Thieser, J., Schuster, G., Horbanski, M., Pöhler, D., Crowley, J. N., Fischer, H., Lelieveld, J., and Harder, H.: Laser-induced fluorescence-based detection of atmospheric nitrogen dioxide and comparison of different techniques during the PARADE 2011 field campaign, *Atmos. Meas. Tech.*, 12, 1461–1481, <https://doi.org/10.5194/amt-12-1461-2019>, 2019.
- Karydis, V. A., Tsimpidi, A. P., Pozzer, A., Astitha, M., and Lelieveld, J.: Effects of mineral dust on global atmospheric nitrate concentrations, *Atmos. Chem. Phys.*, 16, 1491–1509, <https://doi.org/10.5194/acp-16-1491-2016>, 2016.
- Kasibhatla, P., Sherwen, T., Evans, M. J., Carpenter, L. J., Reed, C., Alexander, B., Chen, Q., Sulprizio, M. P., Lee, J. D., Read, K. A., Bloss, W., Crilley, L. R., Keene, W. C., Pszenny, A. A. P., and Hodzic, A.: Global impact of nitrate photolysis in sea-salt aerosol on NO<sub>x</sub>, OH, and O<sub>3</sub> in the marine boundary layer, *Atmos. Chem. Phys.*, 18, 11185–11203, <https://doi.org/10.5194/acp-18-11185-2018>, 2018.
- Kenagy, H. S., Sparks, T. L., Ebben, C. J., Wooldridge, P. J., Lopez-Hilfiker, F. D., Lee, B. H., Thornton, J. A., McDuffie, E. E., Fibiger, D. L., Brown, S. S., Montzka, D. D., Weinheimer, A. J., Schroder, J. C., Campuzano-Jost, P., Day, D. A., Jimenez, J. L., Dibb, J. E., Campos, T., Shah, V., Jaeglé, L., and Cohen, R. C.: NO<sub>x</sub> Lifetime and NO<sub>y</sub> Partitioning During WINTER, *Journal of Geophysical Research: Atmospheres*, 123, 9813–9827, <https://doi.org/10.1029/2018JD028736>, 2018.

- Khan, M. A. H., Miles, B., Jenkin, M. E., Derwent, R. G., Percival, C. J., and Shallcross, D. E.: Investigating the Impacts of Nonacyl Peroxy Nitrates on the Global Composition of the Troposphere Using a 3-D Chemical Transport Model, STOCHEM-CRI, ACS Earth Space Chem., 4, 1201–1212, <https://doi.org/10.1021/acsearthspacechem.0c00133>, 2020.
- Kim, H., Park, R. J., Kim, S., Brune, W. H., Diskin, G. S., Fried, A., Hall, S. R., Weinheimer, A. J., Wennberg, P. O., Wisthaler, A., Blake, D. R., and Ullmann, K.: Observed versus simulated OH reactivity during KORUS-AQ campaign: implications for emission inventory and chemical environment in East Asia, *Elementa* (in review), 2022.
- Kim, S., Huey, L. G., Stickel, R. E., Tanner, D. J., Crawford, J. H., Olson, J. R., Chen, G., Brune, W. H., Ren, X., Leshner, R., Wooldridge, P. J., Bertram, T. H., Perring, A., Cohen, R. C., Lefer, B. L., Shetter, R. E., Avery, M., Diskin, G., and Sokolik, I.: Measurement of HO<sub>2</sub>NO<sub>2</sub> in the free troposphere during the Intercontinental Chemical Transport Experiment–North America 2004, *J. Geophys. Res. Atmos.*, 112, <https://doi.org/10.1029/2006JD007676>, 2007.
- Kleinman, L. I., Springston, S. R., Daum, P. H., Lee, Y.-N., Nunnermacker, L. J., Senum, G. I., Wang, J., Weinstein-Lloyd, J., Alexander, M. L., Hubbe, J., Ortega, J., Canagaratna, M. R., and Jayne, J.: The time evolution of aerosol composition over the Mexico City plateau, *Atmos. Chem. Phys.*, 8, 1559–1575, <https://doi.org/10.5194/acp-8-1559-2008>, 2008.
- Krotkov, N. A., McLinden, C. A., Li, C., Lamsal, L. N., Celarier, E. A., Marchenko, S. V., Swartz, W. H., Bucsela, E. J., Joiner, J., Duncan, B. N., Boersma, K. F., Veeckind, J. P., Levelt, P. F., Fioletov, V. E., Dickerson, R. R., He, H., Lu, Z., and Streets, D. G.: Aura OMI observations of regional SO<sub>2</sub> and NO<sub>2</sub> pollution changes from 2005 to 2015, *Atmos. Chem. Phys.*, 16, 4605–4629, <https://doi.org/10.5194/acp-16-4605-2016>, 2016.
- Krotkov, N. A., Lamsal, L. N., Celarier, E. A., Swartz, W. H., Marchenko, S. V., Bucsela, E. J., Chan, K. L., Wenig, M., and Zara, M.: The version 3 OMI NO<sub>2</sub> standard product, *Atmos. Meas. Tech.*, 10, 3133–3149, <https://doi.org/10.5194/amt-10-3133-2017>, 2017.
- Lamarque, J.-F., Brasseur, G. P., Hess, P. G., and Müller, J.-F.: Three-dimensional study of the relative contributions of the different nitrogen sources in the troposphere, *J. Geophys. Res.*, 101, 22955–22968, <https://doi.org/10.1029/96JD02160>, 1996.
- Lamsal, L. N., Martin, R. V., Padmanabhan, A., van Donkelaar, A., Zhang, Q., Sioris, C. E., Chance, K., Kurosu, T. P., and Newchurch, M. J.: Application of satellite observations for timely updates to global anthropogenic NO<sub>x</sub> emission inventories, *Geophys. Res. Lett.*, 38, <https://doi.org/10.1029/2010GL046476>, 2011.
- Lamsal, L. N., Krotkov, N. A., Celarier, E. A., Swartz, W. H., Pickering, K. E., Bucsela, E. J., Gleason, J. F., Martin, R. V., Philip, S., Irie, H., Cede, A., Herman, J., Weinheimer, A., Szykman, J. J., and Knepp, T. N.: Evaluation of OMI operational standard NO<sub>2</sub> column retrievals using in situ and surface-based NO<sub>2</sub> observations, *Atmos. Chem. Phys.*, 14, 11587–11609, <https://doi.org/10.5194/acp-14-11587-2014>, 2014.
- Lamsal, L. N., Krotkov, N. A., Vasilkov, A., Marchenko, S., Qin, W., Yang, E.-S., Fasnacht, Z., Joiner, J., Choi, S., Haffner, D., Swartz, W. H., Fisher, B., and Bucsela, E.: Ozone Monitoring Instrument (OMI) Aura nitrogen dioxide standard product version 4.0 with improved surface and cloud treatments, *Atmos. Meas. Tech.*, 14, 455–479, <https://doi.org/10.5194/amt-14-455-2021>, 2021.
- Laughner, J. L., Zhu, Q., and Cohen, R. C.: Evaluation of version 3.0B of the BEHR OMI NO<sub>2</sub> product, *Atmos. Meas. Tech.*, 12, 129–146, <https://doi.org/10.5194/amt-12-129-2019>, 2019.
- Levy, H., Moxim, W. J., Klonecki, A. A., and Kasibhatla, P. S.: Simulated tropospheric NO<sub>x</sub>: Its evaluation, global distribution and individual source contributions, *J. Geophys. Res.*, 104, 26279–26306, <https://doi.org/10.1029/1999JD900442>, 1999.



- 1220 Lorente, A., Boersma, K. F., Eskes, H. J., Veeffkind, J. P., van Geffen, J. H. G. M., de Zeeuw, M. B., Denier van der Gon, H. A. C., Beirle, S., and Krol, M. C.: Quantification of nitrogen oxides emissions from build-up of pollution over Paris with TROPOMI, *Sci Rep*, 9, 20033, <https://doi.org/10.1038/s41598-019-56428-5>, 2019.
- Luo, G., Yu, F., and Moch, J. M.: Further improvement of wet process treatments in GEOS-Chem v12.6.0: impact on global distributions of aerosols and aerosol precursors, *Geosci. Model Dev.*, 13, 2879–2903, <https://doi.org/10.5194/gmd-13-2879-2020>, 2020.
- 1225 Mao, J., Paulot, F., Jacob, D. J., Cohen, R. C., Crounse, J. D., Wennberg, P. O., Keller, C. A., Hudman, R. C., Barkley, M. P., and Horowitz, L. W.: Ozone and organic nitrates over the eastern United States: Sensitivity to isoprene chemistry, *J. Geophys. Res. Atmos.*, 118, 11,256–11,268, <https://doi.org/10.1002/jgrd.50817>, 2013.
- Marais, E. A. and Wiedinmyer, C.: Air Quality Impact of Diffuse and Inefficient Combustion Emissions in Africa (DICE-Africa), *Environ. Sci. Technol.*, 50, 10739–10745, <https://doi.org/10.1021/acs.est.6b02602>, 2016.
- 1230 Marais, E. A., Jacob, D. J., Choi, S., Joiner, J., Belmonte-Rivas, M., Cohen, R. C., Beirle, S., Murray, L. T., Schiferl, L. D., Shah, V., and Jaeglé, L.: Nitrogen oxides in the global upper troposphere: interpreting cloud-sliced NO<sub>2</sub> observations from the OMI satellite instrument, *Atmos. Chem. Phys.*, 18, 17017–17027, <https://doi.org/10.5194/acp-18-17017-2018>, 2018.
- Marais, E. A., Roberts, J. F., Ryan, R. G., Eskes, H., Boersma, K. F., Choi, S., Joiner, J., Abuhassan, N., Redondas, A., Grutter, M., Cede, A., Gomez, L., and Navarro-Comas, M.: New observations of NO<sub>2</sub> in the upper troposphere from TROPOMI, *Atmos. Meas. Tech.*, 14, 2389–2408, <https://doi.org/10.5194/amt-14-2389-2021>, 2021.
- 1235 Martin, R. V., Chance, K., Jacob, D. J., Kurosu, T. P., Spurr, R. J. D., Bucsela, E., Gleason, J. F., Palmer, P. I., Bey, I., Fiore, A. M., Li, Q., Yantosca, R. M., and Koelemeijer, R. B. A.: An improved retrieval of tropospheric nitrogen dioxide from GOME, *Journal of Geophysical Research: Atmospheres*, 107, ACH 9-1, <https://doi.org/10.1029/2001JD001027>, 2002.
- Martin, R. V., Jacob, D. J., Chance, K., Kurosu, T. P., Palmer, P. I., and Evans, M. J.: Global inventory of nitrogen oxide emissions constrained by space-based observations of NO<sub>2</sub> columns, *J. Geophys. Res. Atmos.*, 108, <https://doi.org/10.1029/2003JD003453>, 2003.
- 1240 Martin, R. V., Sioris, C. E., Chance, K., Ryerson, T. B., Bertram, T. H., Wooldridge, P. J., Cohen, R. C., Neuman, J. A., Swanson, A., and Flocke, F. M.: Evaluation of space-based constraints on global nitrogen oxide emissions with regional aircraft measurements over and downwind of eastern North America, *J. Geophys. Res.*, 111, D15308, <https://doi.org/10.1029/2005JD006680>, 2006.
- 1245 Matsumoto, J., Hirokawa, J., Akimoto, H., and Kajii, Y.: Direct measurement of NO<sub>2</sub> in the marine atmosphere by laser-induced fluorescence technique, *Atmos. Environ.*, 35, 2803–2814, [https://doi.org/10.1016/S1352-2310\(01\)00078-4](https://doi.org/10.1016/S1352-2310(01)00078-4), 2001.
- McDuffie, E. E., Fibiger, D. L., Dubé, W. P., Lopez-Hilfiker, F., Lee, B. H., Thornton, J. A., Shah, V., Jaeglé, L., Guo, H., Weber, R. J., Michael Reeves, J., Weinheimer, A. J., Schroder, J. C., Campuzano-Jost, P., Jimenez, J. L., Dibb, J. E., Veres, P., Ebben, C., Sparks, T. L., Wooldridge, P. J., Cohen, R. C., Hornbrook, R. S., Apel, E. C., Campos, T., Hall, S. R., Ullmann, K., and Brown, S. S.: Heterogeneous N<sub>2</sub>O<sub>5</sub> Uptake During Winter: Aircraft Measurements During the 2015 WINTER Campaign and Critical Evaluation of Current Parameterizations, *J. Geophys. Res. Atmos.*, 123, 4345–4372, <https://doi.org/10.1002/2018JD028336>, 2018.
- 1250 McDuffie, E. E., Martin, R. V., Spadaro, J. V., Burnett, R., Smith, S. J., O'Rourke, P., Hammer, M. S., van Donkelaar, A., Bindle, L., Shah, V., Jaeglé, L., Luo, G., Yu, F., Adeniran, J. A., Lin, J., and Brauer, M.: Source sector and fuel contributions to ambient PM<sub>2.5</sub> and attributable mortality across multiple spatial scales, *Nat Commun*, 12, 3594, <https://doi.org/10.1038/s41467-021-23853-y>, 2021.

- McKain, K. and Sweeney, C.: Atmospheric Tomography Mission (ATom) ATom: CO<sub>2</sub>, CH<sub>4</sub>, and CO Measurements from Picarro, 2016-2018, <https://doi.org/10.3334/ORNLDAAAC/1732>, 2021.
- 1260 Millero, F. J., Feistel, R., Wright, D. G., and McDougall, T. J.: The composition of Standard Seawater and the definition of the Reference-Composition Salinity Scale, *Deep Sea Research Part I: Oceanographic Research Papers*, 55, 50–72, <https://doi.org/10.1016/j.dsr.2007.10.001>, 2008.
- Miyazaki, K., Bowman, K., Sekiya, T., Eskes, H., Boersma, F., Worden, H., Livesey, N., Payne, V. H., Sudo, K., Kanaya, Y., Takigawa, M., and Ogochi, K.: Updated tropospheric chemistry reanalysis and emission estimates, TCR-2, for 2005–2018, *Earth Syst. Sci. Data*, 12, 2223–2259, <https://doi.org/10.5194/essd-12-2223-2020>, 2020.
- 1265 Mollner, A. K., Valluvadasan, S., Feng, L., Sprague, M. K., Okumura, M., Milligan, D. B., Bloss, W. J., Sander, S. P., Martien, P. T., Harley, R. A., McCoy, A. B., and Carter, W. P. L.: Rate of Gas Phase Association of Hydroxyl Radical and Nitrogen Dioxide, *Science*, 330, 646–649, <https://doi.org/10.1126/science.1193030>, 2010.
- Moore, F. L., Hints, E. J., Nance, D., Dutton, G., Hall, B., and Elkins, J. W.: Atmospheric Tomography Mission (ATom): Trace Gas Measurements from PANTHER Gas Chromatograph, <https://doi.org/10.3334/ORNLDAAAC/1914>, 2022.
- 1270 Mora Garcia, S. L., Pandit, S., Navea, J. G., and Grassian, V. H.: Nitrous Acid (HONO) Formation from the Irradiation of Aqueous Nitrate Solutions in the Presence of Marine Chromophoric Dissolved Organic Matter: Comparison to Other Organic Photosensitizers, *ACS Earth Space Chem.*, 5, 3056–3064, <https://doi.org/10.1021/acsearthspacechem.1c00292>, 2021.
- Moxim, W. J., Levy, H., and Kasibhatla, P. S.: Simulated global tropospheric PAN: Its transport and impact on NO<sub>x</sub>, *J. Geophys. Res.*, 101, 12621–12638, <https://doi.org/10.1029/96JD00338>, 1996.
- 1275 Murphy, J. G., Thornton, J. A., Wooldridge, P. J., Day, D. A., Rosen, R. S., Cantrell, C., Shetter, R. E., Lefer, B., and Cohen, R. C.: Measurements of the sum of HO<sub>2</sub>NO<sub>2</sub> and CH<sub>3</sub>O<sub>2</sub>NO<sub>2</sub> in the remote troposphere, *Atmos. Chem. Phys.*, 4, 377–384, <https://doi.org/10.5194/acp-4-377-2004>, 2004.
- Murray, L. T.: Lightning NO<sub>x</sub> and Impacts on Air Quality, *Curr Pollution Rep*, 2, 115–133, <https://doi.org/10.1007/s40726-016-0031-7>, 2016.
- 1280 Murray, L. T., Jacob, D. J., Logan, J. A., Hudman, R. C., and Koshak, W. J.: Optimized regional and interannual variability of lightning in a global chemical transport model constrained by LIS/OTD satellite data, *Journal of Geophysical Research: Atmospheres*, 117, <https://doi.org/10.1029/2012JD017934>, 2012.
- Nault, B. A., Garland, C., Pusede, S. E., Wooldridge, P. J., Ullmann, K., Hall, S. R., and Cohen, R. C.: Measurements of CH<sub>3</sub>O<sub>2</sub>NO<sub>2</sub> in the upper troposphere, *Atmos Meas. Tech.*, 8, 987–997, <https://doi.org/10.5194/amt-8-987-2015>, 2015.
- 1285 Nault, B. A., Garland, C., Wooldridge, P. J., Brune, W. H., Campuzano-Jost, P., Crounse, J. D., Day, D. A., Dibb, J., Hall, S. R., Huey, L. G., Jimenez, J. L., Liu, X., Mao, J., Mikoviny, T., Peischl, J., Pollack, I. B., Ren, X., Ryerson, T. B., Scheuer, E., Ullmann, K., Wennberg, P. O., Wisthaler, A., Zhang, L., and Cohen, R. C.: Observational Constraints on the Oxidation of NO<sub>x</sub> in the Upper Troposphere, *J. Phys. Chem. A*, 120, 1468–1478, <https://doi.org/10.1021/acs.jpca.5b07824>, 2016.
- 1290 Nault, B. A., Laughner, J. L., Wooldridge, P. J., Crounse, J. D., Dibb, J., Diskin, G., Peischl, J., Podolske, J. R., Pollack, I. B., Ryerson, T. B., Scheuer, E., Wennberg, P. O., and Cohen, R. C.: Lightning NO<sub>x</sub> Emissions: Reconciling Measured and Modeled Estimates With Updated NO<sub>x</sub> Chemistry, *Geophys. Res. Lett.*, 44, 9479–9488, <https://doi.org/10.1002/2017GL074436>, 2017.

- Nault, B. A., Campuzano-Jost, P., Day, D. A., Jo, D. S., Schroder, J. C., Allen, H. M., Bahreini, R., Bian, H., Blake, D. R., Chin, M., Clegg, S. L., Colarco, P. R., Crounse, J. D., Cubison, M. J., DeCarlo, P. F., Dibb, J. E., Diskin, G. S., Hodzic, A.,  
295 Hu, W., Katich, J. M., Kim, M. J., Kodros, J. K., Kupc, A., Lopez-Hilfiker, F. D., Marais, E. A., Middlebrook, A. M., Andrew  
Neuman, J., Nowak, J. B., Palm, B. B., Paulot, F., Pierce, J. R., Schill, G. P., Scheuer, E., Thornton, J. A., Tsigaridis, K.,  
Wennberg, P. O., Williamson, C. J., and Jimenez, J. L.: Chemical transport models often underestimate inorganic aerosol  
acidity in remote regions of the atmosphere, *Commun Earth Environ*, 2, 93, <https://doi.org/10.1038/s43247-021-00164-0>,  
2021.
- 300 Nissenson, P., Dabdub, D., Das, R., Maurino, V., Minero, C., and Vione, D.: Evidence of the water-cage effect on the  
photolysis of  $\text{NO}_3^-$  and  $\text{FeOH}_2^+$ . Implications of this effect and of  $\text{H}_2\text{O}_2$  surface accumulation on photochemistry at the air–  
water interface of atmospheric droplets, *Atmospheric Environment*, 44, 4859–4866,  
<https://doi.org/10.1016/j.atmosenv.2010.08.035>, 2010.
- 305 Nussbaumer, C. M., Parchatka, U., Tadic, I., Bohn, B., Marno, D., Martinez, M., Rohloff, R., Harder, H., Kluge, F.,  
Pfeilsticker, K., Obersteiner, F., Zöger, M., Doerich, R., Crowley, J. N., Lelieveld, J., and Fischer, H.: Modification of a  
conventional photolytic converter for improving aircraft measurements of  $\text{NO}_2$  via chemiluminescence, *Atmos Meas. Tech.*,  
14, 6759–6776, <https://doi.org/10.5194/amt-14-6759-2021>, 2021.
- Osthoff, H. D., Brown, S. S., Ryerson, T. B., Fortin, T. J., Lerner, B. M., Williams, E. J., Pettersson, A., Baynard, T., Dubé,  
W. P., Ciciora, S. J., and Ravishankara, A. R.: Measurement of atmospheric  $\text{NO}_2$  by pulsed cavity ring-down spectroscopy, *J.*  
310 *Geophys. Res.*, 111, D12305, <https://doi.org/10.1029/2005JD006942>, 2006.
- Ott, L. E., Pickering, K. E., Stenchikov, G. L., Allen, D. J., DeCaria, A. J., Ridley, B., Lin, R.-F., Lang, S., and Tao, W.-K.:  
Production of lightning  $\text{NO}_x$  and its vertical distribution calculated from three-dimensional cloud-scale chemical transport  
model simulations, *J. Geophys. Res. Atmos.*, 115, <https://doi.org/10.1029/2009JD011880>, 2010.
- 315 Pai, S. J., Heald, C. L., Pierce, J. R., Farina, S. C., Marais, E. A., Jimenez, J. L., Campuzano-Jost, P., Nault, B. A., Middlebrook,  
A. M., Coe, H., Shilling, J. E., Bahreini, R., Dingle, J. H., and Vu, K.: An Evaluation of Global Organic Aerosol Schemes  
using Airborne Observations, *Atmos. Chem. Phys.*, 20, 2637–2665, <https://doi.org/10.5194/acp-20-2637-2020>, 2020.
- 320 Palmer, P. I., Jacob, D. J., Chance, K., Martin, R. V., Spurr, R. J. D., Kurosu, T. P., Bey, I., Yantosca, R., Fiore, A., and Li,  
Q.: Air mass factor formulation for spectroscopic measurements from satellites: Application to formaldehyde retrievals from  
the Global Ozone Monitoring Experiment, *Journal of Geophysical Research: Atmospheres*, 106, 14539–14550,  
<https://doi.org/10.1029/2000JD900772>, 2001.
- Pickering, K. E., Thompson, A. M., Dickerson, R. R., Luke, W. T., McNamara, D. P., Greenberg, J. P., and Zimmerman, P.  
R.: Model calculations of tropospheric ozone production potential following observed convective events, *J. Geophys. Res.*,  
95, 14049, <https://doi.org/10.1029/JD095iD09p14049>, 1990.
- 325 Platt, U., Meinen, J., Pöhler, D., and Leisner, T.: Broadband Cavity Enhanced Differential Optical Absorption Spectroscopy  
(CE-DOAS) – applicability and corrections, *Atmos. Meas. Tech.*, 2, 713–723, <https://doi.org/10.5194/amt-2-713-2009>, 2009.
- Pollack, I. B., Lerner, B. M., and Ryerson, T. B.: Evaluation of ultraviolet light-emitting diodes for detection of atmospheric  
 $\text{NO}_2$  by photolysis - chemiluminescence, *J Atmos Chem*, 65, 111–125, <https://doi.org/10.1007/s10874-011-9184-3>, 2010.
- 330 Pollack, I. B., Ryerson, T. B., Trainer, M., Parrish, D. D., Andrews, A. E., Atlas, E. L., Blake, D. R., Brown, S. S., Commane,  
R., Daube, B. C., de Gouw, J. A., Dubé, W. P., Flynn, J., Frost, G. J., Gilman, J. B., Grossberg, N., Holloway, J. S., Kofler, J.,  
Kort, E. A., Kuster, W. C., Lang, P. M., Lefer, B., Lueb, R. A., Neuman, J. A., Nowak, J. B., Novelli, P. C., Peischl, J., Perring,  
A. E., Roberts, J. M., Santoni, G., Schwarz, J. P., Spackman, J. R., Wagner, N. L., Warneke, C., Washenfelder, R. A., Wofsy,

- S. C., and Xiang, B.: Airborne and ground-based observations of a weekend effect in ozone, precursors, and oxidation products in the California South Coast Air Basin, *J. Geophys. Res.*, 117, D00V05, <https://doi.org/10.1029/2011JD016772>, 2012.
- Prather, M. J., Holmes, C. D., and Hsu, J.: Reactive greenhouse gas scenarios: Systematic exploration of uncertainties and the role of atmospheric chemistry, *Geophys. Res. Lett.*, 39, L09803, <https://doi.org/10.1029/2012GL051440>, 2012.
- Reed, C., Evans, M. J., Di Carlo, P., Lee, J. D., and Carpenter, L. J.: Interferences in photolytic NO<sub>2</sub> measurements: explanation for an apparent missing oxidant?, *Atmos. Chem. Phys.*, 16, 4707–4724, <https://doi.org/10.5194/acp-16-4707-2016>, 2016.
- Reed, C., Evans, M. J., Crilley, L. R., Bloss, W. J., Sherwen, T., Read, K. A., Lee, J. D., and Carpenter, L. J.: Evidence for renoxification in the tropical marine boundary layer, *Atmos. Chem. Phys.*, 17, 4081–4092, <https://doi.org/10.5194/acp-17-4081-2017>, 2017.
- Richards-Henderson, N. K., Callahan, K. M., Nissenson, P., Nishino, N., Tobias, D. J., and Finlayson-Pitts, B. J.: Production of gas phase NO<sub>2</sub> and halogens from the photolysis of thin water films containing nitrate, chloride and bromide ions at room temperature, *Phys. Chem. Chem. Phys.*, 15, 17636, <https://doi.org/10.1039/c3cp52956h>, 2013.
- Richards-Henderson, N. K., Anderson, C., Anastasio, C., and Finlayson-Pitts, B. J.: The effect of cations on NO<sub>2</sub> production from the photolysis of aqueous thin water films of nitrate salts, *Phys. Chem. Chem. Phys.*, 17, 32211–32218, <https://doi.org/10.1039/C5CP05325K>, 2015.
- Richter, A., Burrows, J. P., Nüß, H., Granier, C., and Niemeier, U.: Increase in tropospheric nitrogen dioxide over China observed from space, *Nature*, 437, 129, 2005.
- Ridley, B. A., Carroll, M. A., Gregory, G. L., and Sachse, G. W.: NO and NO<sub>2</sub> in the troposphere: Technique and measurements in regions of a folded tropopause, *J. Geophys. Res.*, 93, 15813, <https://doi.org/10.1029/JD093iD12p15813>, 1988.
- Rollins, A. W., Rickly, P. S., Gao, R.-S., Ryerson, T. B., Brown, S. S., Peischl, J., and Bourgeois, I.: Single-photon laser-induced fluorescence detection of nitric oxide at sub-parts-per-trillion mixing ratios, *Atmos. Meas. Tech.*, 13, 2425–2439, <https://doi.org/10.5194/amt-13-2425-2020>, 2020.
- Romer, P. S., Wooldridge, P. J., Crounse, J. D., Kim, M. J., Wennberg, P. O., Dibb, J. E., Scheuer, E., Blake, D. R., Meinardi, S., Brosius, A. L., Thames, A. B., Miller, D. O., Brune, W. H., Hall, S. R., Ryerson, T. B., and Cohen, R. C.: Constraints on Aerosol Nitrate Photolysis as a Potential Source of HONO and NO<sub>x</sub>, *Environ. Sci. Technol.*, 52, 13738–13746, <https://doi.org/10.1021/acs.est.8b03861>, 2018.
- Ryerson, T. B., Buhr, M. P., Frost, G. J., Goldan, P. D., Holloway, J. S., Hübler, G., Jobson, B. T., Kuster, W. C., McKeen, S. A., Parrish, D. D., Roberts, J. M., Sueper, D. T., Trainer, M., Williams, J., and Fehsenfeld, F. C.: Emissions lifetimes and ozone formation in power plant plumes, *J. Geophys. Res.*, 103, 22569–22583, <https://doi.org/10.1029/98JD01620>, 1998.
- Ryerson, T. B., Williams, E. J., and Fehsenfeld, F. C.: An efficient photolysis system for fast-response NO<sub>2</sub> measurements, *J. Geophys. Res. Atmos.*, 105, 26447–26461, <https://doi.org/10.1029/2000JD900389>, 2000.
- Sachse, G. W., Collins, Jr., J. E., Hill, G. F., Wade, L. O., Burney, L. G., and Ritter, J. A.: Airborne tunable diode laser sensor for high-precision concentration and flux measurements of carbon monoxide and methane, *Optics, Electro-Optics, and Laser Applications in Science and Engineering*, Los Angeles, CA, 157, <https://doi.org/10.1117/12.46162>, 1991.
- Sandholm, S. T., Bradshaw, J. D., Dorris, K. S., Rodgers, M. O., and Davis, D. D.: An airborne compatible photofragmentation two-photon laser-induced fluorescence instrument for measuring background tropospheric levels of NO, NO<sub>x</sub>, and NO<sub>2</sub>, *J. Geophys. Res.*, 95, 10155–10161, <https://doi.org/10.1029/JD095iD07p10155>, 1990.

- Scharko, N. K., Berke, A. E., and Raff, J. D.: Release of Nitrous Acid and Nitrogen Dioxide from Nitrate Photolysis in Acidic Aqueous Solutions, *Environ. Sci. Technol.*, 48, 11991–12001, <https://doi.org/10.1021/es503088x>, 2014.
- Schmidt, J. A., Jacob, D. J., Horowitz, H. M., Hu, L., Sherwen, T., Evans, M. J., Liang, Q., Suleiman, R. M., Oram, D. E., Le Breton, M., Percival, C. J., Wang, S., Dix, B., and Volkamer, R.: Modeling the Observed Tropospheric BrO Background: Importance of Multiphase Chemistry and Implications for Ozone, OH, and Mercury, *J. Geophys. Res. Atmos.*, 121, 11,819–11,835, <https://doi.org/10.1002/2015JD024229>, 2016.
- Schumann, U. and Huntrieser, H.: The global lightning-induced nitrogen oxides source, *Atmos. Chem. Phys.*, 7, 3823–3907, <https://doi.org/10.5194/acp-7-3823-2007>, 2007.
- Schwantes, R. H., Lacey, F. G., Tilmes, S., Emmons, L. K., Lauritzen, P. H., Walters, S., Callaghan, P., Zarzycki, C. M., Barth, M. C., Jo, D. S., Bacmeister, J. T., Neale, R. B., Vitt, F., Kluzek, E., Roozitalab, B., Hall, S. R., Ullmann, K., Warneke, C., Peischl, J., Pollack, I. B., Flocke, F., Wolfe, G. M., Hanisco, T. F., Keutsch, F. N., Kaiser, J., Bui, T. P. V., Jimenez, J. L., Campuzano-Jost, P., Apel, E. C., Hornbrook, R. S., Hills, A. J., Yuan, B., and Wisthaler, A.: Evaluating the Impact of Chemical Complexity and Horizontal Resolution on Tropospheric Ozone Over the Conterminous US With a Global Variable Resolution Chemistry Model, *J Adv Model Earth Syst*, 14, <https://doi.org/10.1029/2021MS002889>, 2022.
- SEAC4RS Science Team: SEAC4RS Field Campaign Data, <https://doi.org/10.5067/AIRCRAFT/SEAC4RS/AEROSOL-TRACEGAS-CLOUD>, 2014.
- Seltzer, K. M., Vizuete, W., and Henderson, B. H.: Evaluation of updated nitric acid chemistry on ozone precursors and radiative effects, *Atmos. Chem. Phys.*, 15, 5973–5986, <https://doi.org/10.5194/acp-15-5973-2015>, 2015.
- Shah, V., Jacob, D. J., Li, K., Silvern, R. F., Zhai, S., Liu, M., Lin, J., and Zhang, Q.: Effect of changing NO<sub>x</sub> lifetime on the seasonality and long-term trends of satellite-observed tropospheric NO<sub>2</sub> columns over China, *Atmos. Chem. Phys.*, 20, 1483–1495, <https://doi.org/10.5194/acp-20-1483-2020>, 2020.
- Shetter, R. E. and Müller, M.: Photolysis frequency measurements using actinic flux spectroradiometry during the PEM-Tropics mission: Instrumentation description and some results, *J. Geophys. Res.*, 104, 5647–5661, <https://doi.org/10.1029/98JD01381>, 1999.
- Shi, Q., Tao, Y., Krechmer, J. E., Heald, C. L., Murphy, J. G., Kroll, J. H., and Ye, Q.: Laboratory Investigation of Renoxification from the Photolysis of Inorganic Particulate Nitrate, *Environ. Sci. Technol.*, 55, 854–861, <https://doi.org/10.1021/acs.est.0c06049>, 2021.
- Silvern, R. F., Jacob, D. J., Travis, K. R., Sherwen, T., Evans, M. J., Cohen, R. C., Laughner, J. L., Hall, S. R., Ullmann, K., Crounse, J. D., Wennberg, P. O., Peischl, J., and Pollack, I. B.: Observed NO/NO<sub>2</sub> Ratios in the Upper Troposphere Imply Errors in NO-NO<sub>2</sub>-O<sub>3</sub> Cycling Kinetics or an Unaccounted NO<sub>x</sub> Reservoir, *Geophys. Res. Lett.*, 45, 4466–4474, <https://doi.org/10.1029/2018GL077728>, 2018.
- Silvern, R. F., Jacob, D. J., Mickley, L. J., Sulprizio, M. P., Travis, K. R., Marais, E. A., Cohen, R. C., Laughner, J. L., Choi, S., Joiner, J., and Lamsal, L. N.: Using satellite observations of tropospheric NO<sub>2</sub> columns to infer long-term trends in US NO<sub>x</sub> emissions: the importance of accounting for the free tropospheric NO<sub>2</sub> background, *Atmospheric Chemistry and Physics*, 19, 8863–8878, <https://doi.org/10.5194/acp-19-8863-2019>, 2019.
- Simone, N. W., Stettler, M. E. J., and Barrett, S. R. H.: Rapid estimation of global civil aviation emissions with uncertainty quantification, *Transp Res D Transp*, 25, 33–41, <https://doi.org/10.1016/j.trd.2013.07.001>, 2013.

- Singh, H. B., Salas, L. J., and Viezee, W.: Global distribution of peroxyacetyl nitrate, *Nature*, 321, 588–591, <https://doi.org/10.1038/321588a0>, 1986.
- Singh, H. B., Herlth, D., Kolyer, R., Salas, L., Bradshaw, J. D., Sandholm, S. T., Davis, D. D., Crawford, J., Kondo, Y., Koike, M., Talbot, R., Gregory, G. L., Sachse, G. W., Browell, E., Blake, D. R., Rowland, F. S., Newell, R., Merrill, J., Heikes, B., Liu, S. C., Crutzen, P. J., and Kanakidou, M.: Reactive nitrogen and ozone over the western Pacific: Distribution, partitioning, and sources, *J. Geophys. Res.*, 101, 1793–1808, <https://doi.org/10.1029/95JD01029>, 1996.
- Singh, H. B., Salas, L., Herlth, D., Kolyer, R., Czech, E., Avery, M., Crawford, J. H., Pierce, R. B., Sachse, G. W., Blake, D. R., Cohen, R. C., Bertram, T. H., Perring, A., Wooldridge, P. J., Dibb, J., Huey, G., Hudman, R. C., Turquety, S., Emmons, L. K., Flocke, F., Tang, Y., Carmichael, G. R., and Horowitz, L. W.: Reactive nitrogen distribution and partitioning in the North American troposphere and lowermost stratosphere, *J. Geophys. Res.*, 112, D12S04, <https://doi.org/10.1029/2006JD007664>, 2007.
- Sparks, T. L., Ebben, C. J., Wooldridge, P. J., Lopez-Hilfiker, F. D., Lee, B. H., Thornton, J. A., McDuffie, E. E., Fibiger, D. L., Brown, S. S., Montzka, D. D., Weinheimer, A. J., Schroder, J. C., Campuzano-Jost, P., Jimenez, J. L., and Cohen, R. C.: Comparison of Airborne Reactive Nitrogen Measurements During WINTER, *J. Geophys. Res. Atmos.*, 124, 10483–10502, <https://doi.org/10.1029/2019JD030700>, 2019.
- Stettler, M. E. J., Eastham, S., and Barrett, S. R. H.: Air quality and public health impacts of UK airports. Part I: Emissions, *Atmos. Environ.*, 45, 5415–5424, <https://doi.org/10.1016/j.atmosenv.2011.07.012>, 2011.
- Strahan, S. E., Duncan, B. N., and Hoor, P.: Observationally derived transport diagnostics for the lowermost stratosphere and their application to the GMI chemistry and transport model, *Atmos. Chem. Phys.*, 7, 2435–2445, <https://doi.org/10.5194/acp-7-2435-2007>, 2007.
- Strode, S. A., Rodriguez, J. M., Logan, J. A., Cooper, O. R., Witte, J. C., Lamsal, L. N., Damon, M., Van Aartsen, B., Steenrod, S. D., and Strahan, S. E.: Trends and variability in surface ozone over the United States, *J. Geophys. Res. Atmos.*, 120, 9020–9042, <https://doi.org/10.1002/2014JD022784>, 2015.
- Strode, S. A., Steenrod, S.D., Nicely, J.M., Liu, J., Damon, M.R., and Strahan, S.E.: Atmospheric Tomography Mission (ATom): Global Modeling Initiative (GMI) Chemical Transport Model (CTM) Output, <https://doi.org/10.3334/ORNLDAAAC/1897>, 2021.
- Thames, A. B., Brune, W. H., Miller, D. O., Allen, H. M., Apel, E. C., Blake, D. R., Bui, T. P., Commane, R., Crounse, J. D., Daube, B. C., Diskin, G. S., DiGangi, J. P., Elkins, J. W., Hall, S. R., Hanisco, T. F., Hannun, R. A., Hintsä, E., Hornbrook, R. S., Kim, M. J., McKain, K., Moore, F. L., Nicely, J. M., Peischl, J., Ryerson, T. B., St. Clair, J. M., Sweeney, C., Teng, A., Thompson, C. R., Ullmann, K., Wennberg, P. O., and Wolfe, G. M.: Missing OH reactivity in the global marine boundary layer, *Atmos. Chem. Phys.*, 20, 4013–4029, <https://doi.org/10.5194/acp-20-4013-2020>, 2020.
- Thompson, C. R., Wofsy, S. C., Prather, M. J., Newman, P. A., Hanisco, T. F., Ryerson, T. B., Fahey, D. W., Apel, E. C., Brock, C. A., Brune, W. H., Froyd, K., Katich, J. M., Nicely, J. M., Peischl, J., Ray, E., Veres, P. R., Wang, S., Allen, H. M., Asher, E., Bian, H., Blake, D., Bourgeois, I., Budney, J., Bui, T. P., Butler, A., Campuzano-Jost, P., Chang, C., Chin, M., Commane, R., Correa, G., Crounse, J. D., Daube, B., Dibb, J. E., DiGangi, J. P., Diskin, G. S., Dollner, M., Elkins, J. W., Fiore, A. M., Flynn, C. M., Guo, H., Hall, S. R., Hannun, R. A., Hills, A., Hintsä, E. J., Hodzic, A., Hornbrook, R. S., Huey, L. G., Jimenez, J. L., Keeling, R. F., Kim, M. J., Kupc, A., Lacey, F., Lait, L. R., Lamarque, J.-F., Liu, J., McKain, K., Meinardi, S., Miller, D. O., Montzka, S. A., Moore, F. L., Morgan, E. J., Murphy, D. M., Murray, L. T., Nault, B. A., Neuman, J. A., Nguyen, L., Gonzalez, Y., Rollins, A., Rosenlof, K., Sargent, M., Schill, G., Schwarz, J. P., Clair, J. M. St., Steenrod, S. D., Stephens, B. B., Strahan, S. E., Strode, S. A., Sweeney, C., Thames, A. B., Ullmann, K., Wagner, N., Weber, R., Weinzierl, B., Wennberg, P. O., Williamson, C. J., Wolfe, G. M., and Zeng, L.: The NASA Atmospheric Tomography (ATom) Mission:

- Imaging the Chemistry of the Global Atmosphere, *Bull. Amer. Meteor. Soc.*, 103, E761–E790, <https://doi.org/10.1175/BAMS-D-20-0315.1>, 2022.
- Thornton, J. A., Wooldridge, P. J., and Cohen, R. C.: Atmospheric NO<sub>2</sub>: In Situ Laser-Induced Fluorescence Detection at Parts  
 1450 per Trillion Mixing Ratios, *Anal. Chem.*, 72, 528–539, <https://doi.org/10.1021/ac9908905>, 2000.
- Thornton, J. A., Wooldridge, P. J., Cohen, R. C., Williams, E. J., Hereid, D., Fehsenfeld, F. C., Stutz, J., and Alicke, B.: Comparisons of in situ and long path measurements of NO<sub>2</sub> in urban plumes, *J. Geophys. Res.*, 108, 4496, <https://doi.org/10.1029/2003JD003559>, 2003.
- Tian, Y., Yang, G.-P., Liu, C.-Y., Li, P.-F., Chen, H.-T., and Bange, H. W.: Photoproduction of nitric oxide in seawater, *Ocean  
 1455 Sci.*, 16, 135–148, <https://doi.org/10.5194/os-16-135-2020>, 2020.
- Toon, O. B., Maring, H., Dibb, J., Ferrare, R., Jacob, D. J., Jensen, E. J., Luo, Z. J., Mace, G. G., Pan, L. L., Pfister, L., Rosenlof, K. H., Redemann, J., Reid, J. S., Singh, H. B., Thompson, A. M., Yokelson, R., Minnis, P., Chen, G., Jucks, K. W., and Pszenny, A.: Planning, implementation, and scientific goals of the Studies of Emissions and Atmospheric Composition, Clouds and Climate Coupling by Regional Surveys (SEAC<sup>4</sup>RS) field mission, *J. Geophys. Res. Atmos.*, 121, 4967–5009, <https://doi.org/10.1002/2015JD024297>, 2016.  
 1460
- Torres, A. L. and Thompson, A. M.: Nitric oxide in the equatorial Pacific boundary layer: SAGA 3 measurements, *J. Geophys. Res.*, 98, 16949, <https://doi.org/10.1029/92JD01906>, 1993.
- Travis, K. R., Jacob, D. J., Fisher, J. A., Kim, P. S., Marais, E. A., Zhu, L., Yu, K., Miller, C. C., Yantosca, R. M., Sulprizio, M. P., Thompson, A. M., Wennberg, P. O., Crounse, J. D., St. Clair, J. M., Cohen, R. C., Laughner, J. L., Dibb, J. E., Hall, S. R., Ullmann, K., Wolfe, G. M., Pollack, I. B., Peischl, J., Neuman, J. A., and Zhou, X.: Why do models overestimate surface  
 1465 ozone in the Southeast United States?, *Atmos. Chem. Phys.*, 16, 13561–13577, <https://doi.org/10.5194/acp-16-13561-2016>, 2016.
- Travis, K. R., Heald, C. L., Allen, H. M., Apel, E. C., Arnold, S. R., Blake, D. R., Brune, W. H., Chen, X., Commane, R., Crounse, J. D., Daube, B. C., Diskin, G. S., Elkins, J. W., Evans, M. J., Hall, S. R., Hints, E. J., Hornbrook, R. S., Kasibhatla, P. S., Kim, M. J., Luo, G., McKain, K., Millet, D. B., Moore, F. L., Peischl, J., Ryerson, T. B., Sherwen, T., Thames, A. B., Ullmann, K., Wang, X., Wennberg, P. O., Wolfe, G. M., and Yu, F.: Constraining remote oxidation capacity with ATom  
 1470 observations, *Atmos. Chem. Phys.*, 20, 7753–7781, <https://doi.org/10.5194/acp-20-7753-2020>, 2020.
- US EPA Air Pollutant Emissions Trends Data: <https://www.epa.gov/air-emissions-inventories/air-pollutant-emissions-trends-data>, last access: 2 May 2015.
- 1475 US EPA 2011 NEI: <https://www.epa.gov/air-emissions-inventories/2011-national-emissions-inventory-nei-data>, last access: 23 March 2016.
- Vinken, G. C. M., Boersma, K. F., Jacob, D. J., and Meijer, E. W.: Accounting for non-linear chemistry of ship plumes in the GEOS-Chem global chemistry transport model, *Atmos. Chem. Phys.*, 11, 11707–11722, <https://doi.org/10.5194/acp-11-11707-2011>, 2011.
- 1480 Vlemmix, T., Pijters, A. J. M., Berkhout, A. J. C., Gast, L. F. L., Wang, P., and Levelt, P. F.: Ability of the MAX-DOAS method to derive profile information for NO<sub>2</sub> in the boundary layer and free troposphere be separated?, *Atmos. Meas. Tech.*, 4, 2659–2684, <https://doi.org/10.5194/amt-4-2659-2011>, 2011.
- Volkamer, R., Baidar, S., Campos, T. L., Coburn, S., DiGangi, J. P., Dix, B., Eloranta, E. W., Koenig, T. K., Morley, B., Ortega, I., Pierce, B. R., Reeves, M., Sinreich, R., Wang, S., Zondlo, M. A., and Romashkin, P. A.: Aircraft measurements of

- 485 BrO, IO, glyoxal, NO<sub>2</sub> H<sub>2</sub>O, O<sub>2</sub>–O<sub>2</sub> and aerosol extinction profiles in the tropics: comparison with aircraft-/ship-based in situ and lidar measurements, *Atmos. Meas. Tech.*, 8, 2121–2148, <https://doi.org/10.5194/amt-8-2121-2015>, 2015.
- Walega, J. G., Dye, J. E., Grahek, F. E., and Ridley, B. K.: Compact measurement system for the simultaneous determination of NO, NO<sub>2</sub>, NO<sub>y</sub>, and O<sub>3</sub> using a small aircraft, *Optics, Electro-Optics, and Laser Applications in Science and Engineering*, Los Angeles, CA, 232, <https://doi.org/10.1117/12.46167>, 1991.
- 490 Wang, X., Jacob, D. J., Eastham, S. D., Sulprizio, M. P., Zhu, L., Chen, Q., Alexander, B., Sherwen, T., Evans, M. J., Lee, B. H., Haskins, J. D., Lopez-Hilfiker, F. D., Thornton, J. A., Huey, G. L., and Liao, H.: The Role of Chlorine in Global Tropospheric Chemistry, *Atmospheric Chemistry and Physics*, 19, 3981–4003, <https://doi.org/10.5194/acp-19-3981-2019>, 2019.
- Wang, X., Jacob, D. J., Downs, W., Zhai, S., Zhu, L., Shah, V., Holmes, C. D., Sherwen, T., Alexander, B., Evans, M. J., Eastham, S. D., Neuman, J. A., Veres, P. R., Koenig, T. K., Volkamer, R., Huey, L. G., Bannan, T. J., Percival, C. J., Lee, B. H., and Thornton, J. A.: Global tropospheric halogen (Cl, Br, I) chemistry and its impact on oxidants, *Atmos. Chem. Phys.*, 21, 13973–13996, <https://doi.org/10.5194/acp-21-13973-2021>, 2021.
- 495 Wang, Y., Logan, J. A., and Jacob, D. J.: Global simulation of tropospheric O<sub>3</sub>–NO<sub>x</sub>–hydrocarbon chemistry: 2. Model evaluation and global ozone budget, *J. Geophys. Res.*, 103, 10727–10755, <https://doi.org/10.1029/98JD00157>, 1998.
- 500 Warneck, P. and Wurzinger, C.: Product quantum yields for the 305-nm photodecomposition of nitrate in aqueous solution, *J. Phys. Chem.*, 92, 6278–6283, <https://doi.org/10.1021/j100333a022>, 1988.
- Weng, H., Lin, J., Martin, R., Millet, D. B., Jaeglé, L., Ridley, D., Keller, C., Li, C., Du, M., and Meng, J.: Global high-resolution emissions of soil NO<sub>x</sub>, sea salt aerosols, and biogenic volatile organic compounds, *Sci Data*, 7, 148, <https://doi.org/10.1038/s41597-020-0488-5>, 2020.
- 505 Wild, O. and Prather, M. J.: Excitation of the Primary Tropospheric Chemical Mode in a Global Three-Dimensional Model, *J. Geophys. Res.*, 105, 24647–24660, <https://doi.org/10.1029/2000JD900399>, 2000.
- Williams, J. E., Boersma, K. F., Le Sager, P., and Verstraeten, W. W.: The high-resolution version of TM5-MP for optimized satellite retrievals: description and validation, *Geosci. Model Dev.*, 10, 721–750, <https://doi.org/10.5194/gmd-10-721-2017>, 2017.
- 510 Wingen, L. M., Moskun, A. C., Johnson, S. N., Thomas, J. L., Roeselová, M., Tobias, D. J., Kleinman, M. T., and Finlayson-Pitts, B. J.: Enhanced surface photochemistry in chloride–nitrate ion mixtures, *Phys. Chem. Chem. Phys.*, 10, 5668, <https://doi.org/10.1039/b806613b>, 2008.
- Wisthaler, A., Hansel, A., Dickerson, R. R., and Crutzen, P. J.: Organic trace gas measurements by PTR-MS during INDOEX 1999, *J. Geophys. Res.*, 107, 8024, <https://doi.org/10.1029/2001JD000576>, 2002.
- 515 Wofsy, S. C., Afshar, S., Allen, H. M., Apel, E. C., Asher, E. C., Barletta, B., Bent, J., Bian, H., Biggs, B. C., Blake, D. R., Blake, N., Bourgeois, I., Brock, C. A., Brune, W. H., Budney, J. W., Bui, T. P., Butler, A., Campuzano-Jost, P., Chang, C. S., Chin, M., Commane, R., Correa, G., Crounse, J. D., Cullis, P. D., Daube, B. C., Day, D. A., Dean-Day, J. M., Dibb, J. E., DiGangi, J. P., Diskin, G. S., Dollner, M., Elkins, J. W., Erdesz, F., Fiore, A. M., Flynn, C. M., Froyd, K. D., Gesler, D. W., Hall, S. R., Hanisco, T. F., Hannun, R. A., Hills, A. J., Hintsa, E. J., Hoffman, A., Hornbrook, R. S., Huey, L. G., Hughes, S., Jimenez, J. L., Johnson, B. J., Katich, J. M., Keeling, R. F., Kim, M. J., Kupc, A., Lait, L. R., McKain, K., Mclaughlin, R. J., Meinardi, S., Miller, D. O., Montzka, S. A., Moore, F. L., Morgan, E. J., Murphy, D. M., Murray, L. T., Nault, B. A., Neuman, J. A., Newman, P. A., Nicely, J. M., Pan, X., Paplawsky, W., Peischl, J., Prather, M. J., Price, D. J., Ray, E. A., Reeves, J. M., Richardson, M., Rollins, A. W., Rosenlof, K. H., Ryerson, T. B., Scheuer, E., Schill, G. P., Schroder, J. C., Schwarz, J. P.,
- 520



- 1525 St.Clair, J. M., Steenrod, S. D., Stephens, B. B., Strode, S. A., Sweeney, C., Tanner, D., Teng, A. P., Thames, A. B., Thompson, C. R., Ullmann, K., Veres, P. R., Wagner, N. L., Watt, A., Weber, R., Weinzierl, B. B., Wennberg, P. O., Williamson, C. J., Wilson, J. C., et al.: ATom: Merged Atmospheric Chemistry, Trace Gases, and Aerosols, Version 2, , <https://doi.org/10.3334/ORNLDAAC/1925>, 2021.
- 1530 Wooldridge, P. J., Perring, A. E., Bertram, T. H., Flocke, F. M., Roberts, J. M., Singh, H. B., Huey, L. G., Thornton, J. A., Wolfe, G. M., Murphy, J. G., Fry, J. L., Rollins, A. W., LaFranchi, B. W., and Cohen, R. C.: Total Peroxy Nitrates ( $\Sigma$ PNs) in the atmosphere: the Thermal Dissociation-Laser Induced Fluorescence (TD-LIF) technique and comparisons to speciated PAN measurements, *Atmos. Meas. Tech.*, 3, 593–607, <https://doi.org/10.5194/amt-3-593-2010>, 2010.
- Ye, C., Gao, H., Zhang, N., and Zhou, X.: Photolysis of Nitric Acid and Nitrate on Natural and Artificial Surfaces, *Environ. Sci. Technol.*, 50, 3530–3536, <https://doi.org/10.1021/acs.est.5b05032>, 2016a.
- 1535 Ye, C., Zhou, X., Pu, D., Stutz, J., Festa, J., Spolaor, M., Tsai, C., Cantrell, C., Mauldin, R. L., Campos, T., Weinheimer, A., Hornbrook, R. S., Apel, E. C., Guenther, A., Kaser, L., Yuan, B., Karl, T., Haggerty, J., Hall, S., Ullmann, K., Smith, J. N., Ortega, J., and Knote, C.: Rapid cycling of reactive nitrogen in the marine boundary layer, *Nature*, 532, 489–491, <https://doi.org/10.1038/nature17195>, 2016b.
- Ye, C., Heard, D. E., and Whalley, L. K.: Evaluation of Novel Routes for  $\text{NO}_x$  Formation in Remote Regions, *Environ. Sci. Technol.*, 51, 7442–7449, <https://doi.org/10.1021/acs.est.6b06441>, 2017a.
- 1540 Ye, C., Zhang, N., Gao, H., and Zhou, X.: Photolysis of Particulate Nitrate as a Source of HONO and  $\text{NO}_x$ , *Environ. Sci. Technol.*, 51, 6849–6856, <https://doi.org/10.1021/acs.est.7b00387>, 2017b.
- Ye, C., Zhang, N., Gao, H., and Zhou, X.: Matrix effect on surface-catalyzed photolysis of nitric acid, *Sci Rep*, 9, 4351, <https://doi.org/10.1038/s41598-018-37973-x>, 2019.
- 1545 Yu, K., Jacob, D. J., Fisher, J. A., Kim, P. S., Marais, E. A., Miller, C. C., Travis, K. R., Zhu, L., Yantosca, R. M., Sulprizio, M. P., Cohen, R. C., Dibb, J. E., Fried, A., Mikoviny, T., Ryerson, T. B., Wennberg, P. O., and Wisthaler, A.: Sensitivity to grid resolution in the ability of a chemical transport model to simulate observed oxidant chemistry under high-isoprene conditions, *Atmos. Chem. Phys.*, 16, 4369–4378, <https://doi.org/10.5194/acp-16-4369-2016>, 2016.
- 1550 Zatko, M., Geng, L., Alexander, B., Sofen, E., and Klein, K.: The impact of snow nitrate photolysis on boundary layer chemistry and the recycling and redistribution of reactive nitrogen across Antarctica and Greenland in a global chemical transport model, *Atmos. Chem. Phys.*, 16, 2819–2842, <https://doi.org/10.5194/acp-16-2819-2016>, 2016.
- Zhang, R., Gen, M., Huang, D., Li, Y., and Chan, C. K.: Enhanced Sulfate Production by Nitrate Photolysis in the Presence of Halide Ions in Atmospheric Particles, *Environ. Sci. Technol.*, 54, 3831–3839, <https://doi.org/10.1021/acs.est.9b06445>, 2020.
- 1555 Zheng, B., Tong, D., Li, M., Liu, F., Hong, C., Geng, G., Li, H., Li, X., Peng, L., Qi, J., Yan, L., Zhang, Y., Zhao, H., Zheng, Y., He, K., and Zhang, Q.: Trends in China’s anthropogenic emissions since 2010 as the consequence of clean air actions, *Atmos. Chem. Phys.*, 18, 14095–14111, <https://doi.org/10.5194/acp-18-14095-2018>, 2018.
- Zhu, C., Xiang, B., Zhu, L., and Cole, R.: Determination of absorption cross sections of surface-adsorbed  $\text{HNO}_3$  in the 290–330nm region by Brewster angle cavity ring-down spectroscopy, *Chemical Physics Letters*, 458, 373–377, <https://doi.org/10.1016/j.cplett.2008.04.125>, 2008.
- 1560 Zhu, C., Xiang, B., Chu, L. T., and Zhu, L.: 308 nm Photolysis of Nitric Acid in the Gas Phase, on Aluminum Surfaces, and on Ice Films, *J. Phys. Chem. A*, 114, 2561–2568, <https://doi.org/10.1021/jp909867a>, 2010.

Zhu, Q., Laughner, J. L., and Cohen, R. C.: Lightning NO<sub>2</sub> simulation over the contiguous US and its effects on satellite NO<sub>2</sub> retrievals, *Atmos. Chem. Phys.*, 19, 13067–13078, <https://doi.org/10.5194/acp-19-13067-2019>, 2019.

1565 Zhu, Y., Wang, Y., Zhou, X., Elshorbany, Y. F., Ye, C., Hayden, M., and Peters, A. J.: An investigation into the chemistry of HONO in the marine boundary layer at Tudor Hill Marine Atmospheric Observatory in Bermuda, *Atmos. Chem. Phys.*, 22, 6327–6346, <https://doi.org/10.5194/acp-22-6327-2022>, 2022.